

ANALYSIS AND MEASUREMENT OF ANTI-RECIPROCAL SYSTEM

Draft of November 2, 2014 at 17:33

BY

NOORI KIM

DISSERTATION

Submitted in partial fulfillment of the requirements
for the degree of Doctor of Philosophy in Electrical and Computer Engineering
in the Graduate College of the
University of Illinois at Urbana-Champaign, 2014

1

Urbana, Illinois

Doctoral Committee:

Associate Professor Jont B. Allen, Chair

Professor Stephen Boppart

Professor Steven Franke

Associate Professor Michael Oelze

ABSTRACT

2 Loudspeakers, mastoid bone-drivers, hearing-aid receivers, hybrid cars, and more -
3 these “anti-reciprocal” systems are commonly found in our daily lives. However, the
4 depth of understanding about the systems has not been well addressed since McMil-
5 lan in 1946. The goal of this study is to guide an intuitive and clear understanding of
6 the systems, beginning from modeling one of the most popular hearing-aid receivers,
7 a balanced armature receiver (BAR).

8 Models for acoustic transducers are critical in many acoustic applications. This
9 study analyzes a widely used commercial hearing-aid receiver (part number: ED27045),
10 manufactured by Knowles Electronics, Inc. Electromagnetic transducer modeling
11 must consider two key elements: a *semi-inductor* and a *gyrator*. The semi-inductor
12 accounts for electromagnetic eddy-currents, the “skin effect” of a conductor (Van-
13 derkooy, 1989), while the gyrator (McMillan, 1946; Tellegen, 1948) accounts for the
14 anti-reciprocity characteristic [Lenz’s law(Hunt, 1954, p. 113)]. Aside from Hunt
15 (1954), to our knowledge, no publications have included the gyrator element in their
16 electromagnetic transducer models. The most prevalent method of transducer mod-
17 eling evokes the *mobility method*, an ideal transformer alternative to a gyrator fol-
18 lowed by the dual of the mechanical circuit (Beranek, 1954). The mobility approach
19 (Firestone, 1938) greatly complicates the analysis. The present study proposes a
20 novel, simplified and rigorous receiver model. Hunt’s two-port parameters as well
21 as the electrical impedance $Z_e(s)$, acoustic impedance $Z_a(s)$ and electro-acoustic
22 transduction coefficient $T_a(s)$ are calculated using ABCD and impedance matrix
23 methods (Van Valkenburg, 1964). The model has been verified with electrical input
24 impedance, diaphragm velocity *in vacuo*, and output pressure measurements. This

25 receiver model is suitable for designing most electromagnetic transducers, and it can
26 ultimately improve the design of hearing-aid devices by providing a simplified yet
27 accurate, physically motivated analysis.

28 As a utilization of this model, we study the motional impedance (Z_{mot}) that was
29 introduced by Kennelly and Pierce (1912) and highlighted by many researchers early
30 in the 20th century (T.S.Littler, 1934; Fay and Hall, 1933; Hanna, 1925). Our goal for
31 this part of the study is to search for the theoretical explanation of the negative real
32 part (resistance) observed in Z_{mot} in an electro-mechanical system, as it breaks the
33 positive-real (PR) property of Brune's (1931) impedance, as well as the conservation
34 of energy law. Specifically, we specify conditions that cause negative resistance in the
35 motional impedance using simple electro-mechanical network models. Using Hunt's
36 two-port system parameters (a simplified version of an electro-acoustic system), Z_{mot}
37 is defined as $-\frac{T_{em}T_{me}}{Z_m}$, where the subscript m stands for "mechanic," T_{em} and T_{me}
38 are transfer impedances, and Z_m is the mechanical impedance of the system (Hunt,
39 1954). Based on the simplified electro-mechanical model simulation, we demonstrate
40 that $Z_{mot}(s)$ is a minimum-phase function, but does not have to be a positive-real
41 (PR) function. Any electro-mechanical network with shunt losses in the electrical
42 side (including a semi-inductor and a resistor) sees a negative real part in Z_{mot} which
43 may arise when there are frequency-dependent real parts. In conclusion, Z_{mot} is not
44 a PR impedance because of the phase lag.

45 Several significant topics will be discussed in addition to these two larger issues
46 (modeling the balanced armature receiver (BAR) and investigating Z_{mot}). We gen-
47 eralize the gyrator with the non-ideal gyrator, analogous to the ideal *vs.* non-ideal
48 transformer cases. This formula is reinterpreted via electromagnetic fundamentals.
49 This work helps to transparently explain the anti-reciprocal property embedded in a
50 gyrator. Explaining the "matrix composition method" is another contribution, which
51 is characterized by the Möbius transformation. This is a significant generalization
52 of the ABCD (transmission) matrix cascading method. Systems where the quasi-
53 static approximation fails will also be considered (i.e., derivation of KCL, KVL from
54 Maxwell's equations). This leads us to the definition of "wave impedance" which
55 is distinct from the traditional Brune impedance, discussed in modern network the-

Draft of November 2, 2014 at 17:33

56 ory Vanderkooy (1989). The Brune impedance is defined by a reflectance that is
57 minimum phase which is a significant limitation on this classical form of impedance
58 (Brune, 1931). The typical example of a non-Brune impedance is a transmission line.
59 This ‘non-Brune’ distinction is important and we believe it to be a novel topic of
60 research

Draft of November 2, 2014 at 17:33

61

62

To my parents, for their love and support.

Draft of November 2, 2014 at 17:33

ACKNOWLEDGMENTS

63 I cannot express enough thanks to my committee for their continued support and
64 encouragement: Prof. Jont Allen, my committee chair; Prof. Stephen Boppart;
65 Prof. Steven Franke and Prof. Michael Oelze. I offer my sincere appreciation for the
66 learning opportunities provided by my committee.

TABLE OF CONTENTS

67	LIST OF TABLES	ix
68	LIST OF FIGURES	x
69	CHAPTER 1 INTRODUCTION	1
70	1.1 Comparison of a telephone receiver and a moving-coil receiver	4
71	1.2 Goal of this study	7
72	1.3 Historical notes	12
73	CHAPTER 2 THEORETICAL METHODS	15
74	2.1 Two-port anti-reciprocal network with Hunt parameters	15
75	2.2 Network postulates	19
76	2.3 Generalization of the ABCD matrix using Möbius transformation	25
77	2.4 Motional Impedance (Z_{mot})	30
78	2.5 Hidden, quasi-static assumptions in classic circuit theories	42
79	CHAPTER 3 EXPERIMENTAL METHODS	69
80	3.1 Measurements for BAR modeling	69
81	3.2 Technical analysis of an OAE hearing measurement probe	75
82	3.3 A new probe design	84
83	CHAPTER 4 RESULTS	90
84	4.1 Hunt parameter calibration	90
85	4.2 Receiver model	92
86	4.3 Z_{mot} simulation of simplified electro-mechanic systems	99
87	4.4 Calibration results from both the modified and the manufactured	
88	probes	103
89	CHAPTER 5 CONCLUSIONS AND CONTRIBUTIONS	111

Draft of November 2, 2014 at 17:33

90	APPENDIX A	DEFINITION OF ENERGY CONSERVATION, START-	
91		ING FROM MODALITY	113
92	APPENDIX B	TELLEGEN'S THEOREM & KCL/KVL	116
93	APPENDIX C	SENSITIVITY ANALYSIS OF ED SERIES SPICE MODEL	122
94	APPENDIX D	Z_{MOT} : SPATIAL RELATIONSHIPS BETWEEN Φ , I, B,	
95		F, AND I	125
96	APPENDIX E	CALCULATION OF HUNT PARAMETERS	129
97	APPENDIX F	HYSTERESIS LOOP FOR A FERROMAGNETIC MA-	
98		TERIAL: \mathbf{B} VS. \mathbf{H}	131
99	REFERENCES	135

LIST OF TABLES

100	2.1	Example of two-port networks	21
101	4.1	Specific parameters that are used for the suggested model (Knowles BAR	
102		ED7045). c is the speed of sound in the air (334.8[m/s]), $j\omega/c$, z_0 , and l_t are	
103		the propagation function, specific characteristic resistance and length of the	
104		transmission line, respectively. GYR and TRF stand for the gyrator and the	
105		transformer. All model parameters were found by minimizing the RMS error	
106		between the model and electrical input impedance measurements of the receiver. .	94
107	A.1	Example of modalities and their conjugate variables. Upper case symbols are	
108		used for the frequency domain variables. The time domain representation of	
109		each variable can be described using the lower case of the same character,	
110		except in the EM case. But general Electro-Magnetic (EM) theories consider	
111		the time domain and its traditional notation uses capital letter for the time	
112		domain analysis. Note that in the electric field, $\mathbf{E} = -\nabla\Phi$, where Φ is scalar	
113		potential, the voltage.	113
114	A.2	Power and impedance definitions for each modalities in table A.1. In general,	
115		power concept (a product of conjugate variables) can be used in time domain,	
116		however the impedance (a ratio) is thought of in the frequency domain. As-	
117		suming causality, the Laplace transformation can be applied to convert the	
118		impedance to the time domain.	114

LIST OF FIGURES

119	1.1	The Balanced Armature Receiver (BAR) circuit as a model (Kim and Allen, 2013) as defined by a transmission (ABCD) matrix representation. The chained properties of an ABCD matrix are followed by the Möbius transformation. This factored nature of the ABCD matrix is discussed in detail in section 2.3. The electrical and mechanical circuits are coupled by a gyrator (GYR, realizing an anti-reciprocal network), while a transformer (TRF) is used for the coupling of the mechanical and acoustical circuits. The $K1$ is a semi-inductor representing electro-magnetic diffusion due to the skin effect. The $TXLine$ stands for a transmission line to involve a pure delay in the system, violating a quasi-static assumption in this electro-acoustic system. Using this non-quasi-static element is the proper way to model this system. In this model, the input and output potentials for each section are specified as voltage (Φ), force (F), and pressure (P). Current (I), particle velocity (U), and volume velocity (V) represent the flow for each of the three physical sections.	3
120			
121			
122			
123			
124			
125			
126			
127			
128			
129			
130			
131			
132			
133	1.2	(a): The picture of the BAR at the “Cut Z” line in panel (b). There is space for the armature to vibrate vertically between the magnets. Magnets are sandwiching the armature (the blue, dotted line). A laminated iron case surrounds the magnets and the armature. (b): A schematic of a BAR. An electrical current in the coil comes from the transducer’s electrical input terminals; the current induces a Lorentz force on the armature via the induced magnetic field (modified from Knowles documentation of the ED receiver series). Note that the port location of the ED7045 receiver is rotated 90° to the longer side.	4
134			
135			
136			
137			
138			
139			
140			
141	1.3	A picture of the ED7045, a BAR used in this study. The black line shows the depth of the transducer, 2.9 [mm].	6
142			
143	1.4	Sectional view of ring armature receivers (three types) adapted from Mott and Miner (1951), Fig. 2 in the original manuscript.	7
144			

145	1.5	The cross-section view of the moving-coil loudspeaker. Up-and-down motion	
146		of the voice coil around a permanent magnet creates a time-varying magnetic	
147		field. As a voice coil moves around the pole piece, it becomes an “electro-	
148		magnet.” The image is from http://i1-news.softpedia-static.com	8
149	1.6	Overview of this study via the BAR model. All concepts discussed in this	
150		thesis can be tied together to understand the BAR transducer. The important	
151		concepts are highlighted using Roman characters. Note that the <i>quasistatic</i>	
152		(QS) components are marked as dark blue and the non-QS components are in	
153		light blue.	9
154	1.7	(a): A. E. Kennelly (1861, India - 1939, U.S.A.) (b): F. V. Hunt (1905 - 1972,	
155		U.S.A.)	13
156	2.1	A schematic representation of an electro-mechanic system using Hunt param-	
157		eters and Möbius composition of the ABCD matrix (Kim and Allen, 2013).	
158		Note how the ABCD matrix method “factors” the model into 2×2 matrix.	
159		This allows one to separate the modeling from the algebra.	16
160	2.2	Möbius strip sculpture at the Beckman Institute, UIUC. Möbius transfor-	
161		mation matrix is presented underneath of the sculpture.	26
162	2.3	A series impedance (Z) representation with inputs (Φ_1, I_1) and	
163		outputs (Φ_2, I_2). Note that, in this figure, all currents are defined	
164		as going out of the network.	28
165	2.4	Inverted relationship between reflectance (Γ) and the wave impedance	
166		(Z) shown in Eq. 2.33 where the conversion is made from Z to Γ .	
167		When we convert from Γ to Z , the matrix’ diagonal elements are	
168		swapped compared to Eq. 2.33.	30
169	2.5	An example of the motional power diagram introduced by Kennelly and Nukiyama	
170		(1919). The x-axis and y-axis show resistive and reactive parts of the motional	
171		power respectively. When the resistance becomes negative (the left shaded part	
172		of the red line, O-O’, on the circle), power supplied from the electric part of	
173		the system no longer exists (It does not provide the mechanical power onto	
174		the diaphragm). Therefore (referencing at the electrical side) this part of the	
175		power is “active mechanical (motional) power”. All power in this region is	
176		consumed for hysteresis loss when the diaphragm is released (diaphragm is	
177		going back to its original position).	32

178	2.6	The calculated z_m (Eq. 2.36) graph by inverting Z_{mot} and then multiplying by the complex force factor A^2 (Eq. 2.36). Solid curve is obtained by connecting observation values at each frequency point. The dotted line represents the computed (theoretical) values Eq. 2.37. Note that this image is shown as Figure 9 in the original manuscript (Kennelly and Kurokawa, 1921).	34
179			
180			
181			
182			
183	2.7	The corresponding circuits for Fig. 2.8 (1) and (2), before (1) and after (2) mobility networking. Due to the gyrator, the mechanical components becomes dual when they are seen on the electrical side of the network. As investigated in Fig. 2.8, this makes the shape of the Z_{mot} circle.	36
184			
185			
186			
187	2.8	This figure explains the circular shape of Z_{mot} where the motion of the mechanical behavior (i.e., damping (loss), mass, and stiffness) projected to the electrical side defines Z_{mot} . When the mechanical behavior are seen on the electrical input side, due to the gyrator, the series mechanical network becomes a dual network based on the mobility analogy. The blue line shows input impedance based on the series relationship ((1) in Fig. 2.7 without considering the gyrator) while the red line represents the dual. The upper-left, lower-left plots show magnitude and phase of impedance and the right plot (polar plot) shows real and imaginary parts of the impedance. The red circle on the polar plot justifies the circular shape of Z_{mot} . F_c stands for the transition frequency between C (low frequency) and L (high frequency) for both original and dual of magnitude and phase plots. In polar plots, if $\Im Z \rightarrow +\infty$, Z is dominated by L and in case of $\Im Z \rightarrow -\infty$, Z depends on C . Note that this figure only discusses the shape of typical Z_{mot} , not its negative real parts. For simplification, values for L , R , and C are '1' in this simulation.	37
188			
189			
190			
191			
192			
193			
194			
195			
196			
197			
198			
199			
200			
201			
202	2.9	Demonstration of Z_{mot} 's negative real part using a simple circuit example	41
203	2.10	Electrical lumped circuit representations of the cochlea (adapted from Lynch et al. (1982)). (a) and (b) employ the quasi-static assumption where (b) is a simplified version of (a). A transmission line (length l and characteristic resistance r_0) is used in (c), which introduces the pure delay $\tau = l/c$ forcing Z_L to be non-quasi-static.	43
204			
205			
206			
207			
208	2.11	Input impedance simulation based on Fig.2.10. Values for the simulation are followed: Cochlea resistance $R_c = 1.2e6[dyne - s/cm^5]$, stiffness of the annular ligament $C_{al} = 0.37e - 9[cm^5/dyne]$, air density $\rho = 1.14[kg/m^3]$, speed of sound in room temperature $c = 340[m/s]$, area of ear canal $A = r^2 * \pi[m^2]$ with $r = 0.5[cm]$, and length of ear canal $L = 0.7[cm]$	44
209			
210			
211			
212			

213 2.12 An infinitesimal unit of a transmission line (in the limit as $\Delta \rightarrow 0$) having pri-
 214 primary line constants, L (series inductance or mass per unit length [H/m]), R
 215 (series resistance per unit length [Ω/m]), C (shunt capacitance or compliance
 216 per unit length [F/m]), and G (shunt conductance per unit length [S/m]).
 217 The upper figure represents a loss case while the lower figure is lossless case.
 218 Transmission segments are mirrored (shown in blue) to represent reversible
 219 transmission lines. By taking $\Delta \rightarrow \infty$, this goes from a QS to a true trans-
 220 mission line having a delay. 48

221 2.13 Simulation of transmission line input impedance from Eq. 2.59 and 2.63. Val-
 222 ues for this specific example are $L = 1e - 5$ [H/m], $C = 1e - 4$ [F/m]. 50

223 2.14 A simple experiment to display Lenz’s law. The induced flux, Ψ (or emf), gives
 224 rise to a current I whose direction opposes to the direction of the Ψ . Moving
 225 the north pole of a magnet towards the coil causes positive current I . The mo-
 226 tion that the magnet is “pushed into the coil” reveals the negative direction of
 227 the Ψ or emf. If the magnet is “pulled out from the coil” (positive Ψ or emf),
 228 the direction (sign) of the current is reversed. When there is no motion of the
 229 magnet, then the current does not flow. The image is retrieved and modified
 230 from https://bearspace.baylor.edu/Walter_Wilcox/www/courses/phy2435/chap29xxa.pdf
 231 59

232 2.15 Eddy current with a falling magnet inside a conductor (falling from south to
 233 north). When the magnetic field is changed in time in a closed electric field (a
 234 falling magnet in a copper pipe), an “eddy current” is induced on the copper
 235 pipe (red). The direction of the eddy current is perpendicular to the primary
 236 magnetic field (green, it is static when velocity is zero. Also the field is not a
 237 function of θ) followed by right hand rule (thumb-force, 1st finger-electric field,
 238 2nd finger - magnetic field). The eddy current creates the secondary magnetic
 239 loop (blue) whose force is opposite to the force of gravity. At the terminal
 240 velocity, the force of gravity equals the Lenz reactive force. 63

241 2.16 Semi-inductor approximate lumped circuit model via a truncated ladder net-
 242 work. Circuit diagram of the electrical impedance of the semi-inductor model
 243 is defined by the ladder network resistance factor R and shunt inductance fac-
 244 tor L (Weece and Allen, 2010). This circuit follows from a continued fraction
 245 expansion of \sqrt{s} 64

246 3.1 Experimental setup for the electrical input impedance measurement. Where
 247 Φ is the voltage, I is the current, and R is a reference resistance. We varied
 248 the experimental acoustical load impedance by changing Length of a blocked
 249 tube and measured the voltage at two points (A, B) denoted as Φ_A and Φ_B 69

250 3.2 Measured Z_{in} of ED7045 with the eight acoustical load conditions, blocked
251 cavities. Different lengths of the tubes are used to vary the acoustical load.
252 Three different known electrical input impedances are selected to calculate
253 Hunt parameters. 71

254 3.3 This plot shows the electrical input impedance of the ED7045 receiver in
255 blocked/unblocked port, and vacuum conditions. In the unblocked receiver
256 port case, the FR moves to lower frequency (2.5[kHz]) compared to the blocked
257 case, 3.8[kHz]. The FR in vacuum is at the lowest frequency, 2.3[kHz]. The
258 frequency locations of SR for each curve are indicated by arrows in the figures.
259 (a) Magnitude and phase of the electrical input impedance, (b) Polar plot of
260 the electrical input impedance ($\Re Z_{in}$ vs $\Im Z_{in}$). Note that above 5[kHz], the
261 phase of Z_{in} in (a) approaches $\approx .4\pi$ [rad]. Thus in (b), the curves merge at a
262 fixed angle as $\omega \rightarrow \infty$ 72

263 3.4 Experiment setup for the laser mechanical velocity measurement in vacuum.
264 The circled ‘L’ means an input from the laser system. The laser beam is
265 focusing on the plastic window of the transducer to measure the diaphragm
266 velocity (U). 73

267 3.5 Experiment setup for pressure measurement. The circled ‘M’ means an in-
268 put from the ER7C microphone. The ER7C microphone system is factory-
269 calibrated as 50[mV/Pa]. It consists of an amplifier box, a microphone, and
270 a probe tube. Note that the ER7C microphone and the ED7045 receiver is
271 connected carefully to minimize the space between the probe tube’s end and
272 the receiver’s port. 74

273 3.6 (a)A yellow foam tip (14A) is attached to the probe’s head. Note that numbers
274 on the box indicates the system’s serial number. (b)Schematic representation
275 of the ER10C probe. Two speakers and microphones are separated internally
276 across the PCB circuit, microphones are placed ahead of the receivers (speak-
277 ers). 76

278 3.7 Disassembled ER10C. Two parts are inside; (a)microphone holder and (b)circuit
279 board parts. Note that lots of care were needed to see the part (a) as it was
280 permanently attached to the probe’s case. 77

281 3.8 Details of the brass chamber in Fig. 3.7. The recent design of ER10C, an
282 aluminum material chamber is used maintaining the same shape. 77

283 3.9 ER10C circuit board details. A diode package and a capacitor are shown
284 under the wire soldering ends. Only one diode is used to set up to be reverse
285 biased, in series with a capacitor between the microphone’s “output” and the
286 “ground” terminals. It is a traditional approach in the hearing aid industry,
287 to protect the input from spark discharge. 78

288	3.10	ER10C circuit board (Fig. 3.7(b)) and connection details with microphone holder part in Fig. 3.7(a). Note that the speakers are connected to the curved steel tubes via red rubber tubes.	79
289			
290			
291	3.11	(a) Brass material for the middle tube holder part (the brass holder). RTV silicon is used to block the holder's side hole. Calibration passes up to 9-10kHz (ER10C with 3 digits serial number) (b) Aluminum material for the chamber. RTV silicon is not used to block the holder's side hole, but some of black material seals the side hole. Calibration passes up to 6kHz (ER10C with 4 digits serial number). (c) Aluminum chamber is used. None of material seals the holder's side hole, a portion of the hole could be sealed randomly. Calibration totally fails or sometimes it passes but is unstable usually above 4kHz (ER10C with 4 digits serial number). Also (based on the manufacturer), the type of wire used in ER10C has been changed.	81
292			
293			
294			
295			
296			
297			
298			
299			
300			
301	3.12	Original ER10C crosstalk (blue) with ER7C response (red): The sound (0.6V chirp, zero to peak, not RMS) was generated by one of the internal ER10C speakers. The right (blue, ch2) shows the blocked ER10C (serial: 2928) microphone response, and the left (red, ch2) shows the E7C microphone response as a reference of the sound level. Note that we used a small cut syringe with a tiny volume to connect both ER7C microphone and ER10C probe. We blocked the microphone hole on the attached ER10C foam tip for decoupling the microphone path from the sound in the cavity generated by the internal ER10C speaker. Physically and theoretically, internal ER10C's sound paths for the microphones and the receivers are separated. Therefore if the microphone hole is blocked, none of the acoustic signal can go thorough the microphone's diaphragm. any signal that is shown on the right side of this figure (blue) is internal crosstalk of the probe. We read that in high frequency it is approximately increasing proportion to 20dB/octave (capacitive coupling), based on this observation, we hypothesize the source of this crosstalk is in wire of ER10C. This was the motivation of modifying ER10C, including the preamp on the ER10Cs head. Note that this measurement was made on May 14 2014 at Mimosa Acoustics by NK using Stimresp software (Mimosa Acoustics)	82
302			
303			
304			
305			
306			
307			
308			
309			
310			
311			
312			
313			
314			
315			
316			
317			
318			
319	3.13	ER10C crosstalk (blue) after the modification: Crosstalk measurement after the modification, the rising crosstalk behavior in high frequency is apparently reduced. The modified ER10C is inserted in a short cavity with blocked microphone. The probe is connected to the specially modified APU for the modified ER10C.	83
320			
321			
322			
323			
324	3.14	Basic acoustic testing setup	87

325	4.1	Calculated Hunt parameters (Z_e , Z_a , and T_a) of the ED7045. Three	
326		measurements of Z_{in} with acoustic loads (indicated by number as	
327		shown in the legend) are required to find one set of the three Hunt	
328		parameters. The length of each numbered tube is described in	
329		Fig. 3.2. Z_{in} which is measured by blocking the receiver's port	
330		($V = 0$) is plotted with Z_e (green line).	91
331	4.2	Comparison of Hunt parameters (Z_e (red), T_a (black), and Z_a (blue)) from	
332		the model (a) and the measurements (b). Any significant differences between	
333		the model and the data occur above 6[kHz]. All parameters are normalized to	
334		their 1[kHz] values.	95
335	4.3	Comparison the suggested model of Fig. 1.1 and real electrical	
336		input impedance measurement of a balanced armature hearing-	
337		aid receiver (Knowles, ED7045). Blue and red colors represent	
338		vacuum and non-vacuum (ambient) conditions respectively. And	
339		the dashed lines represent the experimental result, whereas the	
340		single lines show the model results. For the vacuum experiment,	
341		the static pressure is less than 0.003[atm]. The left panel shows	
342		the magnitude and the phase of each condition while the real and	
343		imaginary parts of the same data are plotted in the right panel.	
344		Up to 23[kHz], the experimental data is in good agreement with	
345		the modeling result (The sampling rate is 48[kHz], therefore the	
346		maximum measured frequency is 24[kHz]). In the polar plot, above	
347		8[kHz], the impedance behaves as \sqrt{s}	96
348	4.4	Comparison of the diaphragm (mechanical) velocity between the	
349		transducer model and the laser measurement in vacuum, the pres-	
350		sure P is zero. For the model simulation, the acoustical part in	
351		Fig. 1.1 is not included. The laser measurement was performed af-	
352		ter pumping out the air in the receiver. All values are normalized	
353		to one at 1[kHz].	98
354	4.5	Comparison of Thevenin pressure (per voltage) data from various	
355		sources. There are 6 different lines, the first 4 lines are calculated	
356		from the electrical experiments (Hunt parameters), and the orange	
357		colored line is estimated from the model. The last pressure data	
358		(in light-green) are taken from the pressure measurement and are	
359		divided by the electrical input voltage of the receiver. All data	
360		assume the blocked condition, $V=0$ (see text). Every value is nor-	
361		malized to one at 1[kHz].	98

362	4.6	The top left circuit: A simple anti-reciprocal network with a semi-inductor presence. The top right circuit: The dual representation of the left circuit (equivalent) by applying mobility analogy beyond the gyrator. Z_{mot} is reconsidered based on Eq. 2.43. The frequency dependent real parts (shunt loss) of the semi-inductor in $Z_{in} _{F=0}$ (short) experience positive phase shift when the open condition impedance ($Z_{in} _{U=0}$) is subtracted from it.	100
363			
364			
365			
366			
367			
368	4.7	Computed Hunt parameters based on a simple electro-mechanic network shown in Fig. 4.6 (Eq. 4.6-4.9). All parameters K, L, G, and m are set to be 1 for a simple computation.	103
369			
370			
371	4.8	Computed motional impedance(Eq. 4.10), and input impedances with both open(Eq. 4.6) and short circuit conditions(Eq. 4.10+Eq. 4.6) based on a simple electro-mechanic network shown in Fig. 4.6.	104
372			
373			
374	4.9	Real and imaginary parts of a simple electro-mechanic network shown in Fig. 4.6. The the marker's size indicates increment in frequency. Between 8 th and 9 th frequency points, the real parts of Z_{mot} goes to negative.	105
375			
376			
377	4.10	(Left figure) Source parameter calibration result from the modified ER10C to diminish the crosstalk effect. The probe can be calibrated above 10 kHz. Based on this result, we concluded that the crosstalk was interfering with the calibration procedure. (Middle figure) MA16 calibration result. This result demonstrates that we made our own system which can pass the 4C calibration above 10 kHz as well, for the first time. (Right figure) MA17 simulator calibration result. To overcome some drawbacks of the MA16, especially the size, we have proposed a new probe design, namely MA17. Before manufacturing the probe, we simulated acoustics of the probe's structure to support the basic idea of the suggested design.	106
378			
379			
380			
381			
382			
383			
384			
385			
386			
387	4.11	The purpose of this modification is to reduce crosstalk due to the long wire of ER10C probe. This reveals that small changes in the wire may lead significant property changes of the probe. The key idea is to amplify the microphone signal before it passes through the long wire. Near the probe's head we placed amplifier as shown in this picture.	107
388			
389			
390			
391			
392	4.12	This figure shows improvement caused by the ER10C modification before and after. It gives a clear evidence that crosstalk was the source of the problem in the ER10C which has kept users from calibrating the probe above 6 kHz. Now the system can pass 4C calibration above 10 kHz. Note that all data and results are from preliminary tests. Some of the details are Mimoso Acoustics confidential information which will not be addressed here.	108
393			
394			
395			
396			
397			

398	4.13	(a) MA16 is used with the modified APU (right side white box) is used for audio processing. (b) Two speakers (lower two sided) and one microphone (in the middle) are used. The red parts represent acoustic resistors.	109
401	4.14	The MA17 simulator was made to simulate proposed design of the MA17. Due to the lined up transducers, the size of the probe can be greatly minimized.	110
403	B.1	A simple anti-reciprocal network without a semi-inductor	118
404	B.2	Computed Hunt parameters based on a simple electro-mechanic network shown in Fig. B.1 (Eq. B.13-B.16). All parameters L1, L2, G, and m are set to be 1 for a simple computation.	120
407	B.3	Computed motional impedance(Eq. B.18), input impedances with both open(Eq. B.13) and short circuit conditions(Eq. B.18+Eq. B.13) based on a simple electro-mechanic network shown in Fig. B.1.	121
410	C.1	Knowles PSpice model of the ED receiver: The refined PSpice circuit model of ED receiver by reducing ‘small effect’ components which are marked in red. R1, RK512, RK513, and RK514 resistors were added to maintain DC stability of PSpice. Note that the Spice model represents all ED series receivers, including ED7045, ED1744, ED1913, and etc., such that specific parameter value of components vary for each specific receiver.	123
416	C.2	The simulated electrical input impedance’ magnitude, $ Z_{in} $, in dB scale. (a) shows the sensitivity analysis using Matlab based on Fig. C.1 where $s = j\omega$. The ‘A. original model’ and the ‘B. Small effect’ conditions are marked with a thick green line and a dashed red line, respectively. The ‘B. Small effect’ is the simulated result when all ‘small effect’ components in Fig. C.1 are removed in the original PSpice circuit. It represents summed-up sensitivities of ‘small effect’ components in Fig. C.1. (b) represents the sensitivity of the CMAG component only. This analysis is provided by Knowles Electronics using their PSpice library for the CMAG component (This result is plotted in Matlab but the data is acquired via PSpice simulation). Similar to the (a), ‘A. Original model’ shows the PSpice simulation including all components in Fig. C.1, whereas ‘B. Without semi-capacitor’ simulates the original PSpice circuit only without the semi-capacitor. For both simulations (a) and (b), the difference between the original response and the reduced response is calculated based on Eq. C.1 shown as black dashed line.	124
431	D.1	Electro-mechanic system’s variables in spatial domain by BeranekBeranek (1954)	126
432	D.2	Equivalent with Fig. D.1. The choice of each geometry is adapted from Hunt’s book Hunt (1954)	126
433			

- 434 F.1 Simplified magnetization process. Undemagnetized ferromagnetic material's
435 net $\mathbf{B}=0$. When ferromagnetic material is exposure to the magnetic field \mathbf{H} ,
436 the net magnetic intensity (\mathbf{B}) of the material is not longer 0. It becomes
437 magnetized with the same direction of the applied \mathbf{H} . Note that details of
438 this process (i.e., breaking the domain walls) needs heavy duty knowledge in
439 quantum mechanic which is not relevant to discuss in our study Ulaby (2007). . . 132
- 440 F.2 A typical hysteresis curve in ferromagnetic materials. The x-axis represents
441 magnetic field \mathbf{H} that is applied to the material, and the y-axis shows the
442 magnetic intensity (\mathbf{B}) of the material. On the loop, there are five marked
443 points, O , A , B_r , C , D , and two colored points on the x-axis blue(1) and
444 red(2). The blue and red points are two saturation limits of \mathbf{H} in each direction
445 (\pm). The material's initial position starts from O , as strength of the \mathbf{H} is
446 increased to its positive maximum saturation point (1), the material's \mathbf{B} is
447 also increased to reach the point A . Then the \mathbf{H} starts to decrease to be zero,
448 but the material's magnetic property still remains at B_r . This point is named
449 as a residual magnetic point. At this point, the ferromagnetic material has
450 magnetic characteristic without applied magnetic field, therefore it becomes
451 permanent magnet. As \mathbf{H} is increased its amplitude to the opposite direction
452 (the direction of \mathbf{H} is still backward), \mathbf{B} becomes zero at C . The descending
453 from B_r to C is called demagnetization, permanent magnet loses its magnetic
454 characteristic within this process. The line goes down to D , when the \mathbf{H}
455 reaches its (negative) maximum saturation limits at 2 (red). Finally, \mathbf{H} is
456 reversing its direction (i.e., current with sine wave, passing through $f = \pi/2$)
457 and goes through the portion of the hysteresis loop from D to A and repeating
458 $A \rightarrow B_r \rightarrow C \rightarrow D...$ until \mathbf{H} becomes zero 134

CHAPTER 1

INTRODUCTION

459 A typical hearing-aid consists of three parts: a microphone (picks up sound), an
460 amplifier (transforms sound into different frequencies, filters noise, and selectively
461 amplifies each frequency region based on the difference in individual hearing loss¹
462 via multi-band compression), and a receiver (sends the processed signal from the
463 amplifier into the ear). A proper understanding of each component in the hearing-
464 aid can facilitate better and clearer sound quality

465 The current study starts by modeling one of the most important and complex
466 hearing-aid components, the balanced armature receiver (BAR). The BAR is an
467 electromagnetic loudspeaker that converts an electrical signal (current) into acousti-
468 cal pressure (or force, in the case of an electro-mechanical system). It is referred to as
469 an electromagnetic transducer because small magnets are involved. These miniature
470 loudspeakers are widely used and remain one of the most expensive components of
471 modern hearing-aids; they are also the most poorly understood. Therefore, a detailed
472 understanding of these transducers is critical to optimize their design.

473 In the electromagnetic transducer models of both Weece and Allen (2010) and
474 Thorborg et al. (2007), an ideal transformer was used to convert electrical current
475 into mechanical force (or acoustical pressure) in the transducer. As described in Be-
476 ranek (1954), the mobility analogy (Firestone, 1938), along with an ideal transformer,
477 is a valid way to represent electrical-to-mechanical transduction when modeling anti-

¹The percentage of people in the United States who are suffering from Hearing Loss 12.7% in their age of 12 years and older Lin et al. (2011). Also two-thirds of Americans older than 70 years have experienced mild to severe HL. The importance of designing Hearing-aid properly, therefore, is come to the fore in contemporary society along with the Population ageing Population ageing is a shift in the distribution of a country's population towards older ages (http://en.wikipedia.org/wiki/Population_ageing)

478 reciprocal electromagnetic transducers. The mobility method, which requires using
479 the dual network (swapping current and voltage), fails to provide an intuitive expla-
480 nation of the anti-reciprocity characteristic of the electromagnetic transducer, which
481 follows from Maxwell-Faraday’s (1831) law and Lenz’s (1834) law. The impedance
482 and mobility methods are mathematically equivalent, meaning one can use either
483 method to describe the system. However, including the gyrator in transducer models
484 allows for a logical, intuitive, and accurate interpretation of the physical properties.
485 For example, when using a gyrator to represent the mechanical and electrical trans-
486 formation, stiffness can be represented as a capacitor and mass as an inductor in the
487 series combination. Given the mobility (dual) network, it is necessary to swap the
488 inductor and capacitor, placing them in parallel combination. Thus, we feel that the
489 dual network combined with the mobility method is less intuitive and more difficult
490 to quantify when describing the system.

491 Kim and Allen (2013) suggested a two-port network model of the BAR (Fig. 1.1)
492 having a *semi-inductor*, a *gyrator* (two poorly understood elements of special interest
493 in the electromagnetic transducer), and a *pure delay*. Our network has two wave
494 speeds, the speed of light (3×10^8 [m/s]) and the speed of sound (345 [m/s]). Both
495 speeds are important for proper modeling. The acoustic delay becomes significant
496 due to the relatively slow speed of sound. This pure delay is represented using a
497 transmission line in the model. With a *quasi-static* (QS) assumption, there is no
498 pure delay in the system.

499 The semi-inductor component is necessary to account for eddy-current diffusion
500 (the “skin effect”). In 1989, Vanderkooy demonstrated that, at high frequencies, the
501 behavior of the impedance of a loudspeaker changes from the behavior of a normal
502 inductor to that of a semi-inductor because of the eddy-current diffusing into the
503 iron pole structure of the loudspeaker (i.e., the skin effect). Using a Bessel function
504 ratio, Warren and LoPresti (2006) represented Vanderkooy’s semi-inductor model
505 as a “diffusion ladder network,” a continued fraction expansion or a combination
506 of resistors and inductors. In 2010, Weece and Allen used this representation in a
507 bone-driver model. After demagnetizing the bone-driver, they established the \sqrt{s}
508 behavior and determined the ladder network elements from the measured electrical

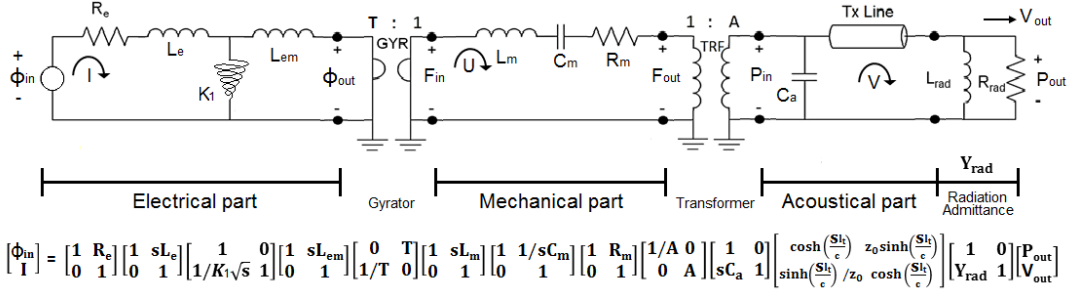


Figure 1.1: The Balanced Armature Receiver (BAR) circuit as a model (Kim and Allen, 2013) as defined by a transmission (ABCD) matrix representation. The chained properties of an ABCD matrix are followed by the Möbius transformation. This factored nature of the ABCD matrix is discussed in detail in section 2.3. The electrical and mechanical circuits are coupled by a gyrator (GYR, realizing an anti-reciprocal network), while a transformer (TRF) is used for the coupling of the mechanical and acoustical circuits. The K_1 is a semi-inductor representing electro-magnetic diffusion due to the skin effect. The $TxLine$ stands for a transmission line to involve a pure delay in the system, violating a quasi-static assumption in this electro-acoustic system. Using this non-quasi-static element is the proper way to model this system. In this model, the input and output potentials for each section are specified as voltage (Φ), force (F), and pressure (P). Current (I), particle velocity (U), and volume velocity (V) represent the flow for each of the three physical sections.

509 impedance of the transducer. Thorborg et al. (2007) also introduced a loudspeaker
 510 model with lumped circuit elements, including a semi-inductor.

511 In 1946, McMillan introduced the anti-reciprocal component as a network element.
 512 Two years later, Tellegen (1948) coined the term gyrator and categorized it as a fifth
 513 network element, along with the capacitor, resistor, inductor, and ideal transformer.
 514 Other than Hunt's 1954 publication, we remain unaware of any publication which
 515 implements anti-reciprocity in its electromagnetic transducer model using a gyrator.

516 Leading to their new circuit model of the BAR (Fig. 1.1), Kim and Allen (2013)
 517 measured the electrical input impedance, solving for the Hunt parameters (1954)²
 518 of the receiver. An intuitive design of an electromagnetic transducer was developed
 519 by using the gyrator and the asymptotic property as $\omega \rightarrow \infty$ (Vanderkooy, 1989)
 520 was properly described by using a parallel relationship between a semi-inductor and
 521 a normal inductor (electrical part in Fig. 1.1). Approximations for two extreme

²The electrical impedance Z_e , the mechanical impedance Z_m , and electro-mechanic transduction coefficients T_{em} , T_{me} . More detail of the Hunt parameters is discussed in section 2.1.

522 frequency limits of the input impedance ($Z_{in} = \sqrt{s}||s$) are defined as follows:

$$Z_{in}(s) = \frac{1}{\frac{1}{\sqrt{s}} + \frac{1}{s}} \approx \begin{cases} \frac{1}{\frac{1}{\sqrt{s}} + \frac{1}{s}} \approx \sqrt{s}, & s \rightarrow \infty \\ \frac{1}{\frac{1}{\sqrt{s}} + \frac{1}{s}} \approx s, & s \rightarrow 0 \end{cases} \quad (1.1)$$

523 where s is the Laplace frequency ($j\omega$). This model is presented in Fig. 1.1, and the modeled BAR³ and its internal structure are shown in Fig. 1.2.

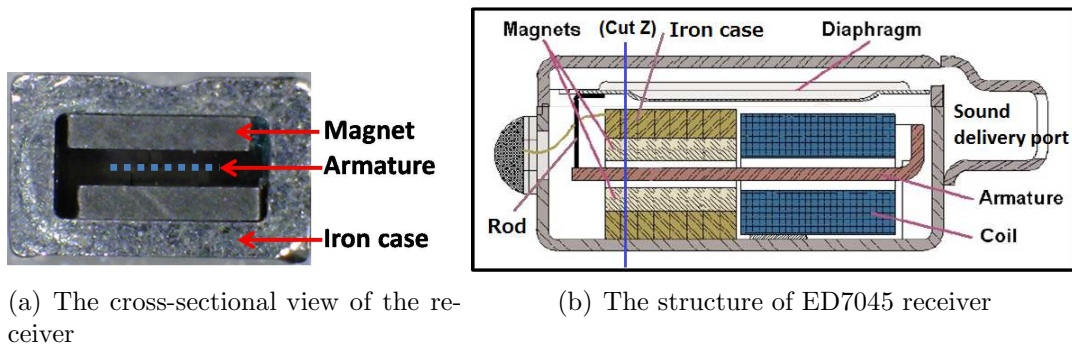


Figure 1.2: (a): The picture of the BAR at the “Cut Z” line in panel (b). There is space for the armature to vibrate vertically between the magnets. Magnets are sandwiching the armature (the blue, dotted line). A laminated iron case surrounds the magnets and the armature. (b): A schematic of a BAR. An electrical current in the coil comes from the transducer’s electrical input terminals; the current induces a Lorentz force on the armature via the induced magnetic field (modified from Knowles documentation of the ED receiver series). Note that the port location of the ED7045 receiver is rotated 90° to the longer side.

524

525 1.1 Comparison of a telephone receiver and a moving-coil 526 receiver

527 The oldest telephone receiver is the BAR type, and it is still in use. The original
528 technology goes back to the invention of the electric loudspeaker by A. G. Bell in

³ED7045 Knowles Electronics, Itasca, IL (<http://www.knowles.com>)

529 1876. Attraction and release of the armature are under the control of the current in
 530 the windings of an electromagnet (Hunt (1954) chapter 7, and Beranek and Mellow
 531 (2014)). As the electrical current goes into the electric terminal of the receiver, it
 532 generates an alternating current (AC) magnetic field surrounded by a coil. Due to
 533 the polarity between the permanent magnet and the generated magnetic field, an
 534 armature, which sits within the core of the coil and the magnet, feels a force. The
 535 very basic principles for explaining this movement are Hooke’s law (F_{hook}) and the
 536 magnetic force due to a current \mathbf{I} (\mathbf{F}_{mag})⁴

$$F_{hook} = k\xi, \quad (1.3)$$

537 where ξ is the displacement, and k is a constant characterizing stiffness of spring (or
 538 armature in our case), and

$$\mathbf{F}_{mag} = \mathbf{I} \times \mathbf{B}_0, \quad (1.4)$$

539 where \mathbf{I} is the current and \mathbf{B}_0 is the static magnetic field.

540 As shown in Fig. 1.2, since a diaphragm is connected to the end of the armature,
 541 when the armature moves, so does the diaphragm. The sound wave is propagated out
 542 of the sound delivery port. A large number of coil turns is required since the generated
 543 magnetic field (from the coil, time-varying magnetic field) should be compatible with
 544 the static direct current (DC) magnetic field (permanent magnet) to balance the
 545 mutual magnetic force. The size, weight, and sensitivity of this type can be greatly
 546 improved by using a light (low-mass) pole piece (i.e., armature) with small permanent

⁴A new theory about operation of the BAR was introduced by Jensen et al. (2011). This paper derives a non-linear time-domain force for the BAR-type receiver. Based on their theory, the input force of the moving-armature transducer system employs “the tractive force,” which attempts to minimize the air gap between the armature and the magnet. According to this theory

$$F_{bar} = \frac{\mathbf{S}_a \mathbf{B}^2}{2\mu_0} = \frac{\Psi_0^2}{2\mu_0 \mathbf{S}_a}, \quad (1.2)$$

where \mathbf{B} [Wb/m²] is the magnetic field across the air gap, S_a [m²] is the transverse area of the armature with the permanent magnet, μ_0 is the permeability in free space ($4\pi 10^{-7}$ [H/m]), and $\Psi_0 (= \mathbf{B}_0 S_a)$ [Wb] is the total magnetic flux in the air gap. To justify this theory, one must construct a relationship between F_{bar} in Eq. 1.2 and current similar to the relationship shown in Eq. 1.4 due to the gyrator nature in electro-magnetic system.

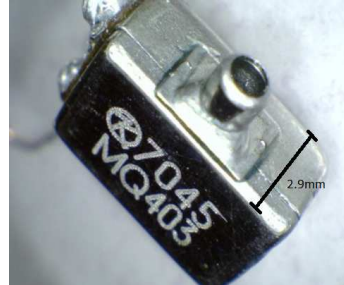


Figure 1.3: A picture of the ED7045, a BAR used in this study. The black line shows the depth of the transducer, 2.9 [mm].

547 magnets. This is the main reason for using this type of transducer in hearing-aid
548 products.

549 Knowles Electronics⁵ ED series receivers shown in Fig. 1.2(a) and Fig. 1.3, includ-
550 ing the ED7045 and ED1913, are BARs, used in all hearing-aids. The ED receiver
551 is 6.32 x 4.31 x 2.9[mm] in size. These receivers consist of a coil, an armature, two
552 magnets, and a diaphragm. Unlike the alternative moving-coil drivers, the coil of the
553 BAR has a fixed position, (Jensen et al., 2011), thereby reducing the internal mass
554 and providing more space for a much longer coil. As a result of the lower mass, the
555 BAR frequency response is higher, and due to the greater coil length, the sensitivity
556 is greater.

557 The armature used for the ED7045 is an E-shaped metal reed (Bauer, 1953),
558 whereas a U-shaped armature was widely used for early telephone instruments (Mott
559 and Miner, 1951). Both shapes have advantages and disadvantages. For example,
560 the U-shaped armature has better acoustic performance (i.e., wide-band frequency
561 response) while the E-shaped armature lowers the vibration of the body more effec-
562 tively. The armature is placed through the center of the coil and in between two
563 magnets, without touching them. The movement of the armature is directly con-
564 nected to the diaphragm through a thin rod (Fig. 1.2 (B)). Figure 1.4 shows the
565 types of ring armature receivers adapted from Mott and Miner (1951).

566 The other popular type of speaker is the moving-coil, or dynamic, speaker proposed
567 by Oliver Lodge in 1898 (Hunt, 1954) (Fig.1.5). In this type of speaker, a voice coil

⁵Knowles Electronics, Itasca, IL (<http://www.knowles.com>)

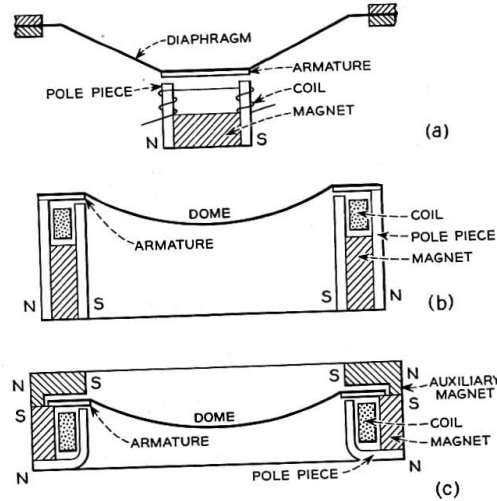


Fig. 2—(a) Early composite diaphragm receiver.
(b) Simple ring armature receiver.
(c) Ring armature receiver with auxiliary magnet.

Figure 1.4: Sectional view of ring armature receivers (three types) adapted from Mott and Miner (1951), Fig. 2 in the original manuscript.

568 surrounds a magnet and the coil is attached to a diaphragm (or sound cone). When
569 there is input through the coil, the coil is forced to move (up and down), as described
570 by Faraday's law. The coil drives the cone, which radiates the sound. As a result,
571 the air particles around the sound cone vibrate; therefore, sound waves are created.

572 To limit the mass of the coil in the dynamic speaker, the number of coil turns must
573 be greatly reduced (e.g., 100 times less than in the BAR case). Rather, the dynamic
574 speaker needs a strong core magnet to float the cone (with the coil), which leads
575 to a size generally larger than the BAR. This acoustic characteristic of the dynamic
576 speaker is easier to understand after controlling the speaker mass and the stiffness
577 of the diaphragm.

578 1.2 Goal of this study

579 The goal of this study is to provide clear insight into anti-reciprocal (or broadly
580 non-reciprocal) system. We are exposed to anti-reciprocal systems in our daily lives;

Draft of November 2, 2014 at 17:33

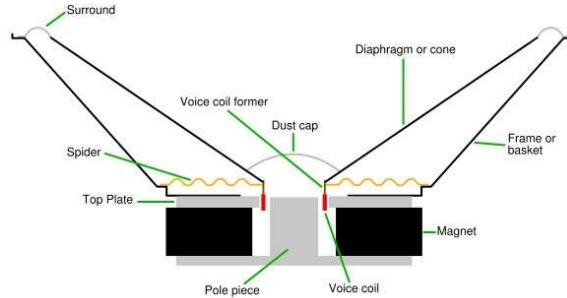


Figure 1.5: The cross-section view of the moving-coil loudspeaker. Up-and-down motion of the voice coil around a permanent magnet creates a time-varying magnetic field. As a voice coil moves around the pole piece, it becomes an “electro-magnet.” The image is from <http://i1-news.softpedia-static.com>.

581 however, the depth of our understanding of them has not been well addressed since
582 McMillan in 1946. The keyword is “anti-reciprocity.”

583 As discussed in the appendix C, the motivation for this study began with a PSPICE
584 simulation using the BAR-type ED series receiver model from Knowles Electronics
585 (Kim and Allen (2013), Fig. C.1). We then proceeded to redefine a new circuit model
586 to characterize a BAR-type receiver, the Knowles ED7045 (Kim and Allen, 2013),
587 and then developed theoretical insights and observations critical to understanding
588 the BAR.

589 The specific concepts covered in this study follow from a conceptual version of the
590 BAR model shown in Fig. 1.6. There are six highlighted parts in this figure labeled
591 with capital Roman numerals. Dark blue represent QS elements, while light blue
592 shows non-QS elements. The left-most resistor (part I) on the electrical side stands
593 for the DC resistance of wire. It depends on the real part of the wire resistance, with
594 the internal noise attributed to the Brownian (thermal) motion of the electrons in
595 the resistor. The second part (II) defines two missing parameters (Lewin, 2002a,b)
596 in classic circuit theory, KVL and KCL, lead inductance due to the emf created
597 by the magnetic field ($\dot{\mathbf{B}}$), and stray capacitance due to displacement current ($\dot{\mathbf{D}}$),
598 respectively. These components are frequency-dependent terms embedded in Fara-
599 day’s law and Ampere’s law. According to Woodson and Melcher (1968) either the
600 lead inductance or the stray capacitance must be zero when defining QS circuits.

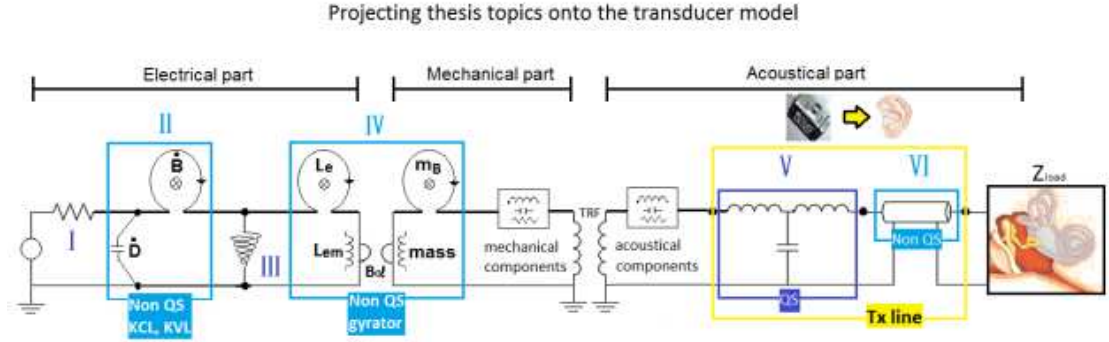


Figure 1.6: Overview of this study via the BAR model. All concepts discussed in this thesis can be tied together to understand the BAR transducer. The important concepts are highlighted using Roman characters. Note that the *quasistatic* (QS) components are marked as dark blue and the non-QS components are in light blue.

601 They define two cases: the stray capacitance (\dot{D}) is zero for electrostatic and the
 602 lead inductance (\dot{B}) is zero for magnetostatic.

603 There are two types of leakage inductances. One is due to the air side of the coil
 604 (L_e in part IV) and the other is from the semi-inductor leakage (part III) due to the
 605 magnetic field diffusion which leads to the eddy-current in the iron core (Vanderkooy,
 606 1989). This diffusive current is described by the skin depth of the ferromagnetic
 607 material ($\sqrt{\frac{2}{\mu\sigma\omega}}$), where μ , σ are the permeability and conductivity of the material
 608 and ω is the angular frequency.

609 Part IV characterizes the behavior of a non-ideal gyration. Two loop inductors (L_e ,
 610 m_B) due to the induced magnetic fields are associated with the self-inductor (mass
 611 in the mechanical side). The ideal gyration, introduced by Tellegen (1948) does not
 612 employ these non-ideal loop inductors, considering only the DC magnetic field of per-
 613 manent magnets and the wire's self-inductances (i.e., ' $F = B_0 l I$ ' relationship from
 614 an ideal gyration, where B_0 is static magnetic field density due to the permanent
 615 magnet and l is the length of the wire). Note that the non-ideal coupling coefficients
 616 (or transfer impedances) are analogues to mutual inductance of a non-ideal trans-
 617 former. Both the ideal and non-ideal gyrations assume the QS approximation. This
 618 gyration describes the transfer impedances of electro-mechanical (or electro-acoustic)

619 systems, namely T_{em} , T_{me} , which have anti-reciprocal characteristics due to Lenz's
620 law (1833).

621 Parts V and VI represent transmission lines, with (V) and without (VI), the QS
622 approximation. The behavior of this line in the low-frequency region can be estimated
623 by lumped circuit elements, as shown in part V. However, any pure delay, identified
624 by the non-QS transmission line, cannot be modeled via the QS approximation.
625 Infinite numbers of resonance and anti-resonance (poles and zeros) are observed in
626 the magnitude of the impedance of the non-QS transmission line (VI). Therefore, it
627 is critical to clearly understand the transmission line, whether it is QS or non-QS,
628 to describe the system correctly. A typical and important application of this kind of
629 transducer is the human ear, as depicted in Fig. 1.6 as the terminating impedance,
630 Z_{load} . The outer ear (i.e, ear canal) and tympanic membrane (TM) can be modeled
631 as a lossless transmission line (Puria and Allen, 1998; Robinson and Allen, 2013;
632 Parent and Allen, 2010), then the specific load is the middle ear.

633 Along with these concepts (parts I - VI), we also study the *motional impedance*
634 Z_{mot} , a unique characteristic of anti-reciprocal systems discovered early in the 20th
635 century. It was first introduced experimentally (Kennelly and Pierce, 1912; Kennelly
636 and Affel, 1915; Kennelly and Nukiyama, 1919; Kennelly and Kurokawa, 1921; Ken-
637 nelly, 1925); however, it has rarely been explained theoretically (Mott and Miner,
638 1951). Along with the modeling work, we investigate Z_{mot} , based on an in-depth
639 analysis of the anti-reciprocal system. For this, we reduce the complexity of the
640 proposed BAR model, leaving only the essential elements, to represent a simpler
641 electro-magnetic motor network.

642 We also reconsider the Z_{mot} formula based on each parameter's spatial relationship.
643 When Maxwell formulated his equations, he used quaternions working in 4D space
644 (x, y, z in the spatial domain plus time t). This work is critical because when we
645 perform circuit simulation we usually do not consider the spatial variation of each
646 variable. Using quaternions to reformulate the definitions of the Hunt parameters and
647 Z_{mot} does not change the original formulas, discussed in previous section (appendix
648 D).

649 The actual contributions from this study which are tied together to understand

650 the BAR transducer “intuitively” can be summarized as follows:

- 651 1. Our distinctive BAR model involves gyrator, semi-inductor, and a transmis-
652 sion line, representing “anti-reciprocal”, “diffusive”, and “non-QS” network
653 (Fig. 1.1).
- 654 2. In-depth investigation of the “anti-reciprocal” network. Reinterpreting the
655 gyrator’s formula via electromagnetic basics and expanding the formula to non-
656 ideal case.
- 657 3. Reinterpretation of the “QS” considering pure delay in the system.

658 A note about the ECE curriculum

659 When modeling transducers, frequency domain tools are critical for both analysis and
660 understanding. These include 1-port and 2-port Network Theory (Van Valkenburg,
661 1964, 1960). This tools naturally include the Fourier and Laplace Transforms, Power,
662 Impedance, and various generalizations of these tools including the Impedance and
663 transmission (ABCD) matrix, scattering matrices, reflectance (Smith Chart). Also
664 important are time domain tools, especially for nonlinear systems. Popular tools
665 include Matlab (ECE310/311) and Spice (ECE-342/343). At the heart of such anal-
666 ysis is the QS approximation, which is typically defined in terms of the ratio of the
667 wavelength over the dimensions of the physical structure being analyzed. This ratio
668 is typically quoted as $ka \ll 1$ where $k = 2\pi/\lambda$ and a is the radius of the system or
669 object being modeled.

670 Digital signal processing (DSP) is based on time domain processing but also uses
671 the frequency domain in the form of the DFT and Z-transform. The quasi-static
672 approximation is not typically assumed in DSP processing, since there is explicit
673 pure delay built into the analysis in terms of the sampling period, based on an
674 estimate of the highest frequency being analyzed. Thus again an upper bound on
675 frequency is assumed, but not in terms of QS. This is a different model that includes
676 explicit the pure delay.

677 Once the student is introduced to Maxwell's equations (ME), all these superficial
678 distinctions are replaced by vector calculus, the wave equation, Gauss's Law, and
679 Poynting's Power theorem ($\mathbf{E} \times \mathbf{H}$) (1884).

680 In this thesis all of these ideas necessarily come into play at the same time. This
681 is in part due to the merging of acoustics, with its slow wave speed, thus short wave-
682 lengths relative to the EM wavelengths (i.e., speed of sound and speed of light). While
683 we use the QS approximation and its associated Brune impedance relationships, we
684 must also generalize impedance to include the *wave impedance* seen in EM and
685 acoustics. These two types of impedance complement each other. Wave impedance
686 requires delay, as we have learned from DSP, whereas the Brune impedance obeys
687 the QS approximation.

688 1.3 Historical notes

689 Two honored people inspired this study.

- 690 1. Arthur Edwin Kennelly (Dec. 17, 1861, Colaba, India - Jun. 18, 1939, Boston,
691 U.S.A.) for the Z_{mot} study, and
- 692 2. Frederick Vinton Hunt (Feb. 15, 1905, Barnesville, OH - Apr. 21, 1972, Buffalo,
693 New York) for the modeling BAR.

694 The first is Arthur Edwin Kennelly (Fig. 1.7 (a)), who was born in 1861 in In-
695 dia. Kennelly was 15 years old when Bell submitted the telephone patent and 16
696 years old when Edison invented the carbon microphone. He is famous for working
697 with Edison starting in 1887 in support of Edison's weaknesses (i.e., math, AC, and
698 electro-magnetic studies); he was 26 years old when he joined Edison's group. He was
699 a professor of electrical engineering at Harvard University from 1902-1930. He wrote
700 his first paper on a loudspeaker in 1912 and worked at the Massachusetts Institute
701 of Technology (MIT) from 1913-1924. Also, he was the first person to use the term
702 impedance for AC circuits (A. E. Kennelly, "Impedance" American Institute of Elec-

703 trical Engineers (AIEE), 1893). In this paper, he discussed the first use of complex
704 numbers as applied to Ohm's law (1827) in alternating current circuit theory.



(a) A. E. Kennelly

(b) F. V. Hunt

Figure 1.7: (a): A. E. Kennelly (1861, India - 1939, U.S.A.) (b): F. V. Hunt (1905 - 1972, U.S.A.)

704 Along with these academic achievements in electro-engineering, the first analysis of
705 the magnetically driven moving-coil speaker's behavior, seen from the electrical side,
706 was highlighted by Kennelly and Pierce (1912) and he, the creator of *impedance* anal-
707 ogy in AC circuits, called it motional *impedance* (Z_{mot}). This concept was intensively
708 studied early in the 20th century based on experimental facts, without theoretical
709 criticism. Kennelly actively published many investigations on Z_{mot} , making him a
710 pioneer in loudspeaker analysis. However, a significant problem regarding Z_{mot} is its
711 negative real part, which appears to be a violation of energy conservation (Eq. A.1).
712 Including Kennelly's papers, the negative real part in Z_{mot} has never been clarified
713 with regard to its physical properties (T.S.Littler (1934); Fay and Hall (1933); Hanna
714 (1925)).
715

716 The second person who inspired this study was Frederick Vinton Hunt (Fig. 1.7
717 (b)), who was born in 1905 in Barnesville, Ohio. He was a professor at Harvard Uni-
718 versity, working in acoustic engineering. He contributed to underwater acoustics dur-
719 ing World War II by developing the first modern sonar system. Other inventions and
720 studies, including room acoustics, regulated power supply, lightweight phonograph
721 pickups, and electronic reproduction equipment, are also important contributions he
722 made to the field of electrical engineering.

723 Hunt published *Electroacoustics* in 1954, which is the basis of the current thesis
724 (Hunt, 1954). In that book, he analyzed and synthesized the electro-acoustic (or
725 electro-mechanical) system by modeling it as 2-by-2 matrix using scalar forms of
726 Lorenz's force and Maxwell's equations (i.e., Ampere's law and Faraday's law).⁶

727 The remainder of this study is structured as follows: Chapter 2 introduces the the-
728 oretical concepts specifically related to designing electro-magnetic transducer models.
729 Chapter 3 presents the experimental methods used in the study of the BAR. Chapter
730 4 includes the results from both the theoretical and experimental methods. Finally,
731 the conclusions and contributions of this study are summarized in Chapter 5.

⁶It was done by distinguishing two constants $j = \sqrt{-1}$ for a 90° phase shift and $k = \sqrt{-1}$ for a 90° spatial phase shift. Hunt (1954) Chapter 3 pp.114, $F = BlkI$, $\Phi = Blku$, where F , I , Φ , u , B , l are force, current, voltage, velocity, magnetic intensity, and length of wire respectively.

CHAPTER 2

THEORETICAL METHODS

732 In this section, we research important theoretical concepts to appreciate anti-reciprocal
733 network, such as Hunt's two port network, Möbius transformation, Carlin's network
734 postulate, a gyrator, a semi-inductor, and the motional impedance.

735 It will be useful to discuss a proper way to choose frequency domains for signals
736 (i.e., Φ , I) and systems (i.e., power and impedance) at this point. Laplace frequency
737 $s = \sigma + j\omega$ is used to indicating a Positive-Real (PR) characteristic of a system. In
738 Laplace frequency plane, the abscissa (x-axis) is for a real part (σ referring to any
739 loss in a system) while the ordinate (y-axis) is for an imaginary part ($j\omega$ where ω is
740 an angular frequency or a Fourier frequency). PR functions are strictly non negative
741 on the right half of the Laplace plane to assume they obey the passive condition (see,
742 C3 in section 2.2). However, Φ and I are classified as signals (not systems). They do
743 not need to obey the PR property. Therefore the angular Fourier frequency ω is used
744 for $\Phi(\omega)$ and $I(\omega)$. For example, one can use Fourier transform to convert a voltage
745 in the time domain to a voltage in the frequency domain. But to convert power from
746 one domain to the other, the Laplace transform must be applied. Since impedance
747 is a necessary part of power, the concept of impedance (\mathcal{Z}) is also described as a
748 system, especially in a frequency domain, therefore we use the Laplace frequency 's'
749 for $\mathcal{Z}(s)$. It is true for one or two port systems.

750 2.1 Two-port anti-reciprocal network with Hunt parameters

751 Hunt (1954) modeled an electro-mechanic system into a simple 2×2 impedance

752 matrix relationship. There are four Hunt’s two-port network parameters, following
 753 Wegel (1921), $Z_e(s)$, $Z_m(s)$, $T_{em}(s)$, and $T_{me}(s)$ where ‘ $s = \sigma + j\omega$ ’ is the Laplace
 754 frequency.

755 To explain each parameter, we convert a two-port ABCD matrix to the Hunt
 756 impedance matrix. A schematic representation of this network is shown in Fig. 2.1
 757 as depicted by Kim and Allen (2013). As shown in Fig. 2.1, each network element may
 758 be represented with a 2 by 2 ABCD matrix, with the velocity U defined as flowing
 759 out of the element (resulting in the ‘-’ sign). Thus multiple elements’ matrices
 760 can be ‘chained’ (i.e., factored) in accordance with different combinations of the
 761 elements (i.e., series or shunt). This allows one to represent the network using matrix
 762 multiplication, which enables convenient algebraic manipulation. Since the current
 763 (flow) is always defined into the port, when we transform the ABCD matrix to an
 764 impedance matrix, it is necessary to force a negative sign for the volume velocity to
 765 maintain tradition matrix requirements.

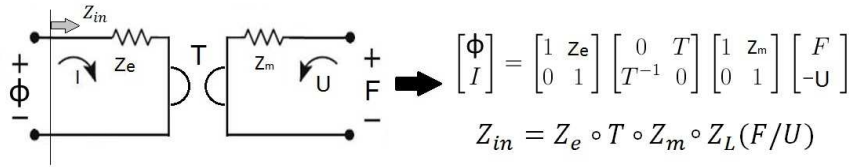


Figure 2.1: A schematic representation of an electro-mechanic system using Hunt parameters and Möbius composition of the ABCD matrix (Kim and Allen, 2013). Note how the ABCD matrix method “factors” the model into 2×2 matrix. This allows one to separate the modeling from the algebra.

766 In practical electro-mechanical systems, all variables in the system (Φ , I , F , U) are
 767 constrained to a fixed direction of action (without considering spatial dependency),
 768 therefore relationships between each quantity become scalar (Hunt, 1954). Especially
 769 when we analyze the system using the ABCD matrix, we must treat all variables as
 770 the scalars.

771 The Hunt impedance matrix representation of the same system is

$$\begin{bmatrix} \Phi(\omega) \\ F(\omega) \end{bmatrix} = \begin{bmatrix} Z_e(s) & T_{em}(s) \\ T_{me}(s) & Z_m(s) \end{bmatrix} \begin{bmatrix} I(\omega) \\ U(\omega) \end{bmatrix}, \quad (2.1)$$

772 where $s = \sigma + j\omega$, and

$$Z_e(s) = \frac{\Phi(\omega)}{I(\omega)} \text{ when } U(\omega)=0, \quad (2.2)$$

773

$$T_{em}(s) = \frac{\Phi(\omega)}{U(\omega)} \text{ when } I(\omega)=0, \quad (2.3)$$

774

$$T_{me}(s) = \frac{F(\omega)}{I(\omega)} \text{ when } U(\omega)=0, \quad (2.4)$$

775

$$Z_m(s) = \frac{F(\omega)}{U(\omega)} \text{ when } I(\omega)=0. \quad (2.5)$$

776 For DC electromagnetic coupling, $-T_{em} = T_{me} = T = B_0 l$, where B_0 and l are DC
 777 magnetic field and length of wire, respectively. Along with Eq. 2.1, the two-port
 778 ‘electro-mechanic’ transducer equation can alternatively be represented in ABCD
 779 (a.k.a. transmission matrix) form, as given by

$$\begin{bmatrix} \Phi(\omega) \\ I(\omega) \end{bmatrix} = \begin{bmatrix} A(s) & B(s) \\ C(s) & D(s) \end{bmatrix} \begin{bmatrix} F(\omega) \\ -U(\omega) \end{bmatrix}. \quad (2.6)$$

780 Here A, B, C, D are functions of s to show they are causal (see, C4 in section 2.2)
 781 and complex analytic “system” variables. The signal variables Φ, I, F, U on the
 782 other hands are functions of ω , to indicate they are neither causal, nor analytic.

783 The fundamental difference between the two matrix representations lies in the cou-
 784 pling of the ‘electro-mechanic’ transducer, between the mechanical and the electric
 785 signals. Specifically, the electrical input parameters Φ and I on the left side of the
 786 network and Eq. 2.6 are expressed in terms of the mechanical variables, the force F
 787 and the velocity U , on the right side of the network, via the four frequency dependent
 788 parameters A, B, C , and D .

789 Conversion between Eq. 2.6 and Eq. 2.1 has the following relationships,

$$\mathcal{Z} = \begin{bmatrix} z_{11}(s) & z_{12}(s) \\ z_{21}(s) & z_{22}(s) \end{bmatrix} = \frac{1}{C} \begin{bmatrix} A(s) & \Delta_T(s) \\ 1 & D(s) \end{bmatrix}, \quad (2.7)$$

790

$$\mathcal{T} \begin{bmatrix} A(s) & B(s) \\ C(s) & D(s) \end{bmatrix} = \frac{1}{T_{me}(s)} \begin{bmatrix} Z_e(s) & \Delta_Z \\ 1 & Z_m(s) \end{bmatrix}. \quad (2.8)$$

791 where $\Delta_Z = Z_e Z_m - T_{em} T_{me}$ and $\Delta_T = AD - BC$. Note that if $C = 0$, Z does
 792 not exist. Eq. 2.8 represents Eq. 2.7's inverse transformation, the conversion from
 793 impedance matrix to transmission matrix.

794 Note that the impedance matrix is useful when making measurements. For in-
 795 stance, system's electrical input impedance and output acoustic impedance (or out-
 796 put mechanical impedance) can be represented with the impedance matrix elements,
 797 z_{11} and z_{22} . The ABCD matrix representation is useful for network modeling,
 798 but then may be transformed into an impedance matrix for experimental verifi-
 799 cation. Symmetry relationships of the network (i.e., reversibility, reciprocity) based
 800 on Eq. 2.7 are discussed in section 2.2.

801 2.1.1 Calibration of Hunt parameters for an electro-acoustic 802 transducer

803 In this section, we employ Hunt parameters to electro-acoustic system, Z_e , Z_a and
 804 T_a , where subscript 'a' stands for 'acoustic.' the electro-acoustic Hunt parameters
 805 can be estimated from Z_{in} given three different acoustic load conditions. Similar to
 806 Eq. 2.1, the BAR can be represented by its electro-acoustic impedance matrix as

$$\begin{bmatrix} \Phi(\omega) \\ P(\omega) \end{bmatrix} = \begin{bmatrix} Z_e(s) & -T_a(s) \\ T_a(s) & Z_a(s) \end{bmatrix} \begin{bmatrix} I(\omega) \\ V(\omega) \end{bmatrix}. \quad (2.9)$$

807 The acoustic load impedance Z_L is defined by Ohm's law as (V is volume velocity
 808 defined as flowing into the port)

$$Z_L \equiv \frac{P}{-V}. \quad (2.10)$$

Draft of November 2, 2014 at 17:33

809 Combining Eq. 2.9 and Eq. 2.10 and solving for V gives

$$V = \frac{-T_a I}{Z_L + Z_a}. \quad (2.11)$$

810 Replacing V in Eq. 2.9 gives an expression for the loaded electrical input impedance
811 ($V \neq 0$)

$$Z_{in} \equiv \frac{\Phi}{I} = Z_e + \underbrace{\frac{T_a^2}{Z_L + Z_a}}_{Z_{mot}}, \quad (2.12)$$

812 where Z_{mot} is denoted the *motional impedance* due to the acoustic load shown in
813 the electric terminals (Hunt, 1954). Note that the sum of Z_a and Z_L in Z_{mot} 's
814 denominator is treated as total acoustic impedance when it is looked at electrical
815 side. Thus the Z_{in} obtained through measurements depends on the acoustic load,
816 Z_L . Varying the acoustic load, which can be done by varying the length of the
817 acoustic tube, results in different Z_{in} values (Fig. 3.2). The algebraic details are
818 provided in Appendix E.

819 2.2 Network postulates

820 An important terminology may be used to describe one-port and two-port networks,
821 as defined in this section. One can relate the limitations of the Brune's impedance
822 based on the one-port network theory (Brune (1931); Serwy (2012)). To cross from
823 one physical modality from the other (Table A.1), a two-port network must be used
824 (Hunt, 1954; Carlin and Giordano, 1964).

825 Carlin and Giordano (1964) summarized two-port networks in terms of 6 pos-
826 tulates: C1-Linearity, C2-time-invariance, C3-passivity, C4-causality, C5-real-time
827 function, and C6-reciprocity. Note that C6 only applies to two-port networks while
828 others are for both one-port or two-port networks.

829 C1 Linearity (*vs.* Non-linearity): A system obeys superposition.

$$\alpha f(x_1) + \beta f(x_2) = f(\alpha x_1 + \beta x_2) \quad (2.13)$$

830 C2 Time-invariance (*vs.* time-variance): A system does not depend on the time of
831 excitation,

$$f(t) = f(x(t)) \rightarrow f(t - t_1) = f(x(t - t_1)). \quad (2.14)$$

832 C3 Passivity (*vs.* Active): Conservation of energy law, Eq. A.1. A system cannot
833 provide more power than supplied amount, where power is defined as

$$power(t) = \int^t i(t) \cdot v(t) dt. \quad (2.15)$$

834 C4 Causality (*vs.* Non-causality *vs.* Anti-causality): A response of a system cannot
835 be affected by a future response.

836 C5 Real-time function (*vs.* Complex-time function): The system's time response
837 is real.

838 The systems' stability can be discussed via the impulse response, the transfer func-
839 tion, and the poles and zeros of the system. An impedance can be interpreted as
840 a transfer function for one-port system, and through the inverse Laplace transform
841 (\mathcal{L}^{-1}), we can have its impulse response. In terms of region of convergence (ROC) of
842 the transfer function, the imaginary axis of the s -plane is included in the ROC for
843 a stable system. Specifically, for a system to be stable and bounded, all poles are
844 in the left half plane (LHP) in a causal system case, whereas all poles must be in
845 the right half plane (RHP) in an anti-causal bounded system case. A third category
846 exists if the system is causal and unbounded, when the poles are in the RHP. In this
847 case, (there may be multiple ROCs but usually) the ROC is the right sided plane
848 from the most right pole.¹ Either BAR or dynamic speaker, both types of transduc-
849 ers are categorized as two-port electro-acoustic systems, converting electrical energy

¹If a pole (s_k) is represented as $s_k = \sigma_0 + j\omega_0$ where σ_0 and ω_0 are the real and the imaginary parts of the pole. Then the 'right-most' pole of the system has the largest, the most positive σ_0 .

850 into acoustic pressure. Other examples of the two-port network can be easily found
 851 in our daily lives. Table 2.1 shows some real life examples of the two-port networks.

Two-port network system	examples
Electro-mechanic	motors, bone vibrators
Electro-acoustic	loud speakers, ear-phones

Table 2.1: Example of two-port networks

852

853 All one-port postulates we discussed (C1-C5), can also be applied to two-port
 854 networks. One strictly two-port postulate is Carlin's last postulate:

855 C6 Reciprocity (*vs.* Non-reciprocity *vs.* Anti-reciprocity): To be a reciprocal net-
 856 work, in terms of conjugate variables described in Table A.1, a generalized
 857 force is swapped to a flow across one modality to the other (Eq. 2.16a). In
 858 other words, the two transfer impedances (the two off-diagonal components)
 859 of the system's impedance matrix must be equal. The anti-reciprocal network
 860 swaps the force and the flow, but one variable changes to the opposite direction
 861 (Eq. 2.16b). A non-reciprocal network is a network which does not have recip-
 862 rocal characteristic. Note that the special case of a non-reciprocal network is
 863 the anti-reciprocal networks (McMillan, 1946).

$$\begin{bmatrix} \Phi \\ F \end{bmatrix} = \begin{bmatrix} 0 & 1 \\ 1 & 0 \end{bmatrix} \begin{bmatrix} I \\ U \end{bmatrix} \quad (2.16a)$$

864

$$\begin{bmatrix} \Phi \\ F \end{bmatrix} = \begin{bmatrix} 0 & -1 \\ 1 & 0 \end{bmatrix} \begin{bmatrix} I \\ U \end{bmatrix} \quad (2.16b)$$

865

$$\begin{bmatrix} \Phi \\ F \end{bmatrix} = \begin{bmatrix} 1 & 0 \\ 0 & 1 \end{bmatrix} \begin{bmatrix} I \\ U \end{bmatrix} \quad (2.16c)$$

866

867 There is another important property denoted 'Reversibility' (Van Valkenburg,
 868 1964), where the diagonal components in a system's impedance matrix are equal

869 (input impedance = output impedance, Eq. 2.16c). In other words, the input force
870 and flow are proportional to the output force and flow, respectively. This postulate
871 is only defined for the two-port network.

872 For the readers benefit, the six types of network symmetry are defined, as followed:

- 873 1. Reciprocal network: If $z_{12} = z_{21} \Leftrightarrow \Delta_T = 1$ with $C \neq 0$.
- 874 2. Non-reciprocal network: all systems that are not reciprocal.
- 875 3. Anti-reciprocal network: $-z_{12} = z_{21} \Leftrightarrow \Delta_T = -1$ with $C \neq 0$.
- 876 4. Reversible network: $z_{11} = z_{22} \Leftrightarrow A = D, C \neq 0$.
- 877 5. Reciprocal and reversible network: $z_{11} = z_{12} \ \& \ z_{21} = z_{22} \Leftrightarrow A = D \ \& \ \Delta_T = 1$
878 with $C \neq 0$.
- 879 6. Anti-reciprocal and reversible network: $-z_{12} = z_{21} \ \& \ z_{11} = z_{22} \Leftrightarrow A = D \ \& \$
880 $\Delta_T = -1$ with $C \neq 0$,

881 where Δ_T is the determinant of the transmission matrix. When $C = 0$ or $z_{21} = 0$,
882 conversion between transmission matrix and impedance matrix is not possible.

883 Note that all categorized postulates are independent² including the reversibility
884 (Carlin and Giordano, 1964).

885 2.2.1 Additional postulates to include Brune's impedance (Brune, 886 1931)

887 In addition to Carlin's postulates for the one-port network (C1-C5), one should
888 consider Brune's impedance as a highly limited extension of the one-port network
889 properties. Otto Brune synthesized the properties of one-port (or two terminals) PR
890 networks in his Ph.D. thesis at MIT (Brune, 1931). However the critical limitation of
891 his network theory is that it assumes a quasi-static approximation. This limitation
892 has been addressed in Roger Serwy's master thesis (Serwy, 2012).

²It is not an absolute statement. There is an exception to this rule.

893 B1 Positive-Real (PR): $Z(s) = \Re(\sigma, \omega) + j\Im(\sigma, \omega)$, where $s = \sigma + j\omega$. Then $\Re(\sigma \geq 0) \geq$
 894 0. Note that PR functions (i.e., impedances) are a subset of minimum phase
 895 functions. Therefore impedance is a Positive-Definite (PD) operator. Moreover
 896 the order difference between numerator and denominator is ± 1 for PR. This
 897 concept is an expanded version of C1-C5.

898 B2 Quasi-static (QS) (*vs.* non quasi-static or “Einstein Causality”): A QS system
 899 always assumes that the system size is much smaller than the wave length λ .
 900 Only when the QS system is bandlimited, it can exhibit a finite system delay.
 901 The complement concept is “Einstein Causality” meaning that the pure delay
 902 ($\tau = \frac{x}{c}$) depends on a distance (x) where ‘ c ’ is the wave speed (sound or light,
 903 $\delta(t - x/c)$).

904 For further explanation of B1, $Z(s)$ is represented as a rational polynomial fraction
 905 (pole-zero pairs). It can be factored into first-order terms in s (Van Valkenburg,
 906 1964)

$$Z(s) = \frac{\prod_{i=1}^L K_i (s - n_i)}{\prod_{k=1}^N K_k (s - d_k)} = \frac{|\rho| e^{j\theta_n}}{|r| e^{j\theta_d}} = \left| \frac{\rho}{r} \right| e^{j(\theta_n - \theta_d)}, \quad (2.17)$$

907 where K_i and K_k are scale factors. The s values for which $Z(s)$ is zero ($s = n_i$) and
 908 infinite ($s = d_k$) are called the system’s zeros and poles. In the first definition of
 909 $Z(s)$ in Eq. 2.17, any poles and zeros that have the same complex location, $n_i = d_k$,
 910 (pairwise pole-zero, aka “removable singularities”) are canceled. Then, the product
 911 of zeros and poles can be represented in polar form (middle definition in Eq. 2.17 with
 912 magnitude: ρ , r , phase: θ_n , θ_d). Finally $Z(s)$ has a reduced form with its magnitude
 913 $\frac{\rho}{r}$ and phase $\theta_n - \theta_d$. If a system satisfies the PR property, then the phase difference
 914 $|\theta_n - \theta_d|$ must be less than $\frac{\pi}{2}$. This means $Z(s)$ is always positive in the Right
 915 Half Plane (RHP). It follows that the difference in order between numerator and
 916 denominator cannot be more than ± 1 or $|L - N| \leq 1$ (Van Valkenburg, 1960).

917 This PR property is closely related to the positive definite (PD) matrix (operator
 918 property). For an example, a (2×2) impedance matrix \mathcal{Z} for a two-port network

919 must have,

$$\begin{bmatrix} \mathcal{I}_1 & \mathcal{I}_2 \end{bmatrix} \begin{bmatrix} z_{11} & z_{12} \\ z_{21} & z_{22} \end{bmatrix} \begin{bmatrix} \mathcal{I}_1 \\ \mathcal{I}_2 \end{bmatrix} \geq 0, \quad \forall \mathcal{I}_1, \mathcal{I}_2, \quad (2.18)$$

920 OR

$$\mathcal{I}^T \cdot \mathcal{Z}(s) \cdot \mathcal{I} \geq 0, \quad \forall \mathcal{I}(\omega). \quad (2.19)$$

921 Note this generalizes to a $\mathcal{Z}_{2 \times 2}$ matrix, for example, $\mathcal{Z}(s)$ and $\mathcal{I}(\omega)$ are (2×2) and
 922 (2×1) matrices respectively. And \mathcal{I}^T is the transpose of \mathcal{I} . Since \mathcal{Z} is PR, the matrix
 923 version of \mathcal{Z} is a PD operator.

924 The quasi-static property (B2) is an alternative way to specify C4. The definition
 925 of quasi-static is “not having pure delay” ($\tau[s] = \frac{\Delta_x[m]}{c[m/s]} = 0$) in a system. An
 926 equivalent definition inherently exists in most classical circuit analysis such as KCL
 927 and KVL. Especially when we deal with an electro-magnetic system, one or both of
 928 the time dependent terms in Maxwell’s equation ($\dot{\mathbf{B}}$ and $\dot{\mathbf{D}}$, where a dot represents
 929 the first-order time derivative) are zero. This point will be discussed later in this
 930 study, section 2.5.2.

931 The antithesis of QS is non-QS, or “Einstein Causality,” a delay existing in a system
 932 proportional to a distance. The most relevant example is reflectance Γ , defined as

$$\Gamma(s) = \frac{Z(s) - 1}{Z(s) + 1}, \quad (2.20)$$

933 where \mathcal{L}^{-1} of $Z(s)$ is $z(t) \leftrightarrow Z(s)$, such that $z(t) = 0 \forall t < 0$. Compared to C4, B32
 934 limits the causal boundary to be physical. Assuming, we live in a world within the
 935 theory of relativity of Einstein, “Einstein Causality” is an appropriate characteristic
 936 to define a network when we talk about the causality. All physical networks must
 937 obey B2.

938 Note that B1-B2 can be applied to both one and two port networks.

939 It is worth discussing the difference between ‘static’ and ‘quasi-static’. The term
 940 ‘quasi-static’ is different from ‘static’. The ‘static’ system is not time-varying ($\frac{d}{dt} =$
 941 0). Serwy (2012) describes two types of QS based on the definition of speed of light,
 942 $c = \frac{1}{\sqrt{\mu_0 \epsilon_0}}$; $\epsilon \rightarrow 0$ and $\mu \rightarrow 0$ to realize $c \rightarrow \infty$. However this definition is inadequate

943 since it conflicts with the definition of characteristic impedance ($\sqrt{\mu/\epsilon}$).

944 The concept of quasi-static still remains vague and needs a better definition. We
945 claim that it is necessary to move beyond quasi-static: one main reason is to handle
946 the case of a physical system, such as ear canal delay (i.e., the canal impedance needs
947 to be factored into a pure delay and a minimum-phase component and this means
948 that it will not be a Brune impedance³ (Robinson and Allen, 2013). Details of this
949 topic is discussed in section 2.5.1.

950 2.3 Generalization of the ABCD matrix using Möbius 951 transformation

952 In this section, we explain how the Möbius transformation or bilinear transformation
953 is an important generalization of the ABCD transformation. In characterizing the
954 ABCD transformation, a cascading series of ABCD matrices is significant to simplify
955 the algebra. It is equivalent to the composition of Möbius transformations (Boas,
956 1987). This is a visual way of describing the ABCD matrix (Fig. 2.2).

957 The relationship (conversion) between the impedance matrix and the ABCD ma-
958 trix formula defined in Eq. 2.8 maybe found in most of the electrical engineering text
959 and is taught in undergraduate classes. The impedance matrix is a generalization of
960 Ohm's law. One side of each equation has a force variable; the other side involves
961 relation between two flows in the system. The conversion to ABCD matrix results
962 once the two equations are rewritten in terms of the first port's two variables, force
963 and flow. The derivation is straightforward; however it is not completely clear why
964 the ABCD cascading method works. One can find the root of this method in the
965 composition of the Möbius transformation.

966 Let's start with an example. The general form of a Möbius transformation is
967 defined as a rational function. We define two rational functions $M_{a,b,c,d}(s)$ and

³The impedance at the probe can be fit to a Brune's form, but the ear canal is definitely better modeled as a delay line



Figure 2.2: Möbius strip sculpture at the Beckman Inastitute, UIUC. Möbius transformation matrix is presented underneath of the sculpture.

968 $M_{A,B,C,D}(z)$,

$$M_{a,b,c,d}(s) = \frac{as + b}{cs + d}, \text{ and } M_{A,B,C,D}(z) = \frac{Az + B}{Cz + D}. \quad (2.21)$$

969 where a, b, c, d, A, B, C , and D are any complex numbers satisfying $AD - BC \neq 0$ and
 970 $ad - bc \neq 0$. When $ad = bc$ or $AD = BC$, Eq. 2.21 are not Möbius transformations.

971 For better visualizing of each Möbius function, 4 steps of transformations (com-
 972 positions) are introduced. Take one of the two formulas in Eq. 2.21, $M_{a,b,c,d}(s)$ can
 973 be decomposed into 4 different functions,

$$M_{a,b,c,d}(s) = M1_{a,b,c,d}(s) \circ M2_{a,b,c,d}(s) \circ M3_{a,b,c,d}(s) \circ M4_{a,b,c,d}(s), \quad (2.22)$$

974 where,

- 975 1. $M1_{a,b,c,d}(s)$: $s + \frac{d}{c}$ translation by $\frac{d}{c}$
- 976 2. $M2_{a,b,c,d}(s)$: $\frac{1}{s}$ taking a inverse
- 977 3. $M3_{a,b,c,d}(s)$: $\frac{bc-ad}{c^2}s$ expansion and rotation
- 978 4. $M4_{a,b,c,d}(s)$: $s + \frac{a}{c}$ translation by $\frac{a}{c}$

979 Composing the two functions in Eq. 2.21 leads the function $Q(z)$,

$$Q(z) = M_{a,b,c,d}(s) \circ M_{A,B,C,D}(z) = \frac{as + b}{cs + d} \circ \frac{Az + B}{Cz + D} = \frac{a \left(\frac{Az+B}{Cz+D} \right) + b}{c \left(\frac{Az+B}{Cz+D} \right) + d}. \quad (2.23)$$

980 Finally we have

$$Q(z) = \frac{(aA + bC)z + (aB + bD)}{(cA + dC)z + (cB + dD)}. \quad (2.24)$$

981 Write two 2X2 matrix, based on the four coefficients in both $M_{a,b,c,d}(s)$, $M_{A,B,C,D}(z)$
 982 in Eq. 2.21 and cascade the two matrix,

$$\begin{bmatrix} a & b \\ c & d \end{bmatrix} \begin{bmatrix} A & B \\ C & D \end{bmatrix} = \begin{bmatrix} aA + bC & aB + bD \\ cA + dC & cB + dD \end{bmatrix}. \quad (2.25)$$

983 It is therefore demonstrated that the composition of Möbius transformations (in
 984 Eq. 2.24 and Eq. 2.23) is equivalent (i.e., isomorphic) to the cascaded matrix of
 985 Eq. 2.25. It also applies to multiple matrix computation. As shown in Eq. 2.23,
 986 computational complexity will be increased as the order of the composition is in-
 987 creased. In such a case, the cascading matrix method is superior over composition.
 988 Cascading ABCD matrices in circuit theory is the best example of Möbius compo-
 989 sition. When we compose a circuit system, we need lots of circuit components (e.g.
 990 Fig. 1.1). Therefore when analyzing a circuit using the ABCD matrix multiplication
 991 method, the algebra becomes trivial.

992 **Example 1**

993 Figure 2.3 depicts a circuit model with a series impedance Z . There are two inputs
 994 (Φ_1, I_1) and two outputs (Φ_2, I_2) to form this simple network. A well-known, ABCD
 995 matrix of a series impedance (Z) is given as

$$\begin{bmatrix} \Phi_1 \\ I_1 \end{bmatrix} = \begin{bmatrix} 1 & Z \\ 0 & 1 \end{bmatrix} \begin{bmatrix} \Phi_2 \\ I_2 \end{bmatrix}, \quad (2.26)$$

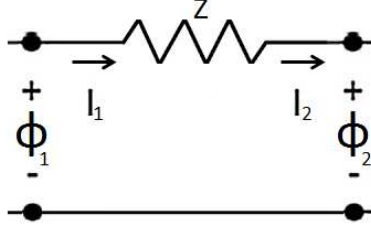


Figure 2.3: A series impedance (Z) representation with inputs (Φ_1, I_1) and outputs (Φ_2, I_2). Note that, in this figure, all currents are defined as going out of the network.

996 where Φ and I are the voltage and the current which is defined as going out of the
 997 network. And the subscripts 1 and 2 stand for the input port and the output port
 998 respectively. To form a rational function using this relationship, take a ratio of the
 999 first and the second rows in Eq. 2.26 to have input impedance Z_{in} as a function of
 1000 the output impedance, Z_{out} ,

$$Z_{in}(Z_{out}) = \frac{\Phi_1}{I_1} = \frac{\Phi_2 + ZI_2}{0 + I_2} = \frac{\Phi_2/I_2 + Z}{0 + 1} = \frac{Z_{out} + Z}{0Z_{out} + 1}, \quad (2.27)$$

1001 where the Eq. 2.27 may be changed by multiple of Z_{in} matrix itself. Representing
 1002 Eq. 2.27 in Möbius composition form,

$$M_{1,Z,0,1}(Z_{out}) = \frac{Z_{out} + Z}{0Z_{out} + 1} : [M] = \begin{bmatrix} 1 & Z \\ 0 & 1 \end{bmatrix}, \quad (2.28)$$

1003 which is identical to the impedance matrix shown in Eq. 2.26. In summary, Eq. 2.26
 1004 is the matrix form while Eq. 2.28 is the composition form.

1005 As discussed early in this section, the parameter C (Eq. 2.6) for Eq. 2.27 is zero,
 1006 therefore $Z_{in}(\infty) = \infty$; conversion to the impedance matrix is impossible for this
 1007 case.

1008 Example 2

1009 This theory can be directly applied into any domain changing relationship such as
 1010 the conversion between reflectance Γ and impedance Z . The relationship between Γ

1011 and Z is

$$\Gamma_{1,-r_0,1,r_0}(Z) = \frac{Z - r_0}{Z + r_0} : [\Gamma] = \begin{bmatrix} 1 & -r_0 \\ 1 & r_0 \end{bmatrix}, \quad (2.29)$$

1012 and its inversion relationship is

$$[\Gamma]^{-1} = Z = \frac{1}{2r_0} \begin{bmatrix} 1 & -r_0 \\ 1 & r_0 \end{bmatrix}, \quad (2.30)$$

1013 where r_0 is surge impedance.

1014 In general we may show this as

$$Z_{A,B,C,D}(s) = \frac{As + B}{Cs + D} : [Z] = \begin{bmatrix} A & B \\ C & D \end{bmatrix}, \quad (2.31)$$

1015 where s is Laplace frequency. It is standard to use round brackets $Z(s)$ on the
 1016 composition form and square brackets $[Z]$ on the matrix form. Composing Eq. 2.31
 1017 with Eq. 2.29,

$$\Gamma(Z) = \frac{\frac{As+B}{Cs+D} - 1}{\frac{As+B}{Cs+D} + 1} = \frac{(A - C)s + B - D}{(A + C)s + B + D}. \quad (2.32)$$

1018 The coefficients in Eq. 2.32 are equivalently shown from the following matrix multi-
 1019 plication, cascading Eq. 2.31 and Eq. 2.29 with $z_0 = 0$ in Eq. 2.29,

$$\begin{bmatrix} 1 & -1 \\ 1 & 1 \end{bmatrix} \begin{bmatrix} A & B \\ C & D \end{bmatrix} = \begin{bmatrix} A - C & B - D \\ A + C & B + D \end{bmatrix}. \quad (2.33)$$

1020 We have shown an example of the conversion relationship from Z to Γ . Now in
 1021 Fig. 2.4 we consider an inverted case, representing a relationship from Γ to Z with
 1022 a simple diagram. We believe that it will give us a better understanding of the
 1023 composition method behind the algebra.

1024 For the case of a lossless transmission line,

$$\Gamma(s) = e^{-s2L/c} \leftrightarrow \delta(t - 2L/c), \quad (2.34)$$

1025 where $L[m]/c[m/s]$ represents delay in the transmission line.

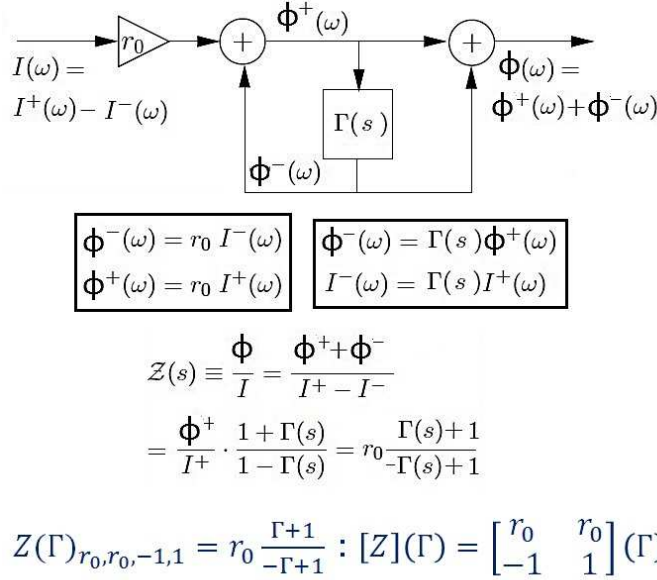


Figure 2.4: Inverted relationship between reflectance (Γ) and the wave impedance (Z) shown in Eq. 2.33 where the conversion is made from Z to Γ . When we convert from Γ to Z , the matrix' diagonal elements are swapped compared to Eq. 2.33.

1026 To summarize, multiplying 2X2 matrices is isomorphic to composition of the bi-
1027 linear transformation.

1028 2.4 Motional Impedance (Z_{mot})

1029 Kennelly's first paper on Z_{mot} was published in 1912 (Kennelly and Pierce, 1912),
1030 it is referenced frequently in the extensive literature. The main point of this 1912
1031 paper is that the impedance of a telephone receiver is different, when the diaphragm
1032 is free to vibrate, from when the diaphragm's motion is damped or blocked (Hunt,
1033 1954). Kennelly defined Z_{mot} as the difference between the two (input) impedances
1034 with different boundary conditions, namely $Z_{mot} = Z_{in}|_{free} - Z_{in}|_{blocked}$. Details of
1035 the Z_{mot} definition maybe found in the next subsection (section 2.4.1)

1036 Three years later, Kennelly published a second paper about Z_{mot} (Kennelly and
1037 Affel, 1915). In this paper, Z_{mot} is characterized in the Z plane (real and imaginary
1038 parts of the impedance, Z) as a circle shaped impedance passing through the ori-
1039 gin of coordinates, with its diameter depressed through a certain angle (depressed
1040 compared to the circle in undamped impedance). Kennelly and Affel addressed these
1041 distinctive features in terms of the electrical and mechanical properties of the system.
1042 They described Z_{mot} using four constants, A (force factor), m (equivalent mass), r
1043 (motional resistance), and k (stiffness constant). There are four unknowns, there-
1044 fore four equations are needed to solve for Z_{mot} . Each of the four constants has the
1045 following relationship,

- 1046 1. The resonant angular frequency $\omega_0 = \sqrt{\frac{k}{m}}$,
- 1047 2. The damping constant $\Delta = \frac{r}{2m}$, and
- 1048 3. The magnitude of the $|Z_{mot}| = \frac{A^2}{r}$.

1049 The missing fourth equation can be supplied by measuring any one of the four con-
1050 stants directly. In practice, what they actually did was to iterate for the four param-
1051 eters (assuming one of the constant is known) using least square method to estimate
1052 the Z_{mot} circle diagram. This is related to Eq. 2.31 From the difference between
1053 two Z_{mot} circle diagrams, the last independent equation can be found. The precise
1054 procedure may be found in Appendix E and in S. Ramo and Duzer (1965) (section
1055 11.07, pp.595).

1056 Kennelly's third paper about Z_{mot} was published in 1919 (Kennelly and Nukiyama,
1057 1919). In this paper, he focused on power concept of Z_{mot} , and introduced the mo-
1058 tional power diagram to better physical understanding. The motional power diagram
1059 is drawn based on m.m.f. (magneto motive force) generated by the vibration of the
1060 diaphragm in the permanent magnetic field. The motional power can be regarded
1061 as a scaled motional impedance diagram. In their view, power is a better concept to
1062 understand the system, compared to impedance.⁴ He explained the motional power

⁴In 1919, impedance had not yet to be defined properly, which finally came about 12 years later in Brune's PhD thesis.

Draft of November 2, 2014 at 17:33

1063 circle by means of “active mechanical power (P_m)”, which is defined as a difference
 1064 between electrical power (P_e) and hysteresis power (P_h)

$$P_m = P_e - P_h. \quad (2.35)$$

1065 The mechanical power observed from electrical side (the motional power circle)
 1066 is depicted in Fig. 2.5. This image is directly adapted from Kennelly and Nukiyama
 1067 (1919), figure 27 in the original paper. Based on the definition of P_m in Eq. 2.35,
 1068 the negative real parts shown in motional power diagram (Fig. 2.5) can be redefined
 as purely active mechanical power looking at the electric part of the system.

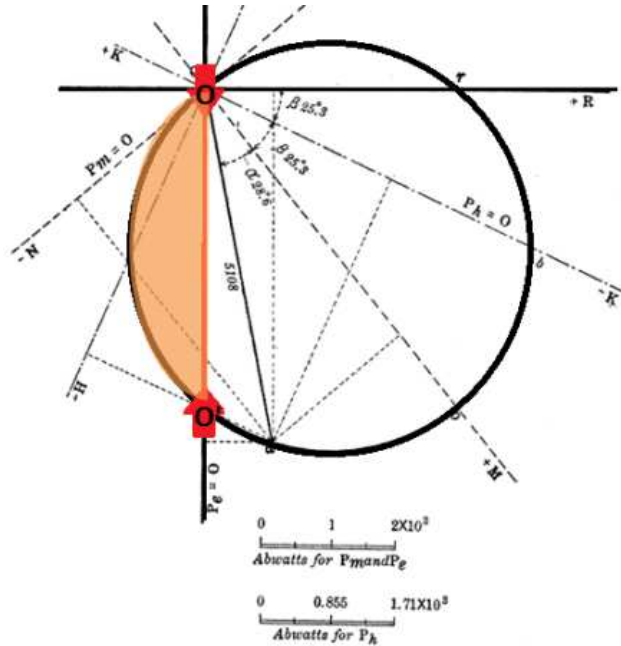


FIG. 27—MOTIONAL POWER DIAGRAM

Figure 2.5: An example of the motional power diagram introduced by Kennelly and Nukiyama (1919). The x-axis and y-axis show resistive and reactive parts of the motional power respectively. When the resistance becomes negative (the left shaded part of the red line, O-O', on the circle), power supplied from the electric part of the system no longer exists (It does not provide the mechanical power onto the diaphragm). Therefore (referencing at the electrical side) this part of the power is “active mechanical (motional) power”. All power in this region is consumed for hysteresis loss when the diaphragm is released (diaphragm is going back to its original position).

1069

1070 Kennelly and Kurokawa published a fourth technical paper in 1921. The objective
1071 of this paper is to describe some techniques to measure acoustic impedance including
1072 various constants introduced in his three previous papers. Starting from definition of
1073 mechanical impedance, the author explains specific ways of measuring the motional
1074 impedance, mechanical impedance, and surge impedance. They also introduce a
1075 method to calculate the mechanical impedance (z_m) from Z_{mot}

$$z_m = \frac{A^2}{Z_{mot}} \text{ [vector ohm]}, \quad (2.36)$$

1076 where A is a complex constant, representing the force factor. Note that this equation
1077 is presented as equation 16 in the original paper (Kennelly and Kurokawa, 1921).
1078 This was before the anti-reciprocal gyrator was invented. Dividing the complex
1079 constant A^2 by the measured Z_{mot} , z_m at a single frequency (including the size
1080 and the slope) is obtained. Repeating this calculation for several frequency points,
1081 the total z_m is determined. An example of z_m is shown in Fig. 2.6, along with its
1082 theoretical value. The theoretical impedance for a shorted transmission line (the
1083 dashed line in Fig. 2.6) is defined as

$$z_0 \tanh(\beta l), \quad (2.37)$$

1084 where z_0 , β are the surge impedance and wavenumber ($\beta = 2\pi/\lambda$, λ is the wave-
1085 length), and l is the length of the transmission line.

1086 Acquiring values to calculate mechanical impedance (z_m , Eq. 2.36) seems some-
1087 what troublesome and inefficient. Historically, this work can be viewed as the
1088 first measurement of a mechanical impedance z_m purely from electrical measure-
1089 ments. Four years later Kennelly published a paper (Kennelly, 1925) specific to
1090 this idea based on the preliminary data from the work with Kurokawa (Kennelly and
1091 Kurokawa, 1921), for measuring acoustic impedance electrically (Hunt, 1954).

1092 **Wegel 1921** Besides Kennelly, Wegel also considered Z_{mot} in his 1921 paper. This
1093 paper is credited by Hunt as the forefather of Hunt's 1954 two-port matrix repre-

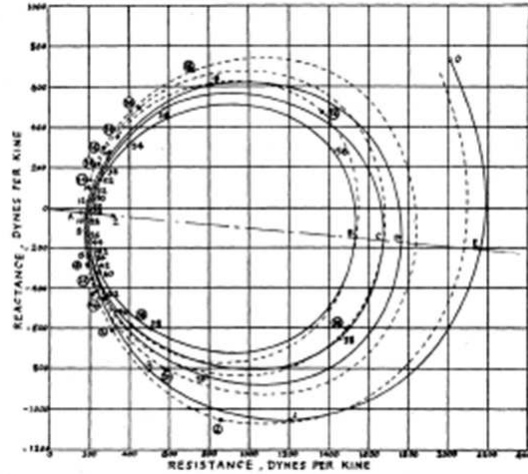


Figure 2.6: The calculated z_m (Eq. 2.36) graph by inverting Z_{mot} and then multiplying by the complex force factor A^2 (Eq. 2.36). Solid curve is obtained by connecting observation values at each frequency point. The dotted line represents the computed (theoretical) values Eq. 2.37. Note that this image is shown as Figure 9 in the original manuscript (Kennelly and Kurokawa, 1921).

1094 sentation (Eq. 2.1). Wegel takes account of the general theory of receiver structures
 1095 using a simple schematic having four coils. As applications, he takes four different
 1096 specific cases of a receiver: a simple receiver, a receiver with eddy currents in the core,
 1097 a simple induction-type receiver, and an electro-dynamics receiver. One interesting
 1098 point is he mentioned the effect of the eddy current, which decreases proportional
 1099 to square root of the frequency when it flows around the core surface (page 797 on
 1100 the last paragraph, Wegel (1921)). However the author did not derive any specific
 1101 formula for this phenomenon, as it was simply an experimental observation. As a
 1102 matter of fact, the observation of this phenomenon (the diffusion wave's impedance
 1103 $\propto \sqrt{\text{frequency}}$) has a long history. To fully appreciate this fact, the observation was
 1104 related to the eddy current, the current flow from primary magnetic field, and finally
 1105 analyzed using Maxwell's equation as carefully analyzed by Vanderkooy (1989), lead-
 1106 ing to the first definition of the semi-inductor with its impedance of $Z_{semi} = K\sqrt{s}$.

1107 **Investigation of the circular shape of Z_{mot}** In terms of the “polar” impedance
 1108 plane, Z_{mot} is a circle passing through the origin (Kennelly and Affel, 1915). Ex-

1109 plaining the unusual shape may be explained in the physical nature of anti-reciprocal
 1110 electro-mechanic system. The left side circuit (1) in Fig. 2.7 describes a (typical)
 1111 mechanical electro-mechanic network. The series of a damper, a mass and a stiff-
 1112 ness of the system are represented as circuit components R , L , and C respectively.
 1113 The Z_{mot} is defined as mechanical characteristic observed in electrical side, therefore
 1114 simulation of these three main mechanical elements on the electrical side is our main
 1115 concern.

1116 Two circuits shown in Fig. 2.7 are functionally equivalent, (1) is physically intuitive
 1117 due to using a gyrator, (2) is dual version of (1) via the mobility analogy (Firestone,
 1118 1938). Figure 2.8 simulates the two circuit cases in Fig. 2.7; blue line (1) without
 1119 gyrator (purely mechanical case) and red line (2) decoding the gyrator using mobility
 1120 method to see mechanical behavior on electrical input side. The upper and lower
 1121 plots in left plane represent magnitude and phase of input impedance and the right
 1122 polar plot shows real and imaginary parts of the impedance.

1123 In Fig.2.8, the red circle on the polar plot (Z_{dual}) shows Z_{mot} which is the dual of
 1124 Z_M namely,

$$Z_M = R + \frac{1}{sC} + sL \Big|_{R,L,C=1} = 1 + \frac{1}{j\omega} + j\omega = \begin{cases} \infty & \omega \rightarrow \infty \\ 1 & \omega \rightarrow 1 \\ -\infty & \omega \rightarrow -\infty \end{cases}, \quad (2.38)$$

1125

$$Z_{dual} = \frac{1}{R} || sC || \frac{1}{sL} \Big|_{R,L,C=1} = \frac{1}{1 + j\omega + \frac{1}{j\omega}} = \begin{cases} 0 & \omega \rightarrow 0 \\ 1 & \omega \rightarrow 1 \\ 0 & \omega \rightarrow \infty \end{cases}. \quad (2.39)$$

1126 The reason we have a circle shape of Z_{mot} is because, we are observing mechanical
 1127 behavior across the gyrator. Note that F_c stands for the transition frequency between
 1128 C (low frequency) and L (high frequency) for both original and dual of magnitude
 1129 and phase plots. In polar plots, when $\Im Z \rightarrow +\infty$, Z is dominated by L and in case
 1130 of $\Im Z \rightarrow -\infty$, Z depends on C .

1131 One may suggests a refined model of Z_{mot} based on Fig. 2.7. The only difference
 1132 between real experimental data of Z_{mot} and the simulation in Fig. 2.8 is angular



Figure 2.7: The corresponding circuits for Fig. 2.8 (1) and (2), before (1) and after (2) mobility networking. Due to the gyrator, the mechanical components becomes dual when they are seen on the electrical side of the network. As investigated in Fig. 2.8, this makes the shape of the Z_{mot} circle.

1133 rotation of the circle (to clockwise direction) pivoted the circle at the origin, which
 1134 will introduce the negative real part in Z_{mot} . One way to realize this model is to add
 1135 a phase delay in the system ($e^{-j\phi(\omega)}$) along with mechanical circuits.

1136 Rotating the circle toward the negative real part is related to any shunt loss in
 1137 electrical part of the system. The details are discussed in section 2.4.3.

1138 2.4.1 Definition of Z_{mot}

1139 Physically, Z_{mot} can be interpreted as the impedance of the mechanical side of the
 1140 system as seen from the electrical input. Z_{mot} was first defined (Kennelly and Pierce,
 1141 1912) by taking a difference between the mechanical open and the short circuit
 1142 conditions, of electrical input impedance.

1143 Starting from Hunt's impedance matrix (Eq. 2.1), we see that

$$\Phi = Z_e I + T_{em} U, \quad (2.40a)$$

1144

$$F = T_{me} I + Z_m U. \quad (2.40b)$$

1145 When the force 'F' is zero, i.e., "shorting out" the mechanical side, the electrical
 1146 input impedance is

$$\frac{\Phi}{I} = Z_e + \frac{T_{em} U}{I}, \quad (2.41a)$$

1147 and

$$\frac{U}{I} = -\frac{T_{me}}{Z_m}. \quad (2.41b)$$

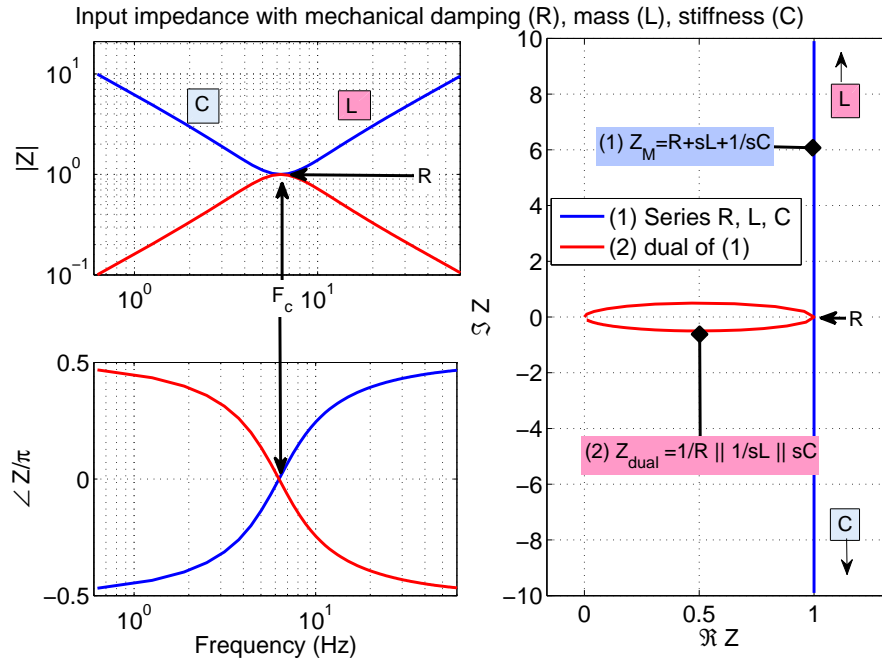


Figure 2.8: This figure explains the circular shape of Z_{mot} where the motion of the mechanical behavior (i.e., damping (loss), mass, and stiffness) projected to the electrical side defines Z_{mot} . When the mechanical behavior are seen on the electrical input side, due to the gyrator, the series mechanical network becomes a dual network based on the mobility analogy. The blue line shows input impedance based on the series relationship ((1) in Fig. 2.7 without considering the gyrator) while the red line represents the dual. The upper-left, lower-left plots show magnitude and phase of impedance and the right plot (polar plot) shows real and imaginary parts of the impedance. The red circle on the polar plot justifies the circular shape of Z_{mot} . F_c stands for the transition frequency between C (low frequency) and L (high frequency) for both original and dual of magnitude and phase plots. In polar plots, if $\Re Z \rightarrow +\infty$, Z is dominated by L and in case of $\Re Z \rightarrow -\infty$, Z depends on C . Note that this figure only discusses the shape of typical Z_{mot} , not its negative real parts. For simplification, values for L , R , and C are '1' in this simulation.

1148 The “shorted” electrical input impedance is

$$Z_{in}|_{F=0} = \frac{\Phi}{I}|_{F=0} = Z_e - \frac{T_{em}T_{me}}{Z_m} = Z_e + Z_{mot}. \quad (2.42)$$

1149 Thus Z_{mot} may be interpreted as the difference between the two mechanical boundary
1150 conditions on the electrical impedance (Z_{in})⁵:

1151 1) Z_{in} with freely oscillating (vibrating) mechanical side (F=0: short circuit con-
1152 dition, Eq. 2.42),

1153 2) $Z_{in} = Z_e$ when the mechanical system is not allowed to move (U=0: open circuit
1154 condition, Eq. 2.2),

$$\boxed{Z_{mot} = Z_{in}|_{F=0} - Z_{in}|_{U=0}}. \quad (2.43)$$

1155 **Z_{mot} definition using Hunt parameters** For the computational benefits, we can
1156 also define Z_{mot} from ABCD matrix parameters introduced in Eq. 2.6,

$$Z_{mot} = \frac{\Phi}{I}|_{F=0} - \frac{\Phi}{I}|_{U=0} = \frac{B}{D} - \frac{A}{C} = -\frac{\Delta_T}{DC} = \frac{1}{DC}, \quad (2.44)$$

1157 where A, B, C, D are the transmission matrix parameters described in Eq. 2.6. Note
1158 that the determinant of the transmission matrix (Δ_T) for an anti-reciprocal network
1159 is always ‘-1’.

1160 To satisfy the positive real (PR) property of Brune’s impedance (Brune, 1931),

$$\Re Z(s) \geq 0. \quad (2.45)$$

1161 In Eq. 2.43, it is obvious the two individual terms $Z_{in}|_{F=0}$ and $Z_{in}|_{U=0}$ are PR
1162 functions as they are physical, real impedances. A sum, or product of two PR
1163 functions has to be PR, but a difference, which is Z_{mot} , will not be a PR function
1164 when $\Re Z_{in}|_{U=0} > \Re Z_{in}|_{F=0}$. Thus Z_{mot} is not a physically realizable impedance.
1165 This because it is a transfer impedance, not a driving point impedance.

⁵The electrical conditions “open” and “short” are equivalent to the mechanical terms, “blocked” and “free”, respectively. Electrically “open” means no current while “blocked” means no velocity.

1166 To be more detail on the problem, Eq. 2.43 may be written as

$$\boxed{Z_{mot} = -\frac{T_{em}T_{me}}{Z_m} = -T_{em}T_{me}Y_m}, \quad (2.46)$$

1167 where $Y_m = \frac{1}{Z_m}$ is mechanical admittance, which is PR. Therefore the answer to
 1168 our question is reduced to investigation of the two transfer impedances' product
 1169 $T_{em}T_{me}$. According to Hunt, $T_{em} = B_0l$, which is real and positive. We know that
 1170 where $T_{em} = T_{me}$ the system is reciprocal and when $T_{em} = -T_{me}$, the system is
 1171 anti-reciprocal.

1172 The question here is, if Z_{mot} is PR. If the transfer impedances are real, then Z_{mot}
 1173 must be PR. However, if they are complex, then Z_{mot} could have negative real parts
 1174 (negative resistance). It has been observed (e.g., Fig. 2.5), the motional power has
 1175 negative real parts.

1176 2.4.2 Z_{mot} interpretation with Eq. 2.46

1177 If we define Z_{mot} using Eq. 2.46 (with Eq. 2.3, Eq. 2.4, and 2.5), Z_{mot} can be rein-
 1178 terpreted as

$$Z_{mot} = -\frac{\Phi_{I=0} F_{U=0} U_{I=0}}{U_{I=0} I_{U=0} F_{I=0}}, \quad (2.47)$$

1179 where $U_{I=0}$ terms are in both T_{em} and Z_m canceled out. This definition is inter-
 1180 preted based on the system's signals, is quite different from Kennelly's experimental
 1181 definition shown in Eq. 2.43. So the remaining four terms represent Z_{mot} , which is

$$Z_{mot} = -\frac{\Phi_{I=0} F_{U=0}}{I_{U=0} F_{I=0}}. \quad (2.48)$$

1182 Lorenz force (\mathbf{F}_L) is

$$\mathbf{F}_L = q(\mathbf{E} + \mathbf{U} \times \mathbf{B}), \quad (2.49)$$

1183 where q , \mathbf{E} , \mathbf{U} , and \mathbf{B} represent a point charge, electric field, particle velocity, and
 1184 magnetic field respectively. From Eq. 2.49 one can infer the two terms $F_{U=0}$, $F_{I=0}$

Draft of November 2, 2014 at 17:33

1185 in Eq. 2.48 are $q\mathbf{E}$, and $q\mathbf{U} \times \mathbf{B}$ (or $q\mu\mathbf{U} \times \mathbf{H}$, $\mathbf{B} = \mu\mathbf{H}$).⁶

1186 Also one may view $\Phi_{I=0}$ in Eq. 2.48 is the Thevenin voltage (Φ_{Th}) considering only
 1187 the electrical side of the network (one-port system's open circuit voltage). And $I_{U=0}$
 1188 is the electrical side's Norton current (I_{No}), as the U across the gyrator becomes Φ ,
 1189 therefore the $U = 0$ is equivalent to $\Phi = 0$, the shorted condition. The ratio of the
 1190 Thevenin voltage and the Norton current is the Thevenin electrical impedance (Z_{Th})
 1191 representing the electrical side of the network ($\frac{\Phi_{Th}}{I_{No}} = Z_{Th}$). Recall and compare Z_{Th}
 1192 to Z_e from Eq. 2.2, the open circuit electrical impedance.

1193 To sum up: Eq. 2.48 can be rewritten as (scalars in frequency domain)

$$Z_{mot} = -\frac{\Phi_{I=0}}{I_{U=0}} \frac{F_{U=0}}{F_{I=0}} = -\frac{\Phi_{Th}}{I_{No}} \frac{q\mathbf{E}}{qU\mathbf{B}} \quad (2.50)$$

1194 where \mathbf{B} , \mathbf{E} represents scalar magnetic flux density and electric field in frequency
 1195 domain respectively.

1196 Finally we have

$$Z_{mot} = -Z_{Th} \frac{q\mathbf{E}}{qU\mathbf{B}} = -Z_{Th} \frac{\mathbf{E}}{\mu U \mathbf{H}}, \quad (2.51)$$

1197 where U , \mathbf{H} are scalars in frequency domain.

1198 From Eq. 2.51, we can consider the motional impedance as affected by the electrical
 1199 impedance (Z_{Th}), as well as the mechanical velocity (U).

1200 The semi-inductor (related to the magnetic diffusion wave) elaborated on Eq. 2.51
 1201 is part of Z_{mot} , causing the negative real parts. When the wave is diffusive, the
 1202 diffusion time constant (delay) can be characterized by the velocity \mathbf{U} . In Vanderkooy
 1203 (1989, p.127), the author says “physically, for an applied voltage step (i.e., \mathbf{E} in
 1204 Eq. 2.51), the coil will try to create a magnetic field (i.e., \mathbf{H} in Eq. 2.51) which takes
 1205 a while to diffuse into the iron. Hence there will be no back emf for the first instant,
 1206 and the current waveform will rise sharply at the leading edge.” Highlighting the
 1207 words “takes a while,” may be interpreted as the delay resulting from the velocity
 1208 \mathbf{U} . Thus the voltage lags behind the current. When $U = 0$, there is no back emf.

⁶The current $I = \int \mathbf{J} \cdot d\mathbf{S}$. Based on Eq. 2.49, \mathbf{J} can be defined in two different ways, $\mathbf{J}_e = \sigma\mathbf{E}$ and $\mathbf{J}_m = q\mathbf{U}$. The zero current specified in $F_{I=0}$ is relevant to $\mathbf{J}_e = 0$, as the condition of U is still unspecified, therefore $F_{I=0}$ indicates the magnetostatic force, $q\mathbf{U} \times \mathbf{B}$.

1209 Note that $\Phi = -B_0 l U$ is the anti-reciprocal equation of the gyrator. Detail discussion
 1210 may be found in section 2.5.3, Eq.2.81.

1211 When the velocity U is zero, there is no magnetic force ($q\mathbf{U} \times \mathbf{B} = q\mu\mathbf{U} \times \mathbf{H} = 0$
 1212 in Eq. 2.49). Because the magnetic force is defined, when and only when, a charge
 1213 is moving. However, the electric force ($q\mathbf{E} = 0$ in Eq. 2.49) exists with a stationary
 1214 charge q (charge is not moving, zero velocity). Therefore the denominator in Eq. 2.51
 1215 lags behind the numerator, and this phase shift can make a part of Z_{mot} 's real parts
 1216 negative.

1217 2.4.3 Z_{mot} interpretation with Eq. 2.43

1218 In this section, we search for a realizable (simple) circuit such that Z_{mot} has a negative
 1219 real part. Figure 2.9 demonstrates a case where a difference of two input impedances
 (Z_{in} with different boundary conditions) goes negative.

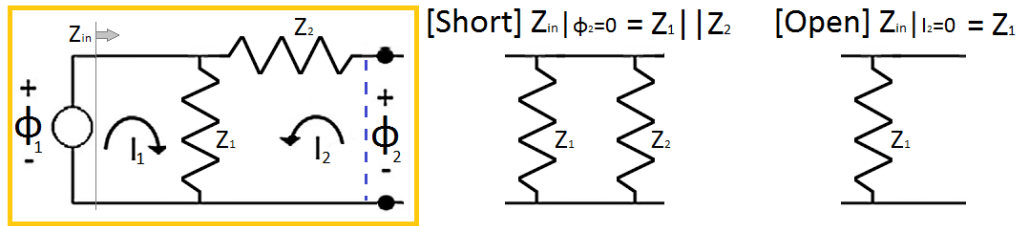


Figure 2.9: Demonstration of Z_{mot} 's negative real part using a simple circuit example

1220
 1221 For example, taking $Z_1 = Z_2 = 100\Omega$. Based on the definition of Z_{mot} (Eq. 2.43),
 1222 subtracting the open circuit impedance from the short circuit impedance results in
 1223 -50Ω ($Z_{in} |_{\phi_2=0} - Z_{in} |_{I_2=0} = Z_1 || Z_2 - Z_1 = 50\Omega - 100\Omega$). This simplest example tells
 1224 us a lot about the nature of Z_{mot} , as well as modeling the electro-mechanic system.

1225 Let's consider a real example, an electro-mechanic system. If there is no **SHUNT**
 1226 resistance (i.e., Z_1) in a system, Z_{mot} cannot have negative real part, as may see
 1227 from Fig. 2.9. The physical meaning of the 'shunt' is this: any current through the
 1228 shunted component cannot be seen from the other components. The only physical
 1229 place for this (shunt component) loss is in the eddy-current, the diffusing current into

1230 magnetic core. It has been shown experimentally since Kennelly and Pierce (1912),
1231 that Z_{mot} has negative real parts. This fact supports the view that a shunt loss in
1232 the electrical side of the system must contribute to this loss (semi-inductor) when
1233 modeling the system (Kim and Allen, 2013).

1234 In the results (section 4.3), we study Z_{mot} from the physically based/simplified
1235 electro-mechanic system. The real part of Z_{mot} (Eq. 2.43, Eq. 2.46) from the sug-
1236 gested two-port network is the target of our investigation. Also in Appendix D, we
1237 reconsider Z_{mot} formula based on each parameter's spatial relationship.

1238 2.5 Hidden, quasi-static assumptions in classic circuit 1239 theories

1240 We revisit classic theories related to the anti-reciprocal circuit networks, such as
1241 KCL, KVL, the gyrator, and the semi-inductor. The purpose is to clarify quasi-
1242 static limitations in each well-known formula with derivations starting with Maxwell's
1243 equations.

1244 2.5.1 Arguments about quasi-static approximation

1245 The objective of this section is to devise another working definition of the quasi-static
1246 assumption. Starting from a physical example, such as the human ear, we claim that
1247 the key feature of the QS approximation is the absence of accuracy to describe a
1248 pure delay. To deal with this pure delay, one must use the reflectance Γ .

1249 Figure 2.10 represents the acoustic impedance of the human ear in terms of elec-
1250 trical elements. Figure 2.10(a) is the network representations of the impedance of
1251 the stapes and cochlea (Lynch et al., 1982). In Fig. 2.10(b), we simplified this origi-
1252 nal model by considering only the significant components, the cochlear resistance R_c
1253 and nonlinear stiffness of the annular ligament C_{AL} . For this simplified version, the

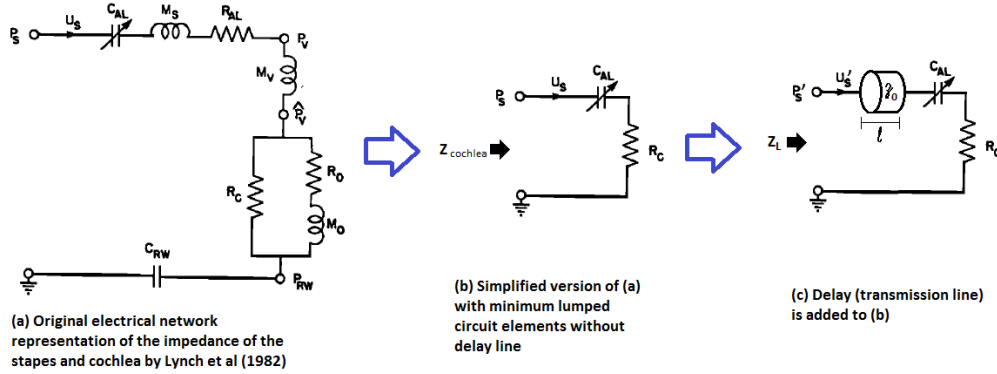


Figure 2.10: Electrical lumped circuit representations of the cochlea (adapted from Lynch et al. (1982)). (a) and (b) employ the quasi-static assumption where (b) is a simplified version of (a). A transmission line (length l and characteristic resistance r_0) is used in (c), which introduces the pure delay $\tau = l/c$ forcing Z_L to be non-quasi-static.

1254 cochlear impedance is

$$Z_{cochlea} = R_C + \frac{1}{sC_{AL}}. \quad (2.52)$$

1255 Note that both Fig. 2.10(a) and Fig. 2.10(b) use lumped (Brune's) circuit elements
 1256 constituting a QS approximation, having a band-limited system delay, not a pure
 1257 delay.

1258 To include the effect of the ear canal and ear drum delay (that is a pure delay)
 1259 (Puria and Allen, 1998), a transmission line (i.e., ear canal) is added, as shown
 1260 in Fig. 2.10(c), with two extra parameters, length l and characteristic impedance
 1261 $r_0 = \frac{\rho c}{A}$. Note that ρ , c , and A are the air density, speed of sound, and area of ear
 1262 canal, respectively. When $l \rightarrow 0$, the reflectance of this network is

$$\Gamma_0 = \frac{Z_{cochlea} - r_0}{Z_{cochlea} + r_0} = \frac{Z_0 - 1}{Z_0 + 1}, \quad (2.53)$$

1263 where $Z_0 = Z_{cochlea}/r_0 = \frac{R_C}{r_0} + \frac{1}{sC_{AL}r_0}$ is the normalized cochlear input impedance.
 1264 Then reflectance at the measurement location L (Γ_L) is

$$\Gamma_L = \Gamma_0 e^{-s\tau} = \Gamma_0 e^{-j\omega 2L/c}, \quad (2.54)$$

1265 where $s = \sigma + j\omega$ is the Laplace frequency and $2L/c$ is the pure delay, τ . Thus, the
 1266 impedance at the measured point L becomes

$$Z_L = r_0 \frac{1 + \Gamma_L}{1 - \Gamma_L}. \quad (2.55)$$

1267 This model has been verified many times (Lynch et al., 1982; Puria and Allen, 1998;
 1268 Parent and Allen, 2010)

1269 The final impedance does not obey the QS assumption (i.e., it is non-QS) due to
 1270 the delay τ . It would require an infinite number of poles and zeros to form a QS
 1271 approximation of this model, due to the delay. Note that the difference between
 1272 Eq. 2.52 and Eq. 2.55 is in the delay $\tau = 2L/c$.

1273 The simulation comparison between Eq. 2.52 (QS) and Eq.2.55 (non-QS) is shown
 1274 in Fig.2.11. The very simple distinction between non-QS and QS is the number of
 1275 poles and zeros. In the case of QS ($Z_{cochlea}$ red line), there is 1 pole and 1 zero, while
 1276 in the non-QS case (Z_L , blue line), the system has an infinite number of poles and
 zeros.

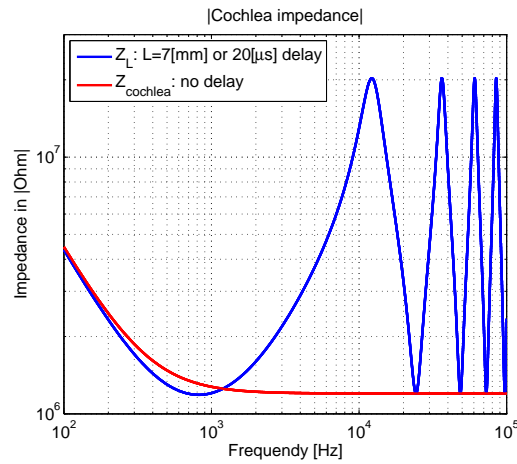


Figure 2.11: Input impedance simulation based on Fig.2.10. Values for the simulation are followed: Cochlea resistance $R_c = 1.2e6[\text{dyn} - \text{s}/\text{cm}^5]$, stiffness of the annular ligament $C_{al} = 0.37e - 9[\text{cm}^5/\text{dyn}]$, air density $\rho = 1.14[\text{kg}/\text{m}^3]$, speed of sound in room temperature $c = 340[\text{m}/\text{s}]$, area of ear canal $A = r^2 * \pi[\text{m}^2]$ with $r = 0.5[\text{cm}]$, and length of ear canal $L = 0.7[\text{cm}]$.

1277

1278 Next, we will show how this example is equivalent to the traditional quasi-static
1279 description, namely, the low-frequency or long-wave approximations.

1280 Quasi-static in electromagnetism

1281 The origin of QS approximation is not clear. However, the QS assumption has been
1282 widely used in classic circuit analysis, such as Kirchhoff's circuit laws (KCL and
1283 KVL, 1845). Efforts to search for the beginning of the QS in history can be found
1284 in Appendix A.

1285 In 1865, James Clerk Maxwell completed his full mathematical description of
1286 electro-magnetic fields using Michael Faraday's theory,⁷

$$\nabla \cdot \mathbf{D} = \rho \quad (2.56a)$$

$$\nabla \cdot \mathbf{B} = 0 \quad (2.56b)$$

$$\nabla \times \mathbf{E} = -\frac{\partial \mathbf{B}}{\partial t} \quad (2.56c)$$

$$\nabla \times \mathbf{H} = \mathbf{J} + \frac{\partial \mathbf{D}}{\partial t}. \quad (2.56d)$$

1290
1291 Regardless of the appreciation for the QS theorem in Maxwell's time, the concept
1292 of QS can be applied to Eq. 2.56 by disregarding either the magnetic induction $\dot{\mathbf{B}}$
1293 (electro-quasi-static, EQS) or the electric displacement current $\dot{\mathbf{D}}$ (magneto-quasi-
1294 static, MQS, Woodson and Melcher (1968)). With either of those terms removed,
1295 there can be no delay, since wave equation does not exist.

1296 In EQS, \mathbf{E} is irrotational since $\nabla \times \mathbf{E} = -\frac{\partial \mathbf{B}}{\partial t} \approx 0$ and $\nabla \cdot \mathbf{D} = \nabla \cdot \epsilon_0 \mathbf{E} = \rho$.
1297 Therefore, the curl and divergence of \mathbf{E} specify the charge density ρ . In the case of
1298 MQS, \mathbf{H} is rotational (solenoidal) as the divergence of \mathbf{H} is zero ($\nabla \cdot \mu_0 \mathbf{H} = 0$) and
1299 $\nabla \times \mathbf{H} = \mathbf{J} + \frac{\partial \mathbf{D}}{\partial t} \approx \mathbf{J}$. Once the current density \mathbf{J} is known, the curl and divergence

⁷The original Maxwell's equations were written in 20 equations with 20 variables using quaternion. It was Oliver Heaviside who reformulated them into four vector equations having 4 variables by using curl and divergence vector operators (1884).

1300 of \mathbf{H} can be solved in MQS.

1301 To illustrate this, one can imagine a source distribution in each case (EQS with
1302 ρ or MQS with \mathbf{J}). The solution for these equations ignores the delay between the
1303 source and measurement points (i.e., functionally, $c \rightarrow \infty$). Thus, each field (EQS
1304 with \mathbf{E} or MQS with \mathbf{H}) at a certain instant will be governed by its source, ρ or \mathbf{J} .

1305 One interesting comparison is that in both the EQS and MQS situations, similar to
1306 Kirchhoff's circuit laws, the time-derivative terms are not considered. EQS ignores
1307 the $\dot{\mathbf{B}}$ term (KVL) and MQS ignores the $\dot{\mathbf{D}}$ (KCL). Sommerfeld (1964) explained
1308 this as "neglecting retardation of fields."

1309 However, the QS definition used for MQS and EQS does not mean setting $\frac{\partial}{\partial t} \rightarrow 0$.
1310 For instance, impedance of lumped circuit elements (i.e., capacitors or inductors)
1311 cannot be defined if $\frac{\partial}{\partial t} \rightarrow 0$. Such elements are also known as the QS "Brune's
1312 impedance" (Brune, 1931; Van Valkenburg, 1960, 1964). Therefore, it is critical to
1313 search for a precise way to define QS systems.

1314 Quasi-static descriptions

1315 The QS assumption is loosely defined via the long wave approximation

$$kl \leq 1, \tag{2.57}$$

1316 where $k = \frac{2\pi}{\lambda} = \frac{2\pi f}{c}$ is the wave number (f is the frequency and c is the speed of
1317 sound or light) and l is the circuit dimension (Sommerfeld, 1964).

1318 This QS description (Eq. 2.57) involves inequalities (i.e., \geq , or \leq operator), which
1319 makes it confusing to specify each system's QS status. Moreover, when we deal with
1320 a physical system, such as the middle ear or a loudspeaker, it becomes even more
1321 difficult to properly characterize the QS system because of the relatively slow speed
1322 of sound. A more precise definition for QS is not based on inequalities. We shall
1323 deal with the proper definition depends on delay (The QS systems have no internal
1324 delay).

1325 Transmission line and a pure delay

1326 Ohm's law (1781) represents the ratio of the voltage over the current as an impedance.⁸
1327 The now classical definition of QS impedance was first stated by Brune (1931). He
1328 characterized a *point impedance* (Eq. 2.57) as a positive-real (PR) quantity (positive-
1329 definite operator in matrix version), meaning that an impedance cannot have a neg-
1330 ative resistance as discussed in section 2.2.1 (postulate B1) which is proved by Van
1331 Valkenburg (1960, 1964).

1332 Brune's impedance is consistently studied with KCL and KVL under the QS con-
1333 dition because it assumes no delay ($\tau = 0$) in the system (Fig. 2.10 (a), (b)). For
1334 instance, wire delay in the system is ignored. A Brune impedance network is rep-
1335 resented using lumped circuit elements such as resistors, inductors, and capacitors,
1336 but not delay. All Brune's impedances are minimum phase (MP), because every PR
1337 function must be MP. Thus a Brune impedance is QS, PR, and MP. We shall see
1338 that the more general "wave impedance" is PR but not QS (section 2.2).

1339 A transmission line is a natural element to represent delay. Under the QS as-
1340 sumption, we assume no delay (i.e., no transmission line). A transmission line is
1341 a two-port network, which can be interpreted as the physical cable connecting the
1342 circuit components. As shown in Fig. 2.10, a transmission line is required for phys-
1343 ical modeling of the middle ear and electro-acoustic transducers, especially where
1344 a delay plays a significant role in understanding the system (Kim and Allen, 2013;
1345 Parent and Allen, 2010). The transmission line becomes critical when the signal's
1346 wavelength is similar to or less than l . A delay (τ) is related to this l , defined as
1347 $\tau = l/c$, where c is the speed of sound or light. Note that any system exhibiting
1348 modes requires a delay.

1349 A low-frequency approximation of a transmission line, using lumped elements,
1350 is effectively a Brune approximation satisfying PR (postulate B1 in section 2.2.1).
1351 A popular and simple loss-transmission line approximation uses four elements: L
1352 (series inductance per unit length), R (DC resistance per unit length), C (shunt
1353 capacitance between the two conductors per unit length), and G (shunt conductance

⁸At that time, the theory of impedance was applied only to resistance. It was Arthur Edwin Kennelly in 1893 who first suggested using the impedance concept in AC circuit.

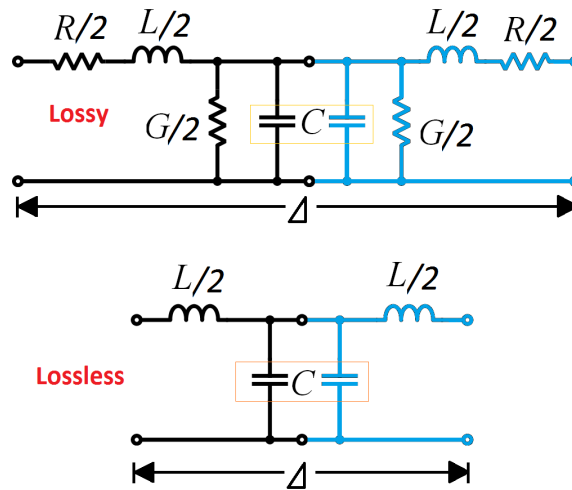


Figure 2.12: An infinitesimal unit of a transmission line (in the limit as $\Delta \rightarrow 0$) having primary line constants, L (series inductance or mass per unit length [H/m]), R (series resistance per unit length [Ω/m]), C (shunt capacitance or compliance per unit length [F/m]), and G (shunt conductance per unit length [S/m]). The upper figure represents a loss case while the lower figure is lossless case. Transmission segments are mirrored (shown in blue) to represent reversible transmission lines. By taking $\Delta \rightarrow \infty$, this goes from a QS to a true transmission line having a delay.

1354 per unit length). In the lossless case, R and G can be ignored.⁹ The remaining
 1355 circuit elements, L and C , represent an elementary unit of the lossless Brune (QS)
 1356 transmission line. Usually infinite numbers of these units are cascaded when defining
 1357 a transmission line. In terms of the transmission line per-length parameters (divided
 1358 by the line length Δ), characteristic impedance r_0 and propagation constant κ are
 1359 computed as

$$r_0 = \sqrt{\frac{\mathcal{Z}}{\mathcal{Y}}}, \kappa = \sqrt{\mathcal{Z}\mathcal{Y}}, \quad (2.58)$$

1360 , where $\mathcal{Z}|_{\Delta \rightarrow 0} = R + sL$, $\mathcal{Y}|_{\Delta \rightarrow 0} = G + sC$, and $s = j\omega$. Note that \mathcal{Z} and \mathcal{Y} are
 1361 function of s (inverse Laplace transform exists, causal, analytic functions). In the
 1362 lossless case $r_0 = \frac{L}{C}$, $\kappa = s\sqrt{LC}$. As shown in Fig. 2.12, the QS input impedance is

$$Z_{in,QS} = s(L/2) + \frac{1}{sC} \Big|_{@lowfreq} \approx \frac{1}{sC}, \quad (2.59)$$

1363 .

1364 However, the model for a true transmission line having delay, such as a coaxial
 1365 cable, will differ from this QS transmission line segment (Eq.2.59). Cascading an
 1366 infinite number of AS transmission line units and using Eq. 2.58, the input impedance
 1367 of the transmission line becomes

$$Z_{in} = \frac{\Phi}{I}. \quad (2.60)$$

1368 The voltage Φ (in frequency domain) and current I are composed with outbound
 1369 (+) and inbound (-) waves as

$$\Phi(x, \omega) = \Phi^+ e^{-\kappa x} + \Phi^- e^{+\kappa x}, \quad (2.61)$$

1370

$$I(x, \omega) = \frac{1}{r_0} (\Phi^+ e^{-\kappa x} - \Phi^- e^{+\kappa x}). \quad (2.62)$$

1371 Note that waves travel between $x = 0$ and $x = l$ based on each direction.

⁹This transmission line model was created by Oliver Heaviside based on Maxwell's equations.

1372 When we short the transmission line ($\Phi = 0$ or $Z_L = 0$),

$$Z_{in,short}(x) = r_0 \tanh(\kappa x), \quad (2.63)$$

1373 and if it is opened ($I = 0$ or $Z_L = \infty$),

$$Z_{in,open}(x) = r_0 \coth(\kappa x). \quad (2.64)$$

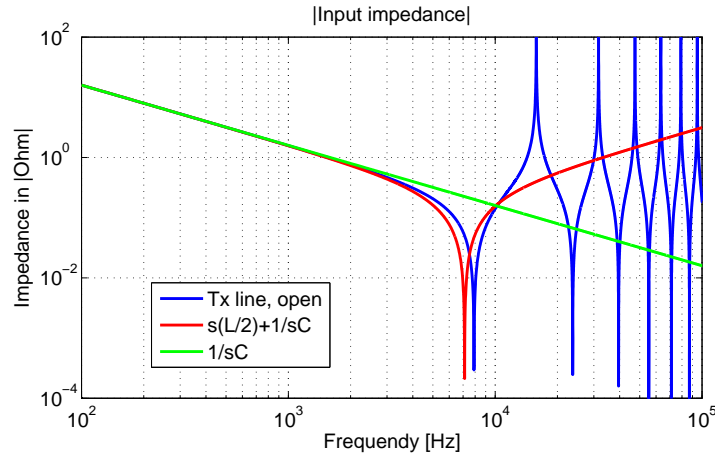


Figure 2.13: Simulation of transmission line input impedance from Eq. 2.59 and 2.63. Values for this specific example are $L = 1e - 5$ [H/m], $C = 1e - 4$ [F/m].

1374 Input impedance (magnitude) simulation results based on Eq. 2.59 and 2.64 are
1375 shown in Fig. 2.13. In this figure,

- 1376 1. **Blue line:** Infinite numbers of poles and zeros exist with the exact transmission
1377 line formula (Eq. 2.64). These poles and zeros (shown in impedance domain)
1378 come from delay (standing waves) based on the length of the line.¹⁰
- 1379 2. **Red line:** Number of poles and zeros is limited. There is one zero and one pole
1380 in this approximation. Compared to the blue line, this approximation works
1381 up to 2kHz.

¹⁰ $Z = \frac{1+\Gamma}{1-\Gamma}$, where the reflectance $\Gamma = e^{-s\frac{eL}{c}}$. When $\Gamma = \pm 1$, poles and zeros appear in impedance domain (magnitude), respectively. Note that L, c stand for the length of the line and speed of sound and the reflection of the wave relates to the standing wave.

1382 3. **Green line**: One pole at the origin, and no zero is found. This approximation
1383 works under 2kHz.

1384 There is a finite number of poles and zeros in the QS (lumped circuit) approximation
1385 (red and green), while poles and zeros are infinite for the transmission line model
1386 (blue).

1387 If a system is QS (having Brune's-type impedance), a finite number of poles and
1388 zeros exists. If it is not QS (non-QS, having a pure delay), then the number of poles
1389 and zeros is infinite. It follows that any system having a pure delay will have infinite
1390 numbers of modes without any exception. This is especially applicable for acoustical
1391 and mechanical systems because of the relatively slow speed of sound compared to
1392 the speed of light.

1393 Reinterpretation of quasi-static

1394 Signals (usually in wave form) and systems are distinguished in terms of causality.
1395 Signals are defined over all time support, $|t| \leq \pm\infty$, whereas in systems, the support
1396 is restricted to $t \geq 0$. The forwarding waves are typically reflected back if the network
1397 has a finite length. A traveling time difference between the forward and backward
1398 waves represents the group delay $\tau(\omega)$. Regardless of the speed of the wave, there is
1399 a system delay given a finite system length l .

1400 The QS approximation is a classic tool used to simulate and analyze electrical
1401 systems, assuming $\lambda \geq l$. However, this assumption does not always describe the
1402 physical reality. Critical examples include electro-acoustic networks, where the sys-
1403 tem's speed transits from one to the other (i.e., from the speed of light to the
1404 speed of sound). The ED7045 receiver (Knowles balanced armature receiver) has
1405 a $4.29 \times 6.5 \times 3$ [mm] dimension. Considering the frequency range of human hearing
1406 (20Hz to 20kHz) with the speed of sound (345[m/s]), the wave length λ calculated at
1407 20kHz is 17 [mm], which is compatible with the width of the receiver ($l = 6.5$ [mm]).
1408 It does not, however, satisfy the rule of thumb for $\lambda \geq l$; the calculated λ is less

1409 than 10 times that of l .¹¹ Also, acoustic networks having a fairly slow system speed
1410 compared to their frequency regions of interest is another example, such as the speed
1411 of sound on the eardrum relative to the speed of sound in air.

1412 Assume a train (1 mile in length, a very long train) has a speed of 60mph and
1413 someone slowly moves inside the train at a speed of 1mph for at least an hour. The
1414 QS approximation may be applied in this scene; an observer outside the train may
1415 think that the train and he are in the same border until he hits the end of the train.
1416 The observer feels that the speed is 60mph for at least an hour. When he hits the
1417 train wall, the QS approximation breaks. After one hour (if he breaks out the train
1418 wall), he and the train will be separated. The outside observer no longer thinks that
1419 he and the train are in the same location or have the same speed. The circumstance
1420 becomes non-QS when the two subjects are physically separated. Then, what is the
1421 meaning of relating the QS to delay? It means that the outside observer can discern
1422 his exact location inside the train at each time frame when he is moving around the
1423 train. This interpretation does not depend on the position of the person, whether
1424 inside or outside the train. The previous portion on the train is similar to the phase
1425 across the object where the phase is due to the delay (i.e., 90° is $\lambda/4$ while 180° is
1426 $\lambda/2$, half way down the train).

1427 In summary, we propose a more fundamental way to characterize the QS approx-
1428 imation. In describing a system as QS or non-QS, delay is the critical parameter as
1429 it determines the pole-zero frequency density. This definition does not violate the
1430 traditional descriptions of QS such as long-wave approximation; rather, it provides
1431 a precise analysis of the system.

¹¹In classical way, to apply QS in a system “ $ka \ll 1$ ” must satisfy. $ka = \frac{2\pi a}{\lambda} = \frac{2\pi 6.5}{17} \approx 2$ for our specific case, which does not satisfy the condition.

Draft of November 2, 2014 at 17:33

1432 2.5.2 Kirchhoff's voltage and current laws (KVL, KCL)

1433 **KVL** Equation 2.65 is the classical definition of KVL,

$$\sum_{k=1}^n \phi_k = 0, \quad (2.65)$$

1434 where ϕ_k is a voltage at each node k in a circuit.

1435 Starting from Faraday's law

$$\nabla \times \mathbf{E} = -\frac{\partial \mathbf{B}}{\partial t}, \quad (2.66)$$

1436 and applying Stoke's theorem, an electric potential (voltage) is defined as a line
1437 integral over an electric field.

$$\int (\nabla \times \mathbf{E}) \cdot d\mathbf{A} = -\frac{\partial}{\partial t} \int \mathbf{B} \cdot d\mathbf{A}, \quad (2.67)$$

1438 it equals to

$$\oint \mathbf{E} \cdot d\mathbf{l} + \frac{\partial}{\partial t} \underbrace{\int \mathbf{B} \cdot d\mathbf{A}}_{\Psi, \text{ flux}} = 0. \quad (2.68)$$

1439 The first term in Eq. 2.68 represents emf, the direction is opposite to the voltage.

$$\text{emf} \equiv \oint \mathbf{E} \cdot d\mathbf{l} = \int_a^b \mathbf{E}' \cdot d\mathbf{l} = -\phi(t), \quad (2.69)$$

1440 where E is the electric field intensity measured by an observer moving with the
1441 contour of the conductor and $\mathbf{E}' = \mathbf{E} - (\mathbf{u} \times \mathbf{B})$ (Woodson and Melcher, 1968) based
1442 on the quasi-static Lorenz force (Eq. 2.49). To arrive at the classical KVL, Eq. 2.65,
1443 the quasi-static assumption ($-\frac{\partial \mathbf{B}}{\partial t} = -\mu_0 \frac{\partial \mathbf{H}}{\partial t} = 0$) must be assumed. In other words,
1444 the classic KVL is valid when the magnetic field is not time-varying (i.e., a constant
1445 \mathbf{B}_0 or very slowly changing in time). The classic KVL equation deals with the quasi-
1446 static electric field with a stationary charge and thus assumes the electric field around
1447 a closed loop to be zero. Therefore Eq. 2.65 is a special, quasi-static case of KVL,

1448 in general form of KVL is

$$- \sum_{k=1}^n \phi_k + \dot{\Psi} = 0, \quad (2.70)$$

1449 where $\dot{\Psi}$ is time derivative of the magnetic flux Ψ . In a frequency domain Eq. 2.70
1450 becomes

$$- \sum_{k=1}^n \Phi_k + j\omega \underline{\Psi} = 0, \quad (2.71)$$

1451 where $\underline{\Psi} = L_m I$ represents the magnetic flux in frequency domain. Finally we have

$$\boxed{\sum_{k=1}^n \Phi_k = sL_m I}, \quad (2.72)$$

1452 meaning that, the sum of the Φ_k is the induced voltage (emf) in the right hand side is
1453 equal to the left hand side which represents the mutual inductance (L_m). Typically
1454 the leakage flux is considered as an undesirable effect (mutual inductive leakage flux).

1455 **KCL** To derive KCL, Gauss's law and Ampere's law (Eq. 2.73 and Eq. 2.74 respec-
1456 tively) must be used. Note that Eq. 2.74 and Eq. 2.102 are equivalent. The Gauss's
1457 law is

$$\nabla \cdot \mathbf{D} = \rho, \quad (2.73)$$

1458 and the Ampere's law is

$$\nabla \times \mathbf{H} = \mathbf{J} + \frac{\partial \mathbf{D}}{\partial t}. \quad (2.74)$$

1459 We apply a divergence theorem on Eq. 2.74, the left term ($\nabla \cdot (\nabla \times \mathbf{H})$) becomes
1460 zero as divergence of the curl is zero. Then assuming a quasi-static magnetic field,
1461 then $\frac{\partial \mathbf{D}}{\partial t} = 0$ (Eq. 2.74),

$$\nabla \cdot \mathbf{J} + \frac{\partial(\nabla \cdot \mathbf{D})}{\partial t} = \nabla \cdot \mathbf{J} + \frac{\partial \rho}{\partial t} = 0. \quad (2.75)$$

1462 Via the Divergence theorem,

$$\int (\nabla \cdot \mathbf{J}) \cdot d\mathbf{V} + \frac{\partial}{\partial t} \int \rho d\mathbf{V} = \int (\nabla \cdot \mathbf{J}) \cdot d\mathbf{V} + \frac{\partial Q}{\partial t} = \underbrace{\int \mathbf{J} \cdot d\mathbf{A}}_{i(t)} + \dot{Q} = 0. \quad (2.76)$$

1463 One can deduce the classical KCL from the Eq. 2.76. The net flux of current at
 1464 a point (node) is zero (the classic KCL assumption, no accumulating current at a
 1465 node) when we ignore the stray capacitance \dot{Q} . Therefore the correct KCL is,

$$\sum_{k=1}^n i_k + \dot{Q} = 0, \quad (2.77)$$

1466 and the frequency domain representation of Eq. 2.77 is,

$$\sum_{k=1}^n I_k + sQ = 0. \quad (2.78)$$

1467 Note that $Q = C\Phi$ is physically interpreted as stray capacitance (C) related to
 1468 current between two adjacent inductors. Usually it is considered to be an undesirable
 1469 effect (capacitive leakage current),

$$\boxed{\sum_{k=1}^n I_k = -sC\Phi}. \quad (2.79)$$

1470 Note that the difference in the sign for Eq. 2.72 and Eq. 2.79 follows from Lenz's
 1471 law.

1472 **Extension of KCL/KVL to include flux coupling and time delay** When
 1473 KVL and KCL are derived from Maxwell's equations, electrostatic and magnetostatic
 1474 assumptions (i.e., quasi-static) are used respectively in section 2.5.2. In the KCL
 1475 derivation, the coupling of a charge, due to a stray capacitance ($\frac{\partial \mathbf{D}}{\partial t}$), is ignored
 1476 while for the KVL the magnetic flux coupling (stray mutual inductance, $-\frac{\partial \mathbf{B}}{\partial t}$ in
 1477 Eq. 2.66) is ignored. That is, in both cases the time-dependent components in the

1478 Maxwell's equations are assumed to be negligible, since

$$\lambda \left(= \frac{c}{f} \right) \geq \text{circuit size} \quad (2.80)$$

1479 where 'c' is the speed of light, and 'f' is frequency of interest. This is a low frequency
1480 approximation where the standard KVL and KCL apply under the quasi-static as-
1481 sumption.

1482 However, the ignored terms in KVL or KCL have their own significance. For
1483 example, when current flows through a wire, there is a magnetic field created around
1484 the wire. The flux in a KVL loop has an induced flux (Ψ) that induces an emf ($\dot{\Psi}$).
1485 This term results in the anti-reciprocal coupling terms that requires the gyrator in
1486 the Hunt matrix (Eq. 2.88 and Eq. 2.89), and it has been ignored in the KCL/KVL
1487 analysis based on the time dependency of the magnetic field in the system. Also
1488 in terms of the wave equation, both $\dot{\mathbf{B}}$ and $\dot{\mathbf{D}}$ terms allow us to derive the wave
1489 equation describing delay, and without them we get diffusion equations.

1490 This discussion can be extended to the limitation of general circuit theory, the
1491 quasi-static assumption. Once we include time delay (elements that include the
1492 wires), one must consider the finite transit time when describing circuits. To clearly
1493 relate the delay to a dimension, we defined a term "Einstein causality" as a general-
1494 ization of causality (B2 in section 2.2.1).

1495 2.5.3 Gyrator

1496 A two-port network, such as an electro-mechanic system has Φ , I , \mathbf{F} , and \mathbf{U} as
1497 the system's variables. A gyrator exists to couple the electric and mechanical sides.
1498 Specifically, through the gyrator, the potential, Φ , maps to the velocity $-\mathbf{U}$ and
1499 the current I maps to the force F . To show this property, one can employ the
1500 impedance matrix of the gyrator

$$Z_{gyrator} = \begin{bmatrix} 0 & -G \\ G & 0 \end{bmatrix}, \quad (2.81)$$

Draft of November 2, 2014 at 17:33

1501 where $G = B_0 l$ is the gyration coefficient, B_0 is the DC magnetic field and l is the
1502 length of the wire. Thus

$$\begin{bmatrix} \Phi(\omega) \\ F(\omega) \end{bmatrix} = \begin{bmatrix} 0 & -B_0 l \\ B_0 l & 0 \end{bmatrix} \begin{bmatrix} I(\omega) \\ U(\omega) \end{bmatrix}. \quad (2.82)$$

1503 namely,

$$\Phi(\omega) = -B_0 l U(\omega) \text{ and } F(\omega) = B_0 l I(\omega). \quad (2.83)$$

1504 When defining an impedance, the flow direction is defined as into the terminals, thus
1505 U is defined as going into the network. Thus, the minus sign of U in Eq. 2.83 follows
1506 from the Lenz's law. Note that Eq. 2.83 explains an ideal gyrator, considering only
1507 a DC magnetic field.

1508 **The non-ideal gyrator** Here we derive the nature of the gyrator from the basics
1509 of electro magnetism. Ulaby (2007) described the induced emf (voltage ϕ) as the
1510 sum of a transformer component (ϕ_{tr}) and a motional component (ϕ_{mot}) namely,

$$\phi(t) = \phi_{tr} + \phi_{mot}. \quad (2.84)$$

1511 The transformer voltage is $\phi_{tr} = -(-\int \frac{\partial \mathbf{B}}{\partial t} \cdot d\mathbf{A}) = \frac{\partial \psi}{\partial t}$, where ψ is magnetic flux. In
1512 the static case ($\frac{d}{dt} = 0$), the time-varying term is zero.

1513 The ϕ_{mot} represents the motion of electrical voltage (Ulaby, 2007)¹² as observed
1514 from the mechanical side (motional voltage due to u). Derivation of ϕ_{mot} starts from
1515 the Lorentz magnetic force (\mathbf{f}_m), acting on a moving charge q inside a magnetic field
1516 \mathbf{B} with a velocity \mathbf{U} ,

$$\mathbf{f}_m = q(\mathbf{U} \times \mathbf{B}). \quad (2.85)$$

1517 Then the motion of magnetic force from the electrical field \mathbf{E}_{mot} is $\mathbf{f}_m = q\mathbf{E}_{mot}$,¹³

¹²The (electrical) voltage which is associated from the motion from the other port (i.e., mechanical). Note that this concept can be applied only in two-port (or higher order) systems.

¹³The unit of q is in coulombs[C], \mathbf{E}_{mot} is in [V/m]=[N/C] as $1V \equiv 1J/C$ and $1N = 1J/m$. Therefore $q\mathbf{E}$ stands for force with a unit of [N]. A positive charge ($q > 0$, proton) is 1.602×10^{19} [C], thus the charge of an electron (negative charge) is -1.602×10^{19} [C]. One Coulomb of charge equals

1518 therefore

$$\mathbf{E}_{mot} = \frac{\mathbf{f}_m}{q} = \mathbf{U} \times \mathbf{B}, \quad (2.86)$$

1519 where \mathbf{E}_{mot} is the motional electric field seen by the charged particle q and its direc-
1520 tion is perpendicular to both \mathbf{U} and \mathbf{B} .

1521 Thus the voltage Φ_{mot} is defined as the line integral of the corresponding electric
1522 field which is \mathbf{E}_{mot} in this case,

$$\phi_{mot} = - \oint_C \mathbf{E}_{mot} \cdot d\mathbf{l} = - \oint_C (\mathbf{U} \times \mathbf{B}) \cdot d\mathbf{l}. \quad (2.87)$$

1523 Note that only this term has been considered in an ideal gyrator.

1524 Finally, the total voltage is

$$\phi = \phi_{tr} + \phi_{mot} = \int \frac{\partial \mathbf{B}}{\partial t} \cdot d\mathbf{A} - \oint_C (\mathbf{U} \times \mathbf{B}) \cdot d\mathbf{l}. \quad (2.88)$$

1525 In the frequency domain with scalars, Eq. 2.88 is rewritten as

$$\Phi = s\Psi - BIU = sL_e I - BIU, \quad (2.89)$$

1526 where L_e is a leakage inductance due to the leakage flux of a self-inductance in the
1527 electrical side, $\Psi = L_e I$.

1528 Assuming a static DC magnetic field (B_0), then $s\Psi = 0$ and we find the ideal
1529 gyrator definition $\Phi = \Phi_{mot} = -UB_0 l$ (Eq. 2.83). Note that the frequency dependant
1530 term shown in Eq. 2.89 ($j\omega\Psi$ and $j\omega L_e I$) is non QS term that is not considered in
1531 an ideal gyrator. The minus sign for the other term $-UBl$ is related to Lenz's law.

1532 Figure 2.14 shows a simple experiment to demonstrate Lenz's law, using a magnet
1533 and an ammeter. Moving the north pole of a magnet towards the coil causes positive
1534 current I . The motion that the magnet is pushed into the coil reveals the negative
1535 direction of the Ψ or emf. If the magnet is pulled out from the coil (positive Ψ or
1536 emf), the direction (sign) of the current is reversed. When there is no motion of the
1537 magnet, then the current does not flow. A faster moving magnet creates a larger

to the charge which can light a 120-watt-bulb for one second.

induced current.

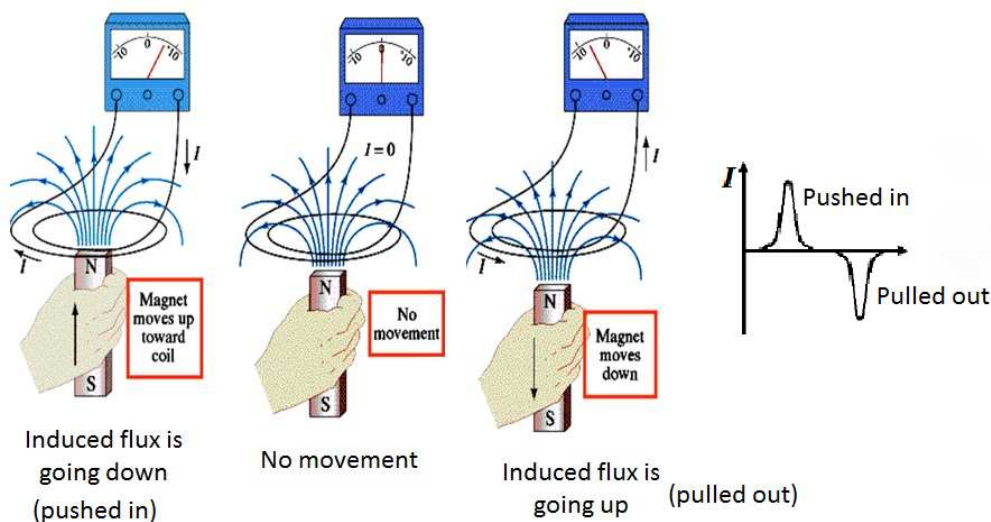


Figure 2.14: A simple experiment to display Lenz's law. The induced flux, Ψ (or emf), gives rise to a current I whose direction opposes to the direction of the Ψ . Moving the north pole of a magnet towards the coil causes positive current I . The motion that the magnet is “pushed into the coil” reveals the negative direction of the Ψ or emf. If the magnet is “pulled out from the coil” (positive Ψ or emf), the direction (sign) of the current is reversed. When there is no motion of the magnet, then the current does not flow. The image is retrieved and modified from https://bearspace.baylor.edu/Walter_Wilcox/www/courses/phy2435/chap29xxa.pdf

1538

1539 Consider a simple circuit of a moving coil loudspeaker, with a resistor R across the
 1540 terminal, voltage $-UBl$ (the induced emf grounded to zero), and current I which is
 1541 moving across the R . By Ohm's law, the current satisfies

$$I(\omega) = \frac{0 - (-UBl)}{R} = \frac{UBl}{R} = \frac{U l}{R A} \Psi, \quad (2.90)$$

1542 where $\Psi = BA$, and l , A are length and area of wire respectively. The direction of
 1543 current is always opposite of the induced emf, this explains the Lenz's law.¹⁴ Note
 1544 the minus signs in Eq. 2.89 requires anti-reciprocity, Carlin's postulate C6.

1545 Similar to Eq. 2.88, one can examine the relation between the force and the current

¹⁴If we consider the emf with its positive sign (UBl), consisting the fixed positive direction in the circuit, we will have $-I$.

1546 in Eq. 2.83, this force term also need two parts; transformer force and motional force,

$$f(t) = f_{tr} + f_{mot}. \quad (2.91)$$

1547 Reconsidering the magnetic force density in Eq. 2.85, the motion of force in electrical
1548 side, $f_{mot}[\text{N}]$ is

$$\mathbf{f}_{mot} = i(t) \oint_C \mathbf{dl} \times \mathbf{B}, \quad (2.92)$$

1549 where $i(t)$ stands for the current.

1550 Assuming that the magnetic field is uniform and the conducting wire is not closed,
1551 starting from a ending at b (if it is closed then the net magnetic force is zero, in
1552 Eq. 2.93 a equals to b .), then Eq. 2.92 becomes

$$\mathbf{f}_{mot} = i \left(\int_a^b \mathbf{dl} \right) \times \mathbf{B}_0 = i\mathbf{l} \times \mathbf{B}_0, \quad (2.93)$$

1553 where \mathbf{l} is a vector, a piece of wire directing from a to b . In frequency domain,
1554 Eq.2.93 is $F = B_0 l$, it is the ideal gyrator's equation discussed in Eq.2.83 which only
1555 considers motional behavior of the network.

1556 Based on the Lorentz force, the transformer force on mechanical side is defined as

$$f_{tr} = m_B \times a = m_B \frac{dU}{dt} \quad (2.94)$$

1557 where m_B is the leakage mass due to imperfect (frequency dependent) mass coupling
1558 in the mechanical side, and $a = \frac{dU}{dt}$ is acceleration. In frequency domain, this term
1559 becomes $F_{tr} = sm_B U$, where $s = j\omega$.

1560 The final force for the non-ideal gyrator is

$$f = f_{tr} + f_{mot} = m_B \frac{dU}{dt} + i\mathbf{l} \times \mathbf{B}, \quad (2.95)$$

1561 in frequency domain with scalars, Eq. 2.95 is reconsidered as

$$F = sm_B U + B_0 l I. \quad (2.96)$$

1562 In conclusion, two types of magnetic fields exist in an electro-mechanic network;
 1563 one is a DC magnetic field and the other is an AC magnetic field. In the ideal
 1564 gyrator formula, only the motional parts (or the DC magnetic field) of the variables
 1565 (voltage and force) are considered. The two modalities in the network (electrical
 1566 and mechanical) share this DC magnetic field which is shown in the motional part of
 1567 each variable. For the non-gyrator case one must use the transduction parts (or AC
 1568 magnetic field) of variables along with the motional parts which do not contribute
 1569 to the opposite modality.

1570 One can convert the impedance matrix form of the ideal gyrator in Eq. 2.81 into
 1571 an ABCD matrix form using Eq. 2.8,

$$T_{i\text{-gyrator}} = \begin{bmatrix} 0 & G \\ G^{-1} & 0 \end{bmatrix}, \quad (2.97)$$

1572 where $G = B_0 l$. The ABCD matrix for of the non-ideal gyrator is,

$$T_{noni\text{-gyrator}} = \frac{1}{G} \begin{bmatrix} sL_e & s^2 L_e m_B + G^2 \\ 1 & sm_B \end{bmatrix}. \quad (2.98)$$

1573 The determinants (Δ) of both Eq. 2.97 and Eq. 2.98 are '-1' which define the anti-
 1574 reciprocal network. When Δ is '1', the network is reciprocal. Note that all of these
 1575 relationships are in the Laplace complex frequency domain $s = j\omega$.

1576 Finally the suggested non-ideal gyrator's impedance matrix formula is

$$Z_{noni\text{-gyrator}} = \begin{bmatrix} sL_e & -G \\ G & sm_B \end{bmatrix}, \quad (2.99)$$

1577 a non-reversible and anti-reciprocal network (if $L_e \neq m_B$).

1578 What provides the coupling between the electrical and mechanical sides? The only
 1579 thing that matters in the electro-mechanic coupling is the magnetic field, $\dot{\mathbf{H}}$. This
 1580 variable is hidden in terms of input and output variables of the system (voltage,
 1581 current, force and velocity). The $\dot{\mathbf{H}}$ generated by the conducting current from the
 1582 coil affects the armature by inducing magnetic polarity on the armature surface.

Draft of November 2, 2014 at 17:33

1583 This induced $\dot{\mathbf{H}}$ and the permanent magnet define the net force on the armature.

1584 Thus the armature moves based on the experienced total net force.

1585 It is intuitive that the electrical current leads to a force, because the system trans-
1586 forms the current signal into a force on the diaphragm, creating sound pressure
1587 waves. Followed by this logic, a gyrator equation relates the electrical current to the
1588 force, $F = B_0 l I$.¹⁵ Therefore we can conclude that the gyrator is a more physically
1589 intuitive convention.

1590 2.5.4 Eddy currents and diffusion waves

1591 Along with the gyrator, the semi-inductor (due to eddy-current¹⁶) is one of key com-
1592 ponents to describe electro-mechanic system (Kim and Allen, 2013). If a magnetic
1593 field near a conductor is changing in time, the traveling magnetic field is described
1594 in terms of the diffusion equation. This is a physical phenomenon which can be
1595 observed in our daily life.

1596 There are two ways to examine Eddy current, (1) direct way and (2) in-direct
1597 way; (1) a magnet traveling inside of a copper pipe can be affected by this diffusive
1598 eddy-current. The magnet falling outside of a conductor does a free fall, while falling
1599 inside of the conducting pipe experiences a significant delay, due to the opposite force
1600 caused by the eddy current. Figure 2.15 describes this phenomenon.

1601 (2) starting from Ampere's law, the current in the wire, namely driven (or con-
1602 ducting) current, induces magnetic field \mathbf{H} . Then, similar to the direct way (1),

¹⁵We may can relate the current to the velocity (transformer and mobility), which seems to be less intuitive.

¹⁶There are three types of currents in electro-magnetic system

1. Conducting current is created by moving charge in conducting medium (\mathbf{J} term in Ampere's law, i.e., current through wire).
2. Displacement current is current due to changing electric field (\mathbf{E}) (\mathbf{D} term in Ampere's law, i.e., capacitors).
3. Eddy current is current due to changing magnetic field (\mathbf{H}). It is directly related to Faraday's (induction) law.

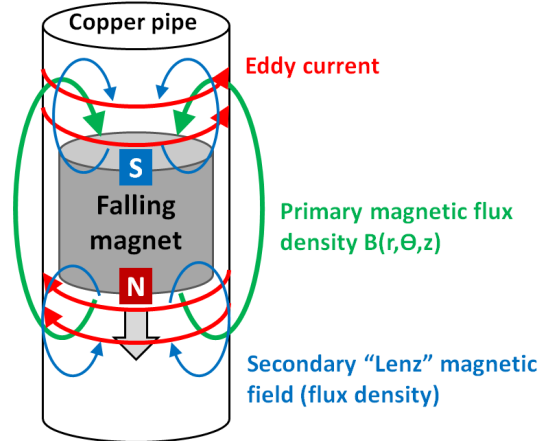


Figure 2.15: Eddy current with a falling magnet inside a conductor (falling from south to north). When the magnetic field is changed in time in a closed electric field (a falling magnet in a copper pipe), an “eddy current” is induced on the copper pipe (red). The direction of the eddy current is perpendicular to the primary magnetic field (green, it is static when velocity is zero. Also the field is not a function of θ) followed by right hand rule (thumb-force, 1st finger-electric field, 2nd finger - magnetic field). The eddy current creates the secondary magnetic loop (blue) whose force is opposite to the force of gravity. At the terminal velocity, the force of gravity equals the Lenz reactive force.

1603 based on the Faraday’s law, the \mathbf{H} creates Eddy current (induced current via \mathbf{H} on
 1604 the surface of the adjacent ferromagnetic material). Note that the magnitude of the
 1605 eddy currents is a function of the drive current with opposite direction.

1606 Vanderkooy (1989) modeled the electrical impedance representation of the semi-
 1607 inductor based on this concept (in-direct way to examine the eddy current). Impedance
 1608 of the semi-inductor is proportional to \sqrt{s} , to realize a diffusive element in circuits.
 1609 A simple impedance formula of the semi-inductor is derived with the assumption
 1610 that the length of a coil sheet is infinite. Neglecting the radius of the coil and the
 1611 air gap between the magnetic material and the wire,

$$Z_{semi} = n^2 \sqrt{\frac{\mu s}{\sigma}} = K \sqrt{s}, \quad (2.100)$$

1612 where K is semi-inductance per unit length in semi-Henrys, n is the number of coil
 1613 winding turns of wire, μ is the iron’s permeability, and σ is the conductivity of

1614 the iron armature.

1615 Semi-inductors, which result from magnetic diffusion, are not commonly found in
 1616 circuit analysis. However, it is a key element in characterizing the ‘eddy-current’ (skin
 1617 effect) in electromagnetic models, such as loudspeakers. In a BAR, the eddy current
 1618 is distributed through the surface of the armature, as well as in the cross section
 1619 of the laminated iron box which surrounds the magnets (Fig. 1.2). In a dynamic
 1620 loudspeaker, the coil is directly connected to the diaphragm and the eddy-current is
 1621 distributed through the surface of an iron core (a pole-piece structure).

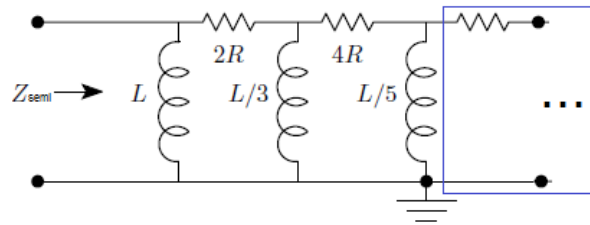


Figure 2.16: Semi-inductor approximate lumped circuit model via a truncated ladder network. Circuit diagram of the electrical impedance of the semi-inductor model is defined by the ladder network resistance factor R and shunt inductance factor L (Weece and Allen, 2010). This circuit follows from a continued fraction expansion of \sqrt{s} .

1622 Warren and LoPresti (2006) noted that the Bessel function ratio in the Vanderkooy
 1623 model (1989) can be expanded as a continued fraction expansion, into a diffusion
 1624 ladder network, so that the electrical impedance can be represented by the circuit
 1625 shown in Fig. 2.16. The semi-inductor model includes two parameters: the diffusion
 1626 resistance R , and the shunt diffusive inductance L which can be represented by the
 1627 physical characteristics of the transducer. The R and L are given by

$$R = \frac{4\pi n^2 l}{\sigma}, \quad L = \mu n^2 \pi r_0^2, \quad (2.101)$$

1628 where n is the number of coil windings, l is the coil length, σ is the conductivity of
 1629 the pole structure, μ is the permeability of the pole structure, and r_0 the coil radius.

1630 Although the combination of the resistor and the inductor should extend to infinity
 1631 (more resistor-inductor pairs), these can only affect higher frequencies (i.e., Fig. 2.16

1632 is a sufficient low frequency approximation). As shown in Fig. 2.16, Weece and Allen
 1633 (2010) determined only 5 elements (L, 2R, L/3, 4R, and L/5), and compared the
 1634 network to the demagnetized condition of their bone driver transducer. Demagne-
 1635 tizing the transducer ($T = B_0 l = 0$) is mathematically equivalent to the open circuit
 1636 condition (i.e., $V = 0$).

1637 Starting from Maxwell's equation, we derive two types of wave equations, normal
 1638 and diffusive cases.

1639 Equation 2.102 has two terms, current from the source, and displacement current.

$$\nabla \times \mathbf{H} = \epsilon \frac{\partial \mathbf{E}}{\partial t} + \sigma \mathbf{E}, \quad (2.102)$$

1640 where $\mathbf{D} = \epsilon \mathbf{E}$ and $\mathbf{J} = \sigma \mathbf{E}$. Via $\mathbf{B} = \mu \mathbf{H}$, Faraday's law (Eq. 2.66) for free space
 1641 written as,

$$\nabla \times \mathbf{E} = -\mu \frac{\partial \mathbf{H}}{\partial t} = -\dot{\mathbf{B}}. \quad (2.103)$$

1642 Also since monopole magnetic charge does not exist, and μ is independent of x
 1643 (i.e., $\nabla \mu = 0$),

$$\nabla \cdot \mathbf{B} = \nabla \cdot \mathbf{H} = 0. \quad (2.104)$$

1644 Taking a curl of Eq. 2.102 using the following vector identity,

$$\nabla \times (\nabla \times \mathbf{H}) = \nabla(\nabla \cdot \mathbf{H}) - \nabla^2 \mathbf{H}. \quad (2.105)$$

1645 then using Eq. 2.103 and Eq. 2.104, Eq. 2.105 becomes

$$\nabla \times (\nabla \times \mathbf{H}) = \epsilon \frac{\partial(\nabla \times \mathbf{E})}{\partial t} + \nabla \times (\sigma \mathbf{E}) = -\mu \epsilon \frac{\partial}{\partial t} \frac{\partial \mathbf{H}}{\partial t} - \mu \sigma \frac{\partial \mathbf{H}}{\partial t} = 0 - \nabla^2 \mathbf{H}. \quad (2.106)$$

1646 Finally we have,

$$\nabla^2 \mathbf{H} = \underbrace{\mu \epsilon \frac{\partial^2 \mathbf{H}}{\partial t^2}}_{\text{loseless wave}} + \underbrace{\mu \sigma \frac{\partial \mathbf{H}}{\partial t}}_{\text{lossy wave}} \leftrightarrow \left(\frac{s^2}{c^2} + \mu \sigma s \right) \underline{\mathbf{H}} = \mu \sigma s (s \epsilon / \sigma + 1) \underline{\mathbf{H}}, \quad (2.107)$$

1647 where $\underline{\mathbf{H}}$ is frequency variable of \mathbf{H} , and $s = j\omega$. When $\omega \leq \sigma / \epsilon = \omega_c$ the wave is

Draft of November 2, 2014 at 17:33

1648 dominated by diffusion, otherwise we have lossy waves. Since the two waves satisfy
1649 superposition, we can separate the two solutions.

1650 **Lossless wave equation ($\mathbf{J} = 0$ or $\sigma = 0$)** When there is zero conductive current
1651 density ($\mathbf{J} = 0$),

$$\nabla \times \mathbf{H} = \frac{\partial \mathbf{D}}{\partial t} + \cancel{\mathbf{J}}^0 = \epsilon \frac{\partial \mathbf{E}}{\partial t}. \quad (2.108)$$

1652 Going through same algebra from Eq. 2.103 to Eq. 2.106 we have the wave equation,

$$\nabla^2 \mathbf{H} = \mu \epsilon \frac{\partial^2 \mathbf{H}}{\partial t^2} = \frac{1}{c^2} \frac{\partial^2 \mathbf{H}}{\partial t^2}. \quad (2.109)$$

1653 **Lossy wave equation: diffusion equation (semi-inductor basics)** Similar
1654 step is used to derive the diffusion equation via Maxwell's equation. The fundamental
1655 difference is in the first step when the medium is a conductor, we can ignore the
1656 displacement current term in Eq. 2.102 as it is small compared to the conducting
1657 current term. Therefore in this case we can set $\frac{\partial \mathbf{D}}{\partial t}$ to zero,

$$\nabla \times \mathbf{H} = \mathbf{J} + \cancel{\frac{\partial \mathbf{D}}{\partial t}}^0 = \sigma \mathbf{E}. \quad (2.110)$$

1658 Based on Eq. 2.103 - Eq. 2.106, finally the diffusion wave equation is derived,

$$\nabla^2 \mathbf{H} = \mu \sigma \frac{\partial \mathbf{H}}{\partial t}. \quad (2.111)$$

1659 The normal wave equation in 3D wave form (Eq. 2.109) describes the propagation
1660 of electromagnetic (EM) waves through a medium whereas the diffusion wave equa-
1661 tion (Eq. 2.111) describes the propagation of EM waves in a conducting magnetic
1662 medium. For both equations the Laplacian on left hand side is same. A diffusion
1663 case has a single time derivative term whereas a normal wave equation has a double
1664 time derivative term. Let's define $\mathbf{H}(x, t)$ assuming a simple geometry,

$$\mathbf{H}(x, t) = H_0 e^{j(\omega t - kx)}, \quad (2.112)$$

Draft of November 2, 2014 at 17:33

1665 where H_0 is the \mathbf{H} , \mathbf{E} propagate in y , z directions, respectively. Note that k is wave
1666 number. Then Eq. 2.111 in frequency domain

$$(jk)^2 = \mu\sigma j\omega, \quad (2.113)$$

1667 then the wave number k is

$$k = \sqrt{\mu\sigma\omega}(\cos 45^\circ - j \sin 45^\circ). \quad (2.114)$$

1668 Thus the wave propagation is proportional to the square-root frequency (\sqrt{s}).

1669 To derive the exact impedance formula of a semi-inductor;

1670 1. substitute Eq. 2.114 into Eq. 2.112

$$\mathbf{H}(x, t) = H_0 e^{j(\omega t - \sqrt{\mu\sigma\omega}x(1-j)/\sqrt{2})}, \quad (2.115)$$

1671 2. calculate the magnetic flux Ψ per unit area, where $\Psi = \int \mathbf{B} \cdot d\mathbf{S} = \mu \int \mathbf{H} \cdot d\mathbf{S}$

1672 3. Then the inductance L per unit length with n numbers of turn with current I
1673 is

$$L = \frac{n}{I} \Psi = n^2 \frac{\mu}{1+j} \sqrt{\frac{2}{\mu\sigma\omega}}. \quad (2.116)$$

1674 4. The impedance of an inductor is $Z(s) = sL$, where $s = j\omega$. Therefore

$$Z_{semi}(s) = n^2 \sqrt{\frac{\mu s}{\sigma}} = K \sqrt{s}, \quad (2.117)$$

1675 where K is the semi-inductance.

1676 The semi-inductor's impedance is proportional to square-root of frequency. More
1677 details considering different geometries are discussed in Vanderkooy (1989)).

One can calculate a propagation cutoff frequency of two waves (diffusion and normal) in a medium. Convert Eq. 2.109 and Eq. 2.111 into frequency domain repre-

sentation via Laplace transform, and set them equal to each other.

$$\mu\sigma\frac{\partial\mathbf{H}}{\partial t} = \mu\epsilon\frac{\partial^2\mathbf{H}}{\partial t^2} \quad (2.118)$$

$$\mu\sigma(j\omega)\mathbf{H} = \mu\epsilon(j\omega)^2\mathbf{H} \quad (2.119)$$

$$\sigma = \epsilon(j\omega), \quad (2.120)$$

1678 the cutoff frequency(f_c) is

$$f_c = \frac{\sigma}{2\pi\epsilon}. \quad (2.121)$$

1679 The f_c of copper, for example, is about 4300[GHz] ($\sigma = 5.96 \times 10^7$, $\epsilon_r = 250,000$, $\epsilon_0 =$
1680 8.854×10^{-12}) meaning that wave below this frequency is diffusive. The corresponding
1681 wave length (λ_c) can be calculated as

$$\lambda_c = \frac{c_{copper}}{f_c} = \frac{3 \times 10^8}{4.3 \times 10^{12} \sqrt{250,000}} \approx 0.14\mu[m], \quad (2.122)$$

1682 where $c_{copper} = \frac{c_0}{\sqrt{\epsilon_r}}$.

CHAPTER 3

EXPERIMENTAL METHODS

1683 3.1 Measurements for BAR modeling

1684 Three different experiments were conducted for modeling the BAR. First, we calcu-
 1685 late the Hunt parameters of a BAR from electrical input impedance measurements
 1686 (Appendix E). The calculation of Hunt parameters may be considered as a two-
 1687 port Thevenin calibration of the receiver, since Z_e , T , and Z_a characterize the initial
 1688 electrical, acoustical and transfer properties of the unloaded receiver. Second, we
 1689 measure of the receiver's diaphragm velocity in vacuum using a laser. This proce-
 1690 dure was needed to verify the mechanical and electrical parts of the model. The last
 1691 step is the pressure measurement of the receiver using an ER7C probe microphone,
 1692 (Etymotic Research). The resulting Thevenin pressure of the receiver from our trans-
 1693 ducer model and Hunt parameters is compared with this experimental pressure data.
 The detail of this result is discussed in chapter 4 (model verification).

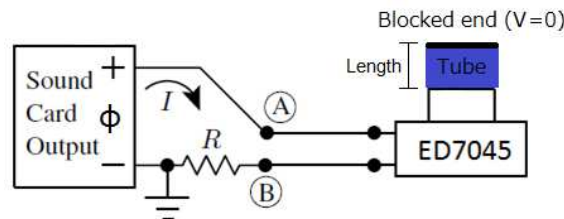


Figure 3.1: Experimental setup for the electrical input impedance measurement. Where Φ is the voltage, I is the current, and R is a reference resistance. We varied the experimental acoustical load impedance by changing Length of a blocked tube and measured the voltage at two points (A, B) denoted as Φ_A and Φ_B .

1694

1695 3.1.1 Electrical input impedance measurements for the Hunt
1696 parameter calculation

1697 Step 1 of calculating the Hunt parameters of the receiver requires a system for mea-
1698 suring electrical impedance as a function of frequency. As shown in Fig. 3.1, all
1699 stimulus signals were generated using a laptop sound card so that voltages could be
1700 recorded. The stimulus waveform was a 24-bit, 2048-point frequency-swept chirp
1701 with a sampling rate of 48[kHz] (bandwidth=24kHz). The signal-to-noise ratio
1702 (SNR) was improved by looping the chirp and averaging between 10 and 1000 con-
1703 secutive frames, depending on the required SNR. The ≤ 1 volt chirp signal from an
1704 Indigo sound card (Echo Audio) was sent to the receiver, which was in series with
1705 a known reference resistor R (1000[Ω], Fig. 3.1). The resistor was located between
1706 one of the receiver's terminals and the sound source ground. The measured electrical
1707 input impedance is expressed as:

$$Z_{in} = \frac{\Phi_A - \Phi_B}{I} = \frac{\Phi_A - \Phi_B}{\Phi_B/R} = R \left(\frac{\Phi_A}{\Phi_B} - 1 \right). \quad (3.1)$$

1708 As shown in Fig. 3.2, eight different acoustic loads were attached to the end of the
1709 receiver output and eight corresponding electrical input impedances were recorded.
1710 Six of the seven tubes (excluding the longest length 6.11[cm], which has the largest
1711 delay among the tubes, due to minimize the discrepancy in the Hunt parameter cal-
1712 culation) were used in the experiments: 0.25, 0.37, 0.88, 1.24, 2.39 and 3.06[cm]. The
1713 inner diameter of the tested tubes (with uniform area) was approximately measured
1714 as 1.5[mm], which is similar to the outer diameter of the ED receiver port. As three
1715 different measurements were required to calculate the three unknown Hunt paramete-
1716 ters (Z_e , Z_a , T_a) (Weece and Allen, 2010), three out of six tubes with different lengths
1717 were selected, resulting in ${}_6C_3 = 20$ possible combinations of the Hunt parameters.
1718 The results from every possible combination are not discussed in this paper; rather,
1719 we focus on the four calculated sets of Hunt parameters. We categorized our testing
1720 tube lengths into short, medium and long tubes, and picked one of each to make a
1721 set of three tubes. An open circuit condition (the volume velocity, V , is zero, rigid

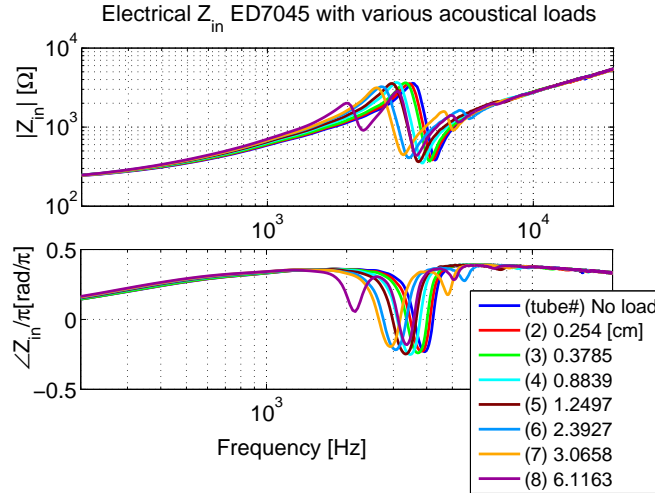


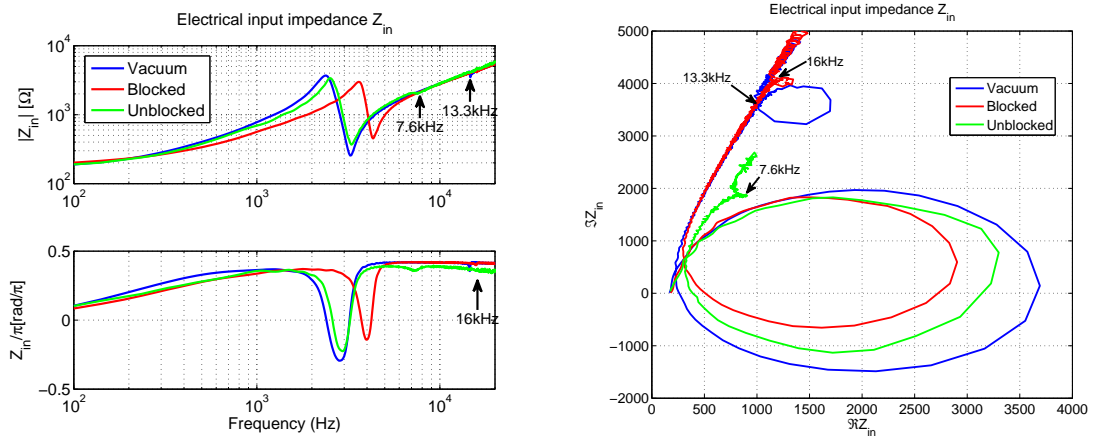
Figure 3.2: Measured Z_{in} of ED7045 with the eight acoustical load conditions, blocked cavities. Different lengths of the tubes are used to vary the acoustical load. Three different known electrical input impedances are selected to calculate Hunt parameters.

1722 termination) was applied, as the ends of the tubes were blocked for the experiment.
 1723 The characteristics of the resulting derived Hunt parameters are discussed in Section
 1724 2.1.1.

1725 When the acoustic load impedance is unblocked, a small second resonance (SR)¹
 1726 appears around 7.6[kHz], following the first resonance (FR)² at 2.5[kHz], as shown
 1727 in Fig. 3.3 (a) (green). In fact, a very small SR appears in *every* case in the figure,
 1728 as clearly seen in the polar plot, Fig. 3.3 (b). The SR of the blocked case (red) is
 1729 not obvious in the magnitude plot, but one sees the SR location from the phase in
 1730 the polar data. Note that a ‘loop’ in the polar data corresponds to the SR in the
 1731 magnitude data. The vacuum data (blue) shows the biggest FR in magnitude (the
 1732 largest circle in the polar plot), and the FR locates at the lowest frequency among
 1733 all the other cases. Compared to the unblocked case (red), the SR frequency of
 1734 the other two cases (blocked and vacuum) is above the frequency range of reliable
 1735 measurements. In detail, it has almost an octave difference ($SR_{unblocked} \approx 7.6[kHz]$,

¹SR: Second Resonance

²FR: First Resonance



(a) Magnitude and phase of Z_{in} of the ED7045 receiver

(b) Z_{in} polar plot

Figure 3.3: This plot shows the electrical input impedance of the ED7045 receiver in blocked/unblocked port, and vacuum conditions. In the unblocked receiver port case, the FR moves to lower frequency (2.5[kHz]) compared to the blocked case, 3.8[kHz]. The FR in vacuum is at the lowest frequency, 2.3[kHz]. The frequency locations of SR for each curve are indicated by arrows in the figures. (a) Magnitude and phase of the electrical input impedance, (b) Polar plot of the electrical input impedance ($\Re Z_{in}$ vs $\Im Z_{in}$). Note that above 5[kHz], the phase of Z_{in} in (a) approaches $\approx .4\pi$ [rad]. Thus in (b), the curves merge at a fixed angle as $\omega \rightarrow \infty$.

Draft of November 2, 2014 at 17:33

1736 $SR_{vacuum} \approx 13.3[kHz]$, $SR_{blocked} \approx 15.7[kHz]$). In addition, the size of $SR_{blocked}$ is
1737 insignificant. For these reasons, we have ignored the SR effect in our model analysis
1738 of the BAR model.

1739 3.1.2 Laser vacuum measurements

1740 Figure 3.4 describes the experimental setup of the laser mechanical velocity mea-
1741 surement in the vacuum environment. In preparation for the laser measurement, a
1742 portion of the transducer's case was carefully removed using a dental drill, to ex-
pose the diaphragm. A thin plastic window was glued on, to reseal the case. The

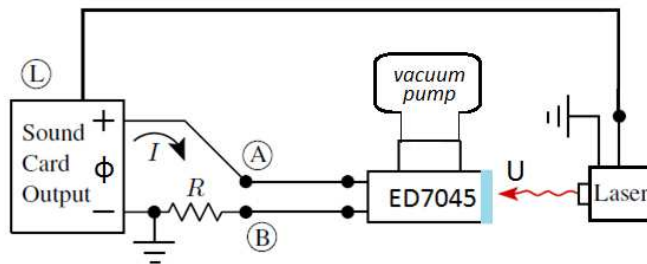


Figure 3.4: Experiment setup for the laser mechanical velocity measurement in vacuum. The circled 'L' means an input from the laser system. The laser beam is focusing on the plastic window of the transducer to measure the diaphragm velocity (U).

1743
1744 laser beam is finely focused on the diaphragm through the window. The measure-
1745 ment was made where the driver rod (Fig. 1.2) connects to the diaphragm. For
1746 the vacuum condition, air inside the receiver was evacuated prior to measurement.
1747 The ambient pressure was maintained at less than $0.003[atm]$ during these measure-
1748 ments. The custom built vacuum system was used with a 'Sergeant Welch' vacuum
1749 pump and a 10-inch bell-shaped jar. A 'Polytec OFV-5000 Vibrometer controller'
1750 was used with a 10x-lens on the laser. The calibration factor for the laser velocity
1751 was $125[mm/sec/volt]$. As before, a chirp was used to measure the complex velocity
1752 frequency response.

1753 3.1.3 Pressure measurements

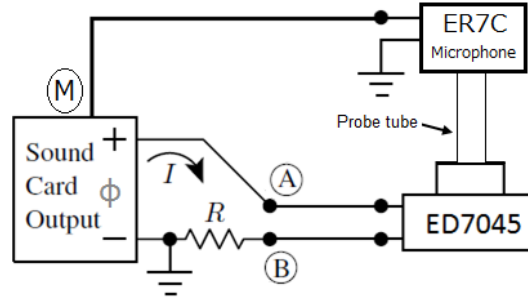


Figure 3.5: Experiment setup for pressure measurement. The circled ‘M’ means an input from the ER7C microphone. The ER7C microphone system is factory-calibrated as 50[mV/Pa]. It consists of an amplifier box, a microphone, and a probe tube. Note that the ER7C microphone and the ED7045 receiver is connected carefully to minimize the space between the probe tube’s end and the receiver’s port.

1754 The purpose of experiment three is to compare the output pressure to the model
 1755 with $V = 0$ (rigid termination). An ER-7C probe microphone (Etymotic Research)
 1756 was used for the transducer pressure measurement (Fig. 3.5). The ER7C microphone
 1757 has an attached probe tube whose dimension was .95 OD x .58 ID x 76[mm], and
 1758 made of medical grade silicon rubber. In fact, it is impossible to connect the mi-
 1759 crophone probe tube with a blocked receiver ($V = 0$, the condition that we want to
 1760 make a comparison with our modeling data) due to the finite load impedance of the
 1761 microphone. The space between the microphone’s tube and the port of the receiver
 1762 is minimized, so the microphone’s tube and the receiver’s port do not touch each
 1763 other. The real part of the characteristic impedance of a tube, $Z_{c_{tube}}$, (without loss)
 1764 is given by

$$Z_{c_{tube}} = \frac{\rho c}{Area_{tube}}, \quad (3.2)$$

1765 where ρ is the air density and c is the speed of sound ($1.21[kg/m^3]$ and $342[m/s]$ at
 1766 $20^\circ[C]$, respectively). The diameter, d , of the receiver’s port and the microphone’s
 1767 tube are $d_{receiver} = 1.4[mm]$ and $d_{mic} = 0.58[mm]$, thus the area of the receiver’s port
 1768 is about 5.8 times larger than the microphone’s. Adding more consideration of the
 1769 length of both cases, $Z_{c_{mic_tube}}$ is much greater than $Z_{c_{receiver_port}}$. Thus we assume

1770 that $Z_{C_{mic.tube}}$ has a negligible loading effect on the source impedance of the receiver.
1771 Recognizing these experimental limitations prior to comparing the measurement data
1772 to theoretical results should give us better understanding of the Thevenin pressure
1773 of the BAR.

1774 Utilization of this experiment can be found in section 4.2.4 for comparing the
1775 model calculated Thevenin pressure (per voltage) to the experimental pressure mea-
1776 surement.

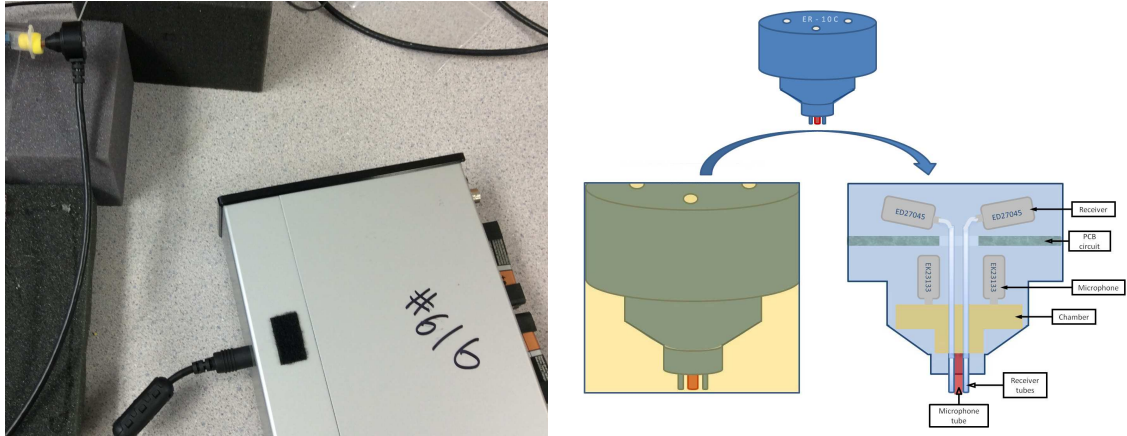
1777 3.2 Technical analysis of an OAE hearing measurement 1778 probe

1779 In this section, we introduce several experimental methods to investigate an existing
1780 hearing measurement probe system, the ER10C by Etymotic Research, for otoacous-
1781 tic emission (OAE) measurements. The ER10C system consists of two parts; a probe
1782 and an amplifier box (Fig. 3.6(a)). The ER10C probe has built-in sound sources (re-
1783 ceivers), which eliminate the need for having external speakers (Fig. 3.6(b)). The
1784 amplifier box contains special circuits for each probe to meet the unified and standard
1785 performance specification of the ER10C system.

1786 For the last decade, the system (or the probe alone with other software such as
1787 HearID or OtoStat by Mimosa Acoustics) has been widely used in clinics for hearing
1788 screening and diagnostics by measuring DPOAEs (Distortion-Product Otoacoustic
1789 Emissions), and middle ear reflectance. Following the probe's Thevenin calibration,
1790 OAE stimuli may be calibrated to have constant forward pressure levels (FPL).

1791 Because of the small number of competitors in the market, users have not had
1792 many alternatives to the system, even though the ER10C has several drawbacks.
1793 First, the size of the probe is too big for infants. Second, because the probe is such a
1794 delicate device, handling it without extreme caution may lead to malfunction of the
1795 probe. Finally, the result of the measurement depends too much on the condition of
1796 the foam tip that is inserted in the subject's ear canal.

1797 Appreciating these facts, we believe that investigation of the properties of the



(a)ER10C with its amplifier box (20dB/40dB)(b)ER10C probe head's schematic cross-sectional view

Figure 3.6: (a)A yellow foam tip (14A) is attached to the probe's head. Note that numbers on the box indicates the system's serial number. (b)Schematic representation of the ER10C probe. Two speakers and microphones are separated internally across the PCB circuit, microphones are placed ahead of the receivers (speakers).

1798 ER10C will provide fundamental and operational understanding of not only the
1799 ER10C system but also hearing measurement devices in general.

1800 3.2.1 Physical structure of ER10C

1801 In this section, we report detailed observations of the ER10C by opening up the
1802 device. Figure 3.7 shows the internal structure of the ER10C probe, which has been
1803 carefully disassembled into two parts; a holder with microphones (Fig. 3.7(a)) and a
1804 circuit board (PCB) with speakers (Fig. 3.7(b)). The microphone holder part has a
1805 chamber in the middle, holding steel tubes to construct the input (microphone) and
1806 the output (speakers) sound paths to each transducer. The microphones are firmly
1807 attached to the chamber while the speakers are attached to steel tubes via a soft
1808 rubber tubes, floated in the air. As the air acts as a best damper, in this way, any
1809 vibrational nonlinear effect (crosstalk) from the speakers can be reduced.

1810 Detailed shape of the chamber (alone) is introduced in Fig. 3.8. The front side of
1811 the chamber has three holes; two small holes are for the two outputs, and one large

Draft of November 2, 2014 at 17:33

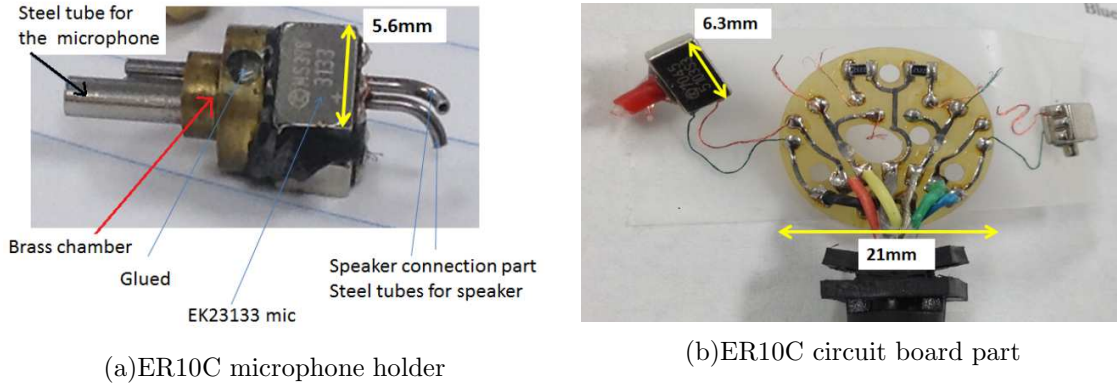


Figure 3.7: Disassembled ER10C. Two parts are inside; (a) microphone holder and (b) circuit board parts. Note that lots of care were needed to see the part (a) as it was permanently attached to the probe's case.

1812 hole is for the input. The back side has four holes; two microphone' ports are directly
1813 plugged into the larger two upper holes, and thin steel tubes (for the speakers) are
passing through the small two lower holes.

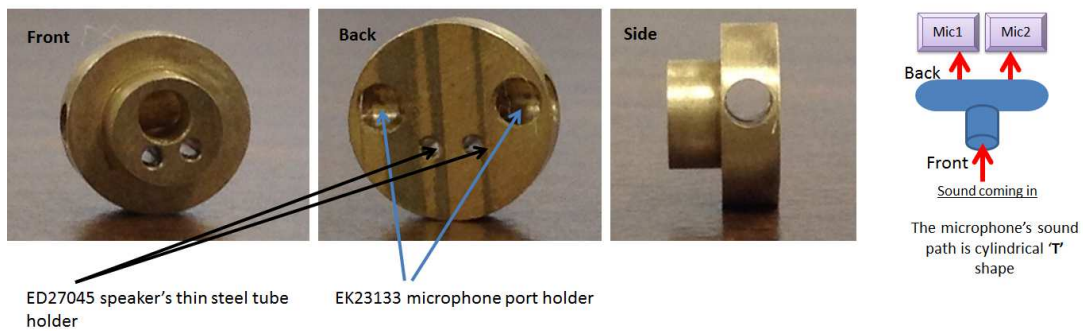


Figure 3.8: Details of the brass chamber in Fig. 3.7. The recent design of ER10C, an aluminum material chamber is used maintaining the same shape.

1814

1815 It may be noted from the structure of the brass cavity (Fig. 3.8) that a unique
1816 point about the input structure of the ER10C (compared to the other hearing mea-
1817 surement probes) is that it has two internal microphones which acts as one input.
1818 The electrical terminals of two microphones are connected with a two-diode package
1819 (i.e., MMBD7000), but only one diode is used, set up to be reverse biased in series

Draft of November 2, 2014 at 17:33

1820 with a capacitor (between the nominal microphone’s “output” and the “ground”
1821 terminals, Fig. 3.9). This is a traditional approach in the hearing aid industry, to
1822 protect the input from spark discharge. The capacitor is to filter out the very large
1823 spark discharge, and take it out (clip it) with the diode. There are two parallel 22K
1824 ohm resistors for two microphones as shown in Fig. 3.7 (black squares with 2122
1825 written on it). But as this system has a single input (this input channel may be
1826 separated as two inputs externally), the resistance of the input channel reads 11 k Ω .

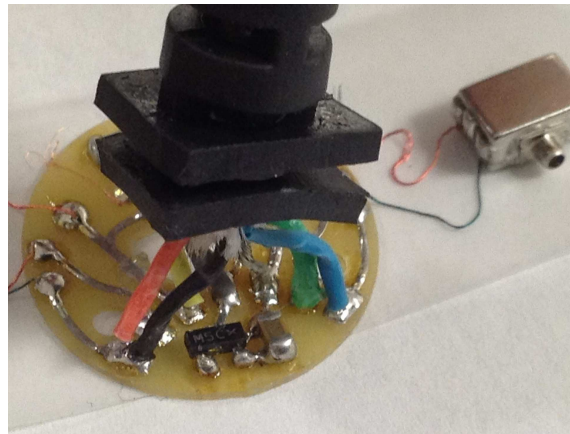


Figure 3.9: ER10C circuit board details. A diode package and a capacitor are shown under the wire soldering ends. Only one diode is used to set up to be reverse biased, in series with a capacitor between the microphone’s “output” and the “ground” terminals. It is a traditional approach in the hearing aid industry, to protect the input from spark discharge.

1827

1828 Figure 3.10 explains the connection details of the two probe parts shown in Fig. 3.7.
1829 The speakers are connected to the curved steel tubes (right side of the upper right
1830 picture) via red rubber tubes attached on speaker port (upper left).

1831 3.2.2 Crosstalk measurement

1832 In this part, we investigate a critical topic to design a hearing measurement probe:
1833 “crosstalk.” Starting from categorizing various types of crosstalk, we describe each
1834 crosstalk measurement.

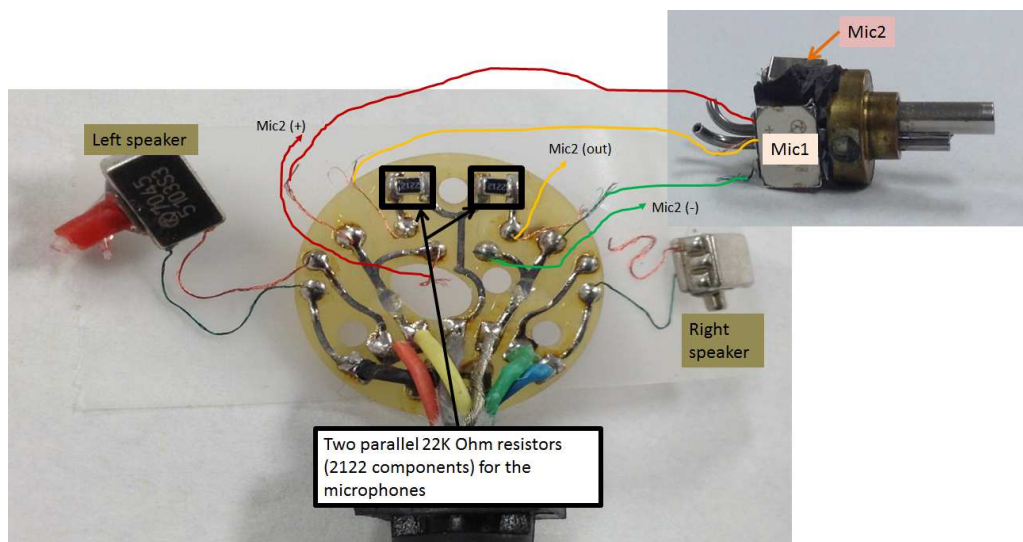


Figure 3.10: ER10C circuit board (Fig. 3.7(b)) and connection details with microphone holder part in Fig. 3.7(a). Note that the speakers are connected to the curved steel tubes via red rubber tubes.

1835 In an electro-acoustic system, crosstalk is undesired signal that is observed in the
1836 system's response. It may contaminate system's signal to and from both the speaker
1837 and the microphone. Our main concern is the crosstalk in the microphone, which
1838 may be categorized into three types,

- 1839 1. Electrical: Coupling of the input signals via the electrical wires, usually affect-
1840 ing the output at high frequencies. To measure this, we may block the probe's
1841 microphone and generate a signal from the speaker, then measure the probe's
1842 microphone response. Ideally, as we blocked the microphone, the signal from
1843 the probe's microphone should be similar to the noise floor. If any signal is
1844 greater than the noise floor, it is the electrical crosstalk.
- 1845 2. Mechanical: vibrational coupling to microphone's diaphragm. Any physical
1846 vibration through probe's body, not through the main input path, the port of
1847 the microphone (i.e., touching the probe' head during measurement can affect
1848 the microphone's diaphragm). To prevent this crosstalk, the probe should be
1849 placed with a 'hands-free' condition during experiments.

1850 3. Acoustical: any signal coming into the system from outside of the region of
1851 measurement (i.e., noise). Typically this is related to poor acoustic seals in the
1852 system, and affects low frequency measurements, increasing the noise floor. To
1853 measure this acoustic crosstalk, we may stimulate output channel 1 (connected
1854 to input channel 1) with a signal and measure the input of channel 2. Ideally,
1855 input channel 2 should have no signal, if the device has zero crosstalk (or similar
1856 to noise floor). However if the acoustic crosstalk is present, some signal that
1857 corresponds to the output of channel 1 will be observed at the channel 2 input.

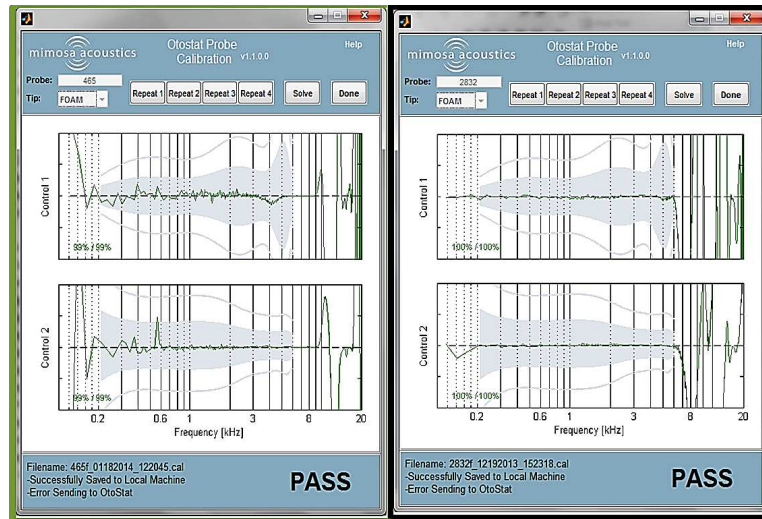
1858 3.2.3 Calibration issues

1859 Figure 3.11 describes calibration details of the ER10C. The ER10C probes may be
1860 categorized into three types based on their calibration pass/fail frequency range.

1861 With careful investigation to find out the reason of the calibration failure both
1862 physically and theoretically, we hypothesized that the problem is in the electrical
1863 crosstalk based on the experimental data shown in Fig. 3.12 and Fig. 3.13. When we
1864 blocked the ER10C microphone, sound signal cannot pass through the acoustic sound
1865 path of the microphone. Therefore the acquired data from the microphone should
1866 be similar to noise floor. The result that we had in Fig. 3.12 does not agree with this
1867 point, meaning that it is experiencing electrical cross talk. One might assume that
1868 imperfectly blocking the hole may cause this result, but the signal would have been
1869 shown in low frequency, not in high frequency.

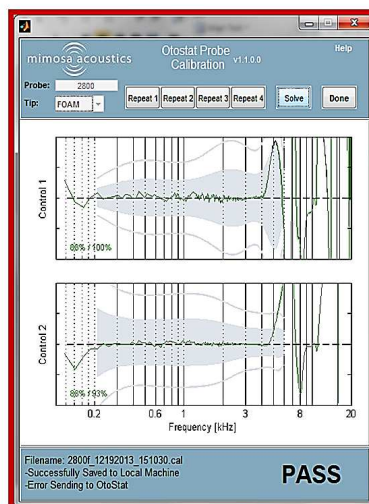
1870 The long electric wire attached on ER10C probe head is the source of the elec-
1871 trical crosstalk. One ER10C was specially modified as requested to eliminate, the
1872 capacitive coupling in blocked ER10Cs microphone response, approximately 20dB
1873 per octave or 60dB per decade curve in high frequency (Fig. 3.12). To remove the
1874 capacitive coupling caused by the ER10Cs long wire, we put the amplifier near the
1875 probe head (The improved crosstalk result is introduced in Fig. 3.13). A theoretical
1876 explanation of this can be found in Eq. 2.74, $\frac{\partial \mathbf{D}}{\partial t}$ term in Ampere's law, which is
1877 underestimated in the probe's design process.

Draft of November 2, 2014 at 17:33



(a) Old good ER10C

(b) New good ER10C



(c) New bad ER10C

Figure 3.11: (a) Brass material for the middle tube holder part (the brass holder). RTV silicon is used to block the holder's side hole. Calibration passes up to 9-10kHz (ER10C with 3 digits serial number) (b) Aluminum material for the chamber. RTV silicon is not used to block the holder's side hole, but some of black material seals the side hole. Calibration passes up to 6kHz (ER10C with 4 digits serial number). (c) Aluminum chamber is used. None of material seals the holder's side hole, a portion of the hole could be sealed randomly. Calibration totally fails or sometimes it passes but is unstable usually above 4kHz (ER10C with 4 digits serial number). Also (based on the manufacturer), the type of wire used in ER10C has been changed.

Draft of November 2, 2014 at 17:33

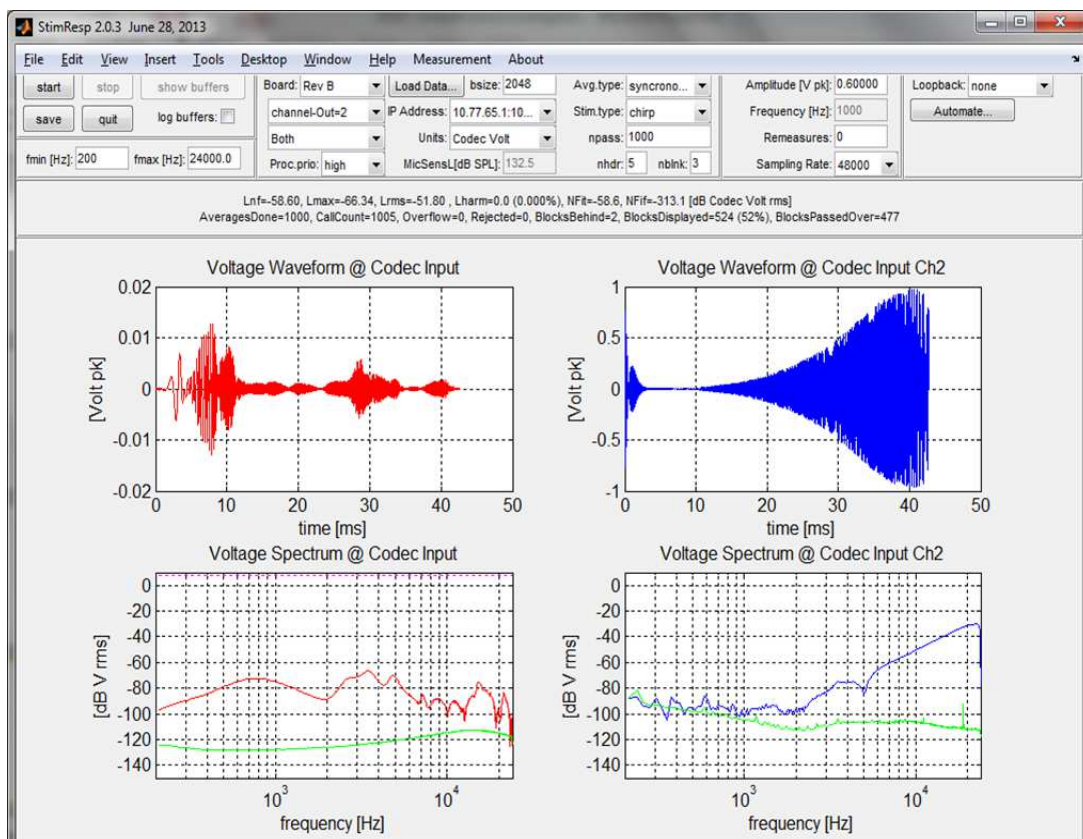


Figure 3.12: Original ER10C crosstalk (blue) with ER7C response (red): The sound (0.6V chirp, zero to peak, not RMS) was generated by one of the internal ER10C speakers. The right (blue, ch2) shows the blocked ER10C (serial: 2928) microphone response, and the left (red, ch2) shows the E7C microphone response as a reference of the sound level. Note that we used a small cut syringe with a tiny volume to connect both ER7C microphone and ER10C probe. We blocked the microphone hole on the attached ER10C foam tip for decoupling the microphone path from the sound in the cavity generated by the internal ER10C speaker. Physically and theoretically, internal ER10C's sound paths for the microphones and the receivers are separated. Therefore if the microphone hole is blocked, none of the acoustic signal can go through the microphone's diaphragm. any signal that is shown on the right side of this figure (blue) is internal crosstalk of the probe. We read that in high frequency it is approximately increasing proportion to 20dB/octave (capacitive coupling), based on this observation, we hypothesize the source of this crosstalk is in wire of ER10C. This was the motivation of modifying ER10C, including the preamp on the ER10Cs head. Note that this measurement was made on May 14 2014 at Mimosa Acoustics by NK using Stimresp software (Mimosa Acoustics)

Draft of November 2, 2014 at 17:33

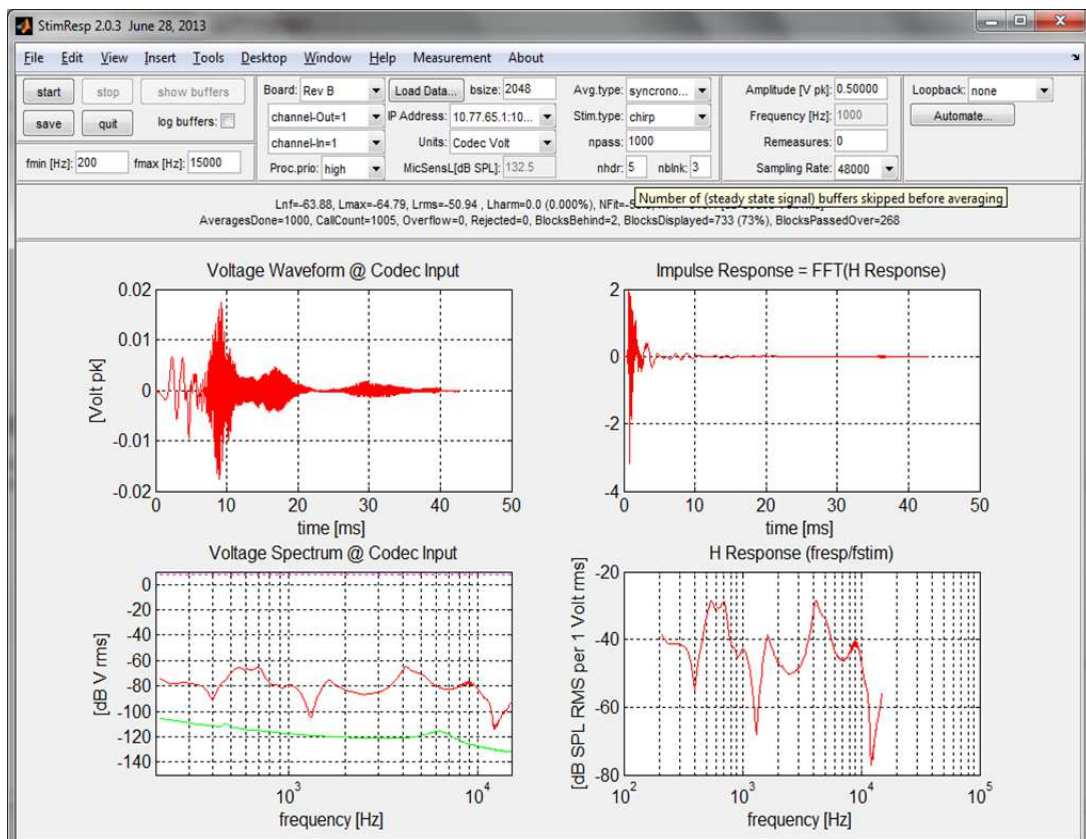


Figure 3.13: ER10C crosstalk (blue) after the modification: Crosstalk measurement after the modification, the rising crosstalk behavior in high frequency is apparently reduced. The modified ER10C is inserted in a short cavity with blocked microphone. The probe is connected to the specially modified APU for the modified ER10C.

1878 3.3 A new probe design

1879 Motivated by the published transducer model (Kim and Allen, 2013) as well as
1880 the experimental investigation of ER10C, we have designed improved measurement
1881 probes to extend middle ear diagnostics. These new acoustic probes, the MA16
1882 and MA17, have been considered to enhance characteristics of the ER10C, such as
1883 sensitivity, frequency response, noise floor and linearity.

1884 We explain how we designed our hearing measurement probe based on the theoret-
1885 ical understanding of probe's functions as well as trials and errors from experiments.

1886 3.3.1 Choice of transducers

1887 Two kinds of transducers are needed, a microphone and receiver. Based on the
1888 linearity of the receiver, (usually) we may need two receivers in a probe to measure
1889 such as DPOAE.

1890 Using an absolute microphone (i.e., BK2137 or ER7C), sensitivities of both mi-
1891 crophone and receivers should be measured in mV/Pa and Pa/mV. The industry
1892 standard for the microphone sensitivity is 50 [mV/Pa] at 1kHz.

1893 Dynamic range (or linearity) of the probe defines the usable range of the probe in
1894 terms of both frequency range and the level of the signal.

1895 Based on the all of the above, we can choose the right combination of microphone
1896 and receiver.

1897 3.3.2 Sound delivery path for the microphone

1898 The microphone picks up the sound inside a space such as a testing cavity, ear canal,
1899 or artificial ear. Though there are many modes in the spreading waves, namely higher
1900 order modes (HOMs) in the space, what we really consider is the plane wave, which
1901 is easy to analyze especially for the source calibration procedure; the HOMs may be
1902 ignored if there is a sufficiently large distance in the system over which they will die

Draft of November 2, 2014 at 17:33

1903 out exponentially. Here are experimental technics for performing a simple calibration
1904 procedure assuming the microphone is used to measure an ideal cylindrical cavity.

- 1905 1. centering the microphone port, pointing the cavity end.
- 1906 2. about 3[mm] of tube is needed in front of the microphone's port to pick up
1907 the plane wave. Note that the HOMs die out within a few mm once the wave
1908 starts to spread from the source.
- 1909 3. when the frequency response of the microphone is not flat (dividing the micro-
1910 phone response to an ideal microphone), introducing peaks, it usually means
1911 the microphone tube is too long. You may use a loosely packed cotton or
1912 acoustic resistor, to minimize the tube effect.

1913 3.3.3 Sound delivery path for the receiver

1914 When sound is generated from a receiver, it is guided by its port and then spreads
1915 out. An ideal speaker has a flat frequency response regardless of the signal level,
1916 maintaining a constant level across all frequencies. But the reality is that distortions
1917 are observed due to high peaks (in pressure) at certain frequencies if we derive high
1918 voltage level to the receiver. There is not a linear relationship between the level of
1919 the distortion and the level of signal, due to the hysteresis effect of electro-magnetic
1920 system. Indeed the BAR is a really noisy device to deal with. Here are systematic
1921 procedures to handle this device when we make a probe.

- 1922 1. Finding out the linear region of this transducer (dynamic range) based on the
1923 given sensitivity is critical.
- 1924 2. Instead of acoustic resistors, a small piece of cotton (loosely packed) can be
1925 applied to the sound spreading area inside the probe. This will help not only
1926 to damp out the pressure peak at the certain frequency point but also to design
1927 the wave spreading space close to the ideal shape (i.e., cylinder).

1928 **3.3.4 Probe evaluation**

1929 The following is a list of specifications to evaluate a hearing measurement probe:

- 1930 1. Frequency responses of both microphone and speaker should be as flat as possible,
1931 especially within the frequency range of human hearing (ideally up to
1932 20kHz for the microphone and up to 16kHz for the speaker)
- 1933 2. Thevenin parameters must be stable over time. This can be evaluated via
1934 source calibration (i.e., 4 cavity calibration, Allen (1986))
- 1935 3. Output levels for loudspeakers should be higher for amplification of signal,
1936 especially for measuring hearing impaired ears. (i.e., 85dB SPL desirable)
- 1937 4. Dynamic range as large as possible. Dynamic range is defined as the subtraction
1938 between the first harmonic level and the total harmonic level at each frequency
1939 (i.e., 50-60dB is acceptable).
- 1940 5. Linearity superior to current probes. Dynamic range should be linear across
1941 the frequency range of interest.
- 1942 6. Impulse response should be short and exact. The duration of impulse ringing
1943 should be less than 1 ms. This result is critical to TEOAE measurement.
- 1944 7. Crosstalk issues including all noise sources must be addressed - microphone,
1945 loudspeaker,
- 1946 8. Good seal and stability in the ear canal. This needs good earplug design to fit
1947 a range of adult ear-canal sizes and shapes easily.

1948 The size of the probe is an especially critical factor in the clinic for measurements of
1949 infant ears, due to their very small ear canals. There are other serious issues relevant
1950 to manufacturing a probe, such as handling ear tips, removing ear wax, etc, which
1951 must take into account in the probe design.

1952 A general acoustic measurement setup (to test the itemized evaluation categories)
1953 is found in Fig. 3.14.

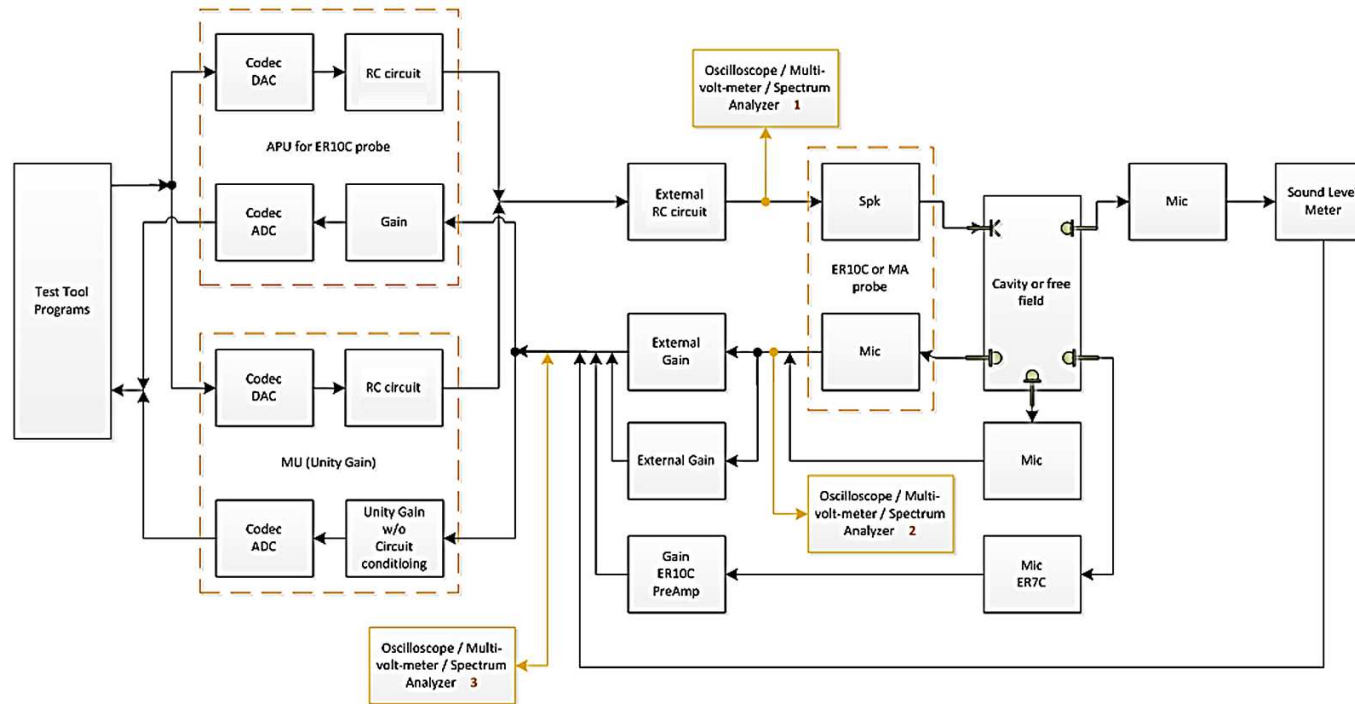


Figure 3.14: Basic acoustic testing setup

Draft of November 2, 2014 at 17:33

1954 The ‘cavity or free field’ block can be DB100 or B&K4157 artificial ear coupler, a
1955 cut-off syringe, any tube, or any rigid cavity in which the probe may be sealed. The
1956 ‘probe’ block can be any probe containing a loudspeaker and a microphone (or two
1957 microphones). The probes we have used include the ER10C and MA probes. We
1958 also use a probe simulator³ to evaluate the electronic part of the system, in order to
1959 provide a baseline for the probe’s performance characteristics.

1960 In our specific experiments, two audio processing units were used, an APU and
1961 MU (‘Audio Processing Unit’ and ‘Modified Unit’ by Mimoso Acoustics). The APU
1962 is built for use with the ER10C probe. The other, the MU, is built to by-pass the
1963 internal RC (a parallel combination of a resistor R and a capacitor C to boost up
1964 the signal level in the high frequency region) of the ER10C probe, setting the gain to
1965 unity. The MU is used for the other probes, such as the MA probes (and ILO probe
1966 from Otodynamics). When using the MU with these other probes, an external RC
1967 circuit and pre-amp can be added for evaluation.

1968 Several microphones can be used for calibration of the transducers used in the
1969 probe, to measure the receiver and microphone sensitivities, frequency responses,
1970 and other characteristics. The microphone (‘Mic’, the previous stage of the ‘Sound
1971 Level Meter’ in Fig. 3.14) and ER7C microphone (‘Mic ER7C’ in Fig. 3.14) are
1972 reference microphones, which have wide and flat frequency responses. When both
1973 the reference microphones and the tested probe microphone pick up the response
1974 from the test cavity, the tested microphone’s response is divided by the reference
1975 microphone’s response to obtain the test microphone frequency response.

1976 An oscilloscope, spectrum analyzer, or multi-meter can be used to monitor the
1977 voltage at various points of the setup. In this setup, the specific points of interest
1978 are at

- 1979 1. the input to the tested probe speaker for computing the receiver sensitivity,
- 1980 2. the output of the tested probe microphone, and
- 1981 3. the output of the external gain for computing the microphone sensitivity.

³a package of circuit elements to simulate electrical part of the probe excluding the acoustic elements

Draft of November 2, 2014 at 17:33

1982 To check the frequency response of the transducers, it is necessary to calibrate
1983 the transducers (receivers and microphone inside the probe). Once we calculate the
1984 sensitivity of the transducer, we can compute the frequency response of the probe by
1985 applying a chirp signal and normalizing the response with the sensitivity at 1kHz.

CHAPTER 4

RESULTS

1986 In this section, we represent key results based on our theoretical and experimental
1987 study (chapter 2 and 3). Details of modeling BAR and its calibration results us-
1988 ing Hunt parameters are discussed. Then, we reduce the BAR model to a simple
1989 electro-mechanic system, only involving essential circuit components for composing
1990 the system. This minimized model is used for Z_{mot} simulations to justify our theory
1991 discussed in chapter 2.

1992 4.1 Hunt parameter calibration

1993 The calculated Hunt parameters of the BAR derived from various Z_{in} (Fig. 3.2) are
1994 shown in Fig. 4.1. Some considerations for the Hunt parameters of the BAR are as
1995 follows:

- 1996 1. Z_e : Compared to $Z_a(s)$ and $T_a(s)$, $Z_e(s)$ has the smallest dependency on the
1997 choice of load cavities (the three of six chosen load impedances: loads (2)-(7)
1998 in Fig. 3.2). Below 200[Hz], $Z_e(s)$ converges to a fixed resistance (ED7045:
1999 $\approx 195[\Omega]$). The frequency range between 0.5-2.5[kHz] is proportional to ‘s’
2000 (Z_e shows a slope of 1 in this frequency range). It is not clearly shown at
2001 frequencies below 10[kHz], however when the frequency increases, the slope
2002 of Z_e approaches that of ‘ \sqrt{s} ’. More precise evidence of ‘ \sqrt{s} ’ domination at
2003 high frequency is shown in Fig.3.3 in the polar plot. This frequency depen-
2004 dant impedance behavior (e.g., proportional to a constant, ‘s’ and ‘ \sqrt{s} ’) is
2005 determined by the coil properties, which are closely related the DC resistance,

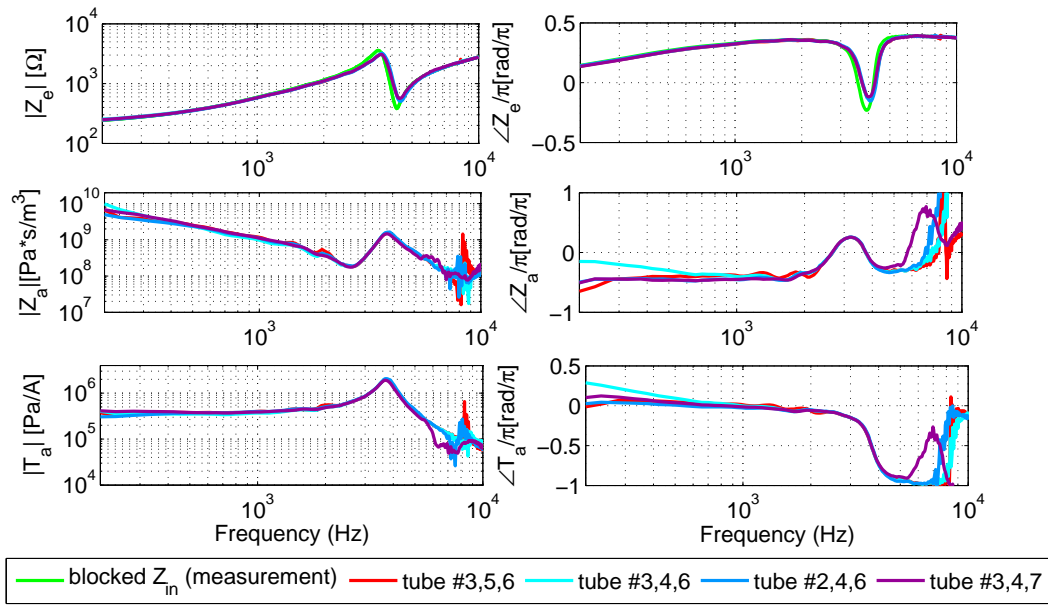


Figure 4.1: Calculated Hunt parameters (Z_e , Z_a , and T_a) of the ED7045. Three measurements of Z_{in} with acoustic loads (indicated by number as shown in the legend) are required to find one set of the three Hunt parameters. The length of each numbered tube is described in Fig. 3.2. Z_{in} which is measured by blocking the receiver's port ($V = 0$) is plotted with Z_e (green line).

2006 inductance and the semi-inductance. Note that Z_{in} (measured) $\rightarrow Z_e$ (calcu-
2007 lated) as $V \rightarrow 0$.

2008 2. **Z_a**: For frequencies below 2.5[kHz], Z_a is stiffness dominated (i.e., a capaci-
2009 tance), and between 2.5-4[kHz] it is dominated by the mass of the diaphragm
2010 and armature. Those properties determine the first anti-resonance (zero, near
2011 2.5[kHz]). The resonance (pole) at 3.7[kHz] is the frequency where the transfer
2012 impedance, T_a , is maximum. The pole of Z_e is also introduced in this same
2013 frequency. As T_a and Z_a are tied more closely, they move together when the
2014 set of Hunt parameter is changed while Z_e is almost identical over every set
2015 of the Hunt parameters (Fig. 4.2). Above 4[kHz] the transmission line and
2016 acoustic properties dominates given the small volume inside the receiver. The
2017 error above 6-7[kHz] is primarily caused by the experimental limitations, such
2018 as the manual manipulation of the tubes.

2019 3. **T_a**: It is nearly constant below 2-3[kHz] and is 4×10^5 [Pa/A] at 1[kHz]. The
2020 phase shift in T_a is due to acoustic delay. Although the frequencies above
2021 6[kHz] are obscured by the noise, T_a behaves as an all-pole function, which
2022 depends on the system delay τ . To account for this delay, a transmission line
2023 (Tx line) is added to the acoustic model, as shown in Fig. 1.1.

2024 4.2 Receiver model

2025 In this section, we discuss details of our refined BAR model introduced in Fig. 1.1.
2026 The electrical circuit elements are shown to the left of the gyrator. R_e is approxi-
2027 mated to the DC resistance. The source of the armature movement is the Lorentz
2028 force ($F = \int J \times BdA$) due to the interaction of the current in the coil and the
2029 static magnetic field B_0 of the magnets. The current in the coil and the core of
2030 the E-shaped armature give rise to the inductance L_{em} , while the penetration of the
2031 magnetic field into the core induces an eddy current, depicted by a semi-inductor
2032 element K_1 in Fig. 1.1 Vanderkooy (1989). L_e represents any leakage flux, in air gap,

2033 which explains an additional small stored energy.

2034 There should be a transition frequency, $f_t = \frac{1}{2\pi} \left(\frac{K_0}{L_0} \right)^2$, between the inductor (L_0)
2035 and the semi-inductor (K_0). Since we used two inductors and one semi-inductor
2036 (total 3) for our receiver model, it is unclear exactly how to calculate the f_t from
2037 these components as we discussed in section 4.1. However as shown in Fig. 4.3 (polar
2038 plot), the slope of the impedance is approaching \sqrt{s} (45°) as ω increases. Based on
2039 Thorborg et al. (2007), the f_t of a dynamic loudspeaker is 100-200[Hz], which means
2040 the f_t for the balanced armature receiver is much higher than for the moving coil
2041 loudspeaker.

2042 The gyrator relates the electrical and the mechanical sections with parameter
2043 $T = B_0 l$. The wire inside the ED7045 receiver is made of 49 AWG copper, which
2044 has a resistivity of 26.5[Ω /m]. Since the measured DC resistance of the receiver is
2045 around 190[Ω] we can calculate the length of the wire is approximately 7.1[m]. In
2046 general, the dynamic moving-coil speaker's l is shorter than the BAR's. Therefore
2047 we can expect a larger 'T' value for the BAR ($n \propto l, 1/d_{coil}$).

2048 To the right of the gyrator are the mechanical and acoustical sections of the trans-
2049 ducer. We can simply describe the mechanical section as composed of a series com-
2050 bination of the armature and the diaphragm's stiffness, mass and damping. The
2051 transformer's coupling ratio of the acoustic side to the mechanical side is related to
2052 the diaphragm's area. The capacitor (C_a) and a transmission line in the acoustical
2053 part account for the back (rear) volume and sound delay. Because we are using a
2054 gyrator, the mobility analogy method is not used (Beranek, 1954; Hunt, 1954).

2055 The Thevenin pressure of the BAR is defined given that the volume velocity (V)
2056 at the port is zero ('blocked' port), meaning the load impedance is set to ∞ .

2057 Several comparisons are made to verify the transducer model. First, the Hunt
2058 parameters are calculated from the model to support the transfer relation between
2059 electrical and acoustical parts (Section 3.1.1). The mechanical part of the transducer
2060 model was verified by conducting laser mechanical velocity measurements in a vac-
2061 uum condition (Section 3.1.2). Along with these results, we simulated the Thevenin
2062 pressure of the transducer from our model and compared the result to the pres-
2063 sure measurement (when $V=0$) (Section 3.1.3). These three comparisons (electrical,

Electrical elements
$R_e = 195 [\Omega]$,
$L_e = 9 [\text{mH}]$,
$K_1 = 27.5 [\text{Semi-Henry}]$, $L_{em} = 52 [\text{mH}]$
GYR = 7.5
Mechanical elements
$C_m = 1.25\text{e-}3 [\text{F}]$, $L_m = 4.3\text{e-}6 [\text{H}]$, $R_m = 0.003 [\Omega]$
TRF (1/Area) = $1/(2.4\text{e-}6)$
Acoustical elements
$C_a = 4.3\text{e-}15 [\text{F}]$
Tx Line: $z_0 = 1\text{e}9 [\text{kg/sec}]$, $l_t = 1\text{e-}4 [\text{m}]$
Radiation impedance
$L_{rad} = 10^{10} [\text{Acoustic-Henry}]$, $R_{rad} = 10^{11} [\text{Acoustic-Ohm}]$

Table 4.1: Specific parameters that are used for the suggested model (Knowles BAR ED7045). c is the speed of sound in the air (334.8[m/s]), $j\omega/c$, z_0 , and l_t are the propagation function, specific characteristic resistance and length of the transmission line, respectively. GYR and TRF stand for the gyrator and the transformer. All model parameters were found by minimizing the RMS error between the model and electrical input impedance measurements of the receiver.

2064 mechanical, and acoustical) justify and verify the transducer model (Fig. 1.1).

2065 4.2.1 Hunt parameters comparison

2066 The Hunt parameters, from the model and the experimental calculation, are com-
 2067 pared in Fig. 4.2. The discrepancies of Z_a above 6 - 7[kHz] are presumably caused
 2068 by the manual adjustment of the experimental conditions. This error is insignificant
 2069 in Z_e . However the small noise in electrical impedance impacts the parameter esti-
 2070 mation far from the electrical side. In other words, we can see the largest variation
 2071 in acoustical parameter (Z_a), as the transition order goes from $Z_e \rightarrow T_a \rightarrow Z_a$.

2072 Another interesting parameter is the resonant frequency (3-4kHz). The frequency
 2073 of the pole (f_p) in Fig. 4.2 looks almost identical to each parameter: Z_e . Z_a and
 2074 T_a slightly differ by the set, but the f_p of the three parameters occurs at the same
 2075 location for the same set of Hunt parameters. The three parameters assume the
 2076 zero-loaded condition which means, in theory, the f_p should be identical for all cases.

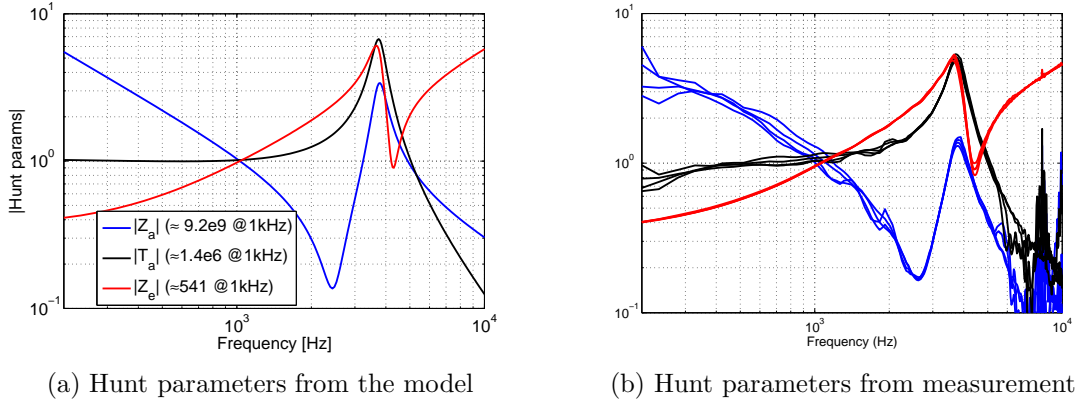


Figure 4.2: Comparison of Hunt parameters (Z_e (red), T_a (black), and Z_a (blue)) from the model (a) and the measurements (b). Any significant differences between the model and the data occur above 6[kHz]. All parameters are normalized to their 1[kHz] values.

2077 Because of small measurement differences, this is not exactly the case. This resonant
 2078 frequency can thus be interpreted as one of the most fundamental characteristics
 2079 (eigenmode) of an electro-magnetic transducer.

2080 4.2.2 Verification 1: Electrical impedance *in vacuo*

2081 The acoustical part in the transducer model is removed for the vacuum case, while all
 2082 the electrical and mechanical parameters in Fig. 1.1 during the experiments remain
 2083 the same as the no-vacuum condition.

2084 In Fig. 4.3, the simulated electrical input impedance results are expressed in two
 2085 ways; the magnitude-phase and the polar plot (real vs. imaginary parts). For both
 2086 the vacuum and the blocked port condition, the model (solid lines) and the experi-
 2087 ment result (dashed lines) show reasonable agreement below ≈ 12 [kHz].

2088 The transducer model, including acoustical elements ('blocked' output port) is
 2089 in red, and the model excluding acoustical elements (vacuum condition) is in blue.
 2090 Both cases give similar shape, a pole, followed by a zero, with increasing frequency
 2091 (≈ 890 [Hz] in vacuum, ≈ 750 [Hz] in blocked case). We conclude that the trapped air
 2092 (between the diaphragm and the port of the receiver) influences the resonance by

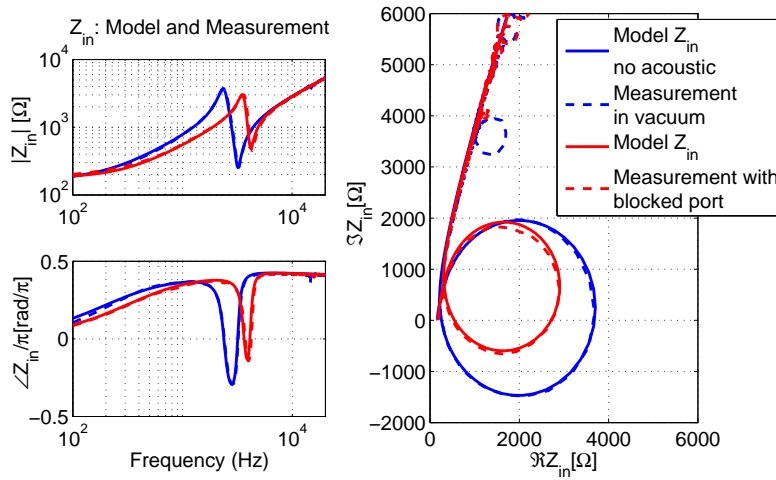


Figure 4.3: Comparison the suggested model of Fig. 1.1 and real electrical input impedance measurement of a balanced armature hearing-aid receiver (Knowles, ED7045). Blue and red colors represent vacuum and non-vacuum (ambient) conditions respectively. And the dashed lines represent the experimental result, whereas the single lines show the model results. For the vacuum experiment, the static pressure is less than 0.003[atm]. The left panel shows the magnitude and the phase of each condition while the real and imaginary parts of the same data are plotted in the right panel. Up to 23[kHz], the experimental data is in good agreement with the modeling result (The sampling rate is 48[kHz], therefore the maximum measured frequency is 24[kHz]). In the polar plot, above 8[kHz], the impedance behaves as \sqrt{s} .

2093 pushing it to higher frequencies due to the increased stiffness to mass ratio. Also
2094 because of the acoustical properties (including mechanical-acoustical coupling), the
2095 magnitude of the vacuum resonance is reduced by 1.9dB compared to the blocking
2096 the receiver's output port (in air).

2097 By looking at the polar plot (the right panel in Fig. 4.3), we can clearly see that the
2098 high frequency impedance is dominated by \sqrt{s} , clear evidence of the eddy-current,
2099 in the BAR. The many small loops appearing above 16[kHz] may be a measurement
2100 artifact, however the second resonance at 15[kHz] is real.

2101 4.2.3 Verification 2: Mechanical velocity measurement using Laser 2102 *in vacuo*

2103 As shown in Fig. 4.4, the mechanical velocity is also calculated from the transducer
2104 model and compared with the laser velocity measurement result. The model and the
2105 experiment are well matched below 10[kHz].

2106 However small magnitude difference is observed; the laser measured data has about
2107 1[dB] higher velocity at the FR and the low frequency area. There are some possible
2108 solutions to improve the model. First, as explained in section 3.1.2, when we make
2109 the measurement, we put the laser's focus near at the rod (where the armature and
2110 the diaphragm is connected). And secondly, when modeling the data, we could add
2111 or remove mechanical damping in the transducer model (i.e., increasing or decreasing
2112 the value of R_m in our model Fig. 1.1) relative to the present value. The problem
2113 below 200[Hz] is due to a very small hole that is burned into the diaphragm, to act
2114 as a very low frequency leak.

2115 The mechanical velocity is calculated by assuming the force (F) in vacuum is zero.
2116 In reality, it is impossible to reach an absolute vacuum condition. Our experiment
2117 condition of 0.003[atm] seems adequate to understand the nature of the mechanical
2118 velocity of the transducer as the measurement gives a reasonable agreement with the
2119 model.

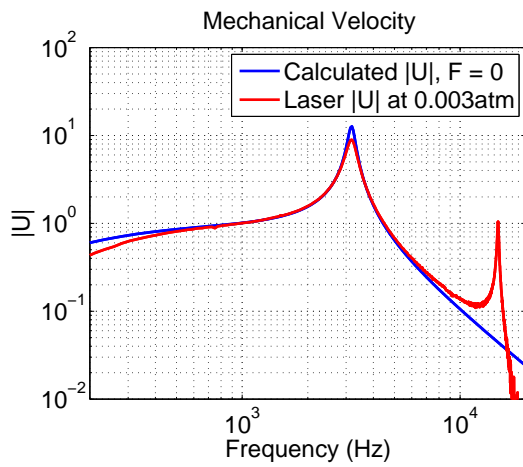


Figure 4.4: Comparison of the diaphragm (mechanical) velocity between the transducer model and the laser measurement in vacuum, the pressure P is zero. For the model simulation, the acoustical part in Fig. 1.1 is not included. The laser measurement was performed after pumping out the air in the receiver. All values are normalized to one at 1[kHz].

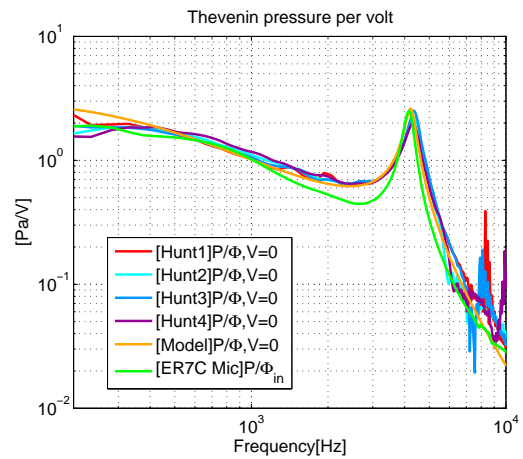


Figure 4.5: Comparison of Thevenin pressure (per voltage) data from various sources. There are 6 different lines, the first 4 lines are calculated from the electrical experiments (Hunt parameters), and the orange colored line is estimated from the model. The last pressure data (in light-green) are taken from the pressure measurement and are divided by the electrical input voltage of the receiver. All data assume the blocked condition, $V=0$ (see text). Every value is normalized to one at 1[kHz].

2120 4.2.4 Verification 3: Thevenin pressure comparison

2121 The model and measured Thevenin pressure are plotted in Fig. 4.5. Two indirect
 2122 pressure estimation methods are used; one using the Hunt parameters, and the other
 2123 using the simulation of our transducer model. There is a reasonable agreement among
 2124 these measures up to 6-7[kHz]. The mathematical definitions of these data are the
 2125 Thevenin pressure per unit voltage (P/Φ), with a zero volume velocity ($V = 0$),

$$\frac{P}{\Phi} \Big|_{V=0} = \frac{T_a}{Z_e} \Big|_{V=0} . \quad (4.1)$$

2126 Note that $\frac{P}{T}$ and $\frac{P}{\Phi}$ differ in the theoretical meaning as well as in the definition;
 2127 $T_a \equiv \frac{P}{T} \Big|_{V=0}$ is one of the Hunt parameters, while the Thevenin pressure (per volt)
 2128 in Eq. 4.1 is a more realistic experimental function, when one uses a voltage drive.
 2129 For the comparison, the pressure data is divided by the voltage (Φ_{in}) across the
 2130 two electrical terminals of ED7075 (A and B in Fig. 3.5) when $V = 0$. The data
 2131 from section 3.1.1 is imported for Φ_{in} , assuming $V = 0$ at the port in the pressure
 2132 measurement.

2133 The green line in Fig. 4.5 shows the Thevenin pressure data derived from the ER-7C
 2134 probe microphone. Other than the direct pressure measurement (green), all responses
 2135 are derived from the Hunt parameter calculation introduced in the Appendix E, using
 2136 the ‘electrical input impedance measurements’ for acoustical loads.

2137 4.3 Z_{mot} simulation of simplified electro-mechanic systems

2138 For further application, we will investigate a simple electro-mechanic network model
 2139 including a semi-inductor. The goal is to demonstrate some condition that $\Re Z_{mot} < 0$
 2140 based on the simplified electro-mechanic model. The simple electro-mechanic model
 2141 has been reduced from the Kim and Allen’s original work (Fig. 1.1: the electro-
 2142 acoustic network model, Kim and Allen (2013)). Related theories are discussed in
 2143 section 2.4 and Appendix B.

2144 Left sided figure in Fig. 4.6 shows a oversimplified two-port network from Fig. 1.1

2145 containing only essential components for better and easier understanding of the phys-
 2146 ical electro-mechanic system. In this simple model, any acoustic or resistive compo-
 2147 nents are eliminated.

2148 In this figure we have four components: a semi-inductor, an inductor in the elec-
 2149 trical port, a mass in the mechanical port, and a gyrator that links two ports.

2150 The two circuits in Fig. 4.6 represent equivalent circuits via the mobility (dual)
 2151 analogy. In both, very low and high frequencies the capacitor ‘m’ is opened. The
 2152 parallel relation of semi-inductor and inductor enables the semi-inductor’s high fre-
 2153 quency dominance Vanderkooy (1989). The mid frequency is governed by the induc-
 2154 tor L and the capacitor m. If we ignore the semi-inductor in Fig. 4.6, the system looks
 2155 like a Helmholtz resonator with neck mass L and barrel compliance m. Therefore
 these two components act like a resonator in the system.

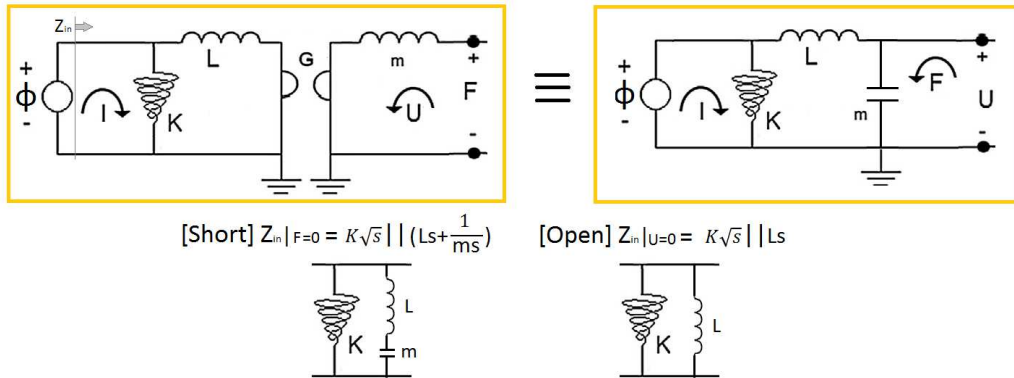


Figure 4.6: The top left circuit: A simple anti-reciprocal network with a semi-inductor presence. The top right circuit: The dual representation of the left circuit (equivalent) by applying mobility analogy beyond the gyrator. Z_{mot} is reconsidered based on Eq. 2.43. The frequency dependent real parts (shunt loss) of the semi-inductor in $Z_{in}|_{F=0}$ (short) experience positive phase shift when the open condition impedance ($Z_{in}|_{U=0}$) is subtracted from it.

2156

2157 To realize this system into a matrix form, we can use ABCD matrix cascading
 2158 method which results in Eq. 4.2.

$$\begin{bmatrix} \Phi(\omega) \\ I(\omega) \end{bmatrix} = \begin{bmatrix} 1 & 0 \\ \frac{1}{K\sqrt{s}} & 1 \end{bmatrix} \begin{bmatrix} 1 & sL \\ 0 & 1 \end{bmatrix} \begin{bmatrix} 0 & G \\ \frac{1}{G} & 0 \end{bmatrix} \begin{bmatrix} 1 & sm \\ 0 & 1 \end{bmatrix} \begin{bmatrix} F(\omega) \\ -U(\omega) \end{bmatrix}, \quad (4.2)$$

2159 where s is the Laplace frequency ($\sigma + j\omega$) and ‘ L ’, ‘ K ’, ‘ G ’, and ‘ m ’ are the inductance,
 2160 the semi-inductance, the gyration coefficient, and the mass of the system respectively.

2161 Let’s isolating the ABCD matrix part in Eq. 4.2 and setting ‘ L ’, ‘ K ’, ‘ G ’, and ‘ m ’
 2162 to be ‘1’ for a simple to make the algebra simple calculation, the equation is reduced
 2163 to

$$\begin{bmatrix} 1 & 0 \\ \frac{1}{\sqrt{s}} & 1 \end{bmatrix} \begin{bmatrix} 1 & s \\ 0 & 1 \end{bmatrix} \begin{bmatrix} 0 & 1 \\ 1 & 0 \end{bmatrix} \begin{bmatrix} 1 & s \\ 0 & 1 \end{bmatrix} = \begin{bmatrix} 1 & s \\ \frac{1}{\sqrt{s}} & \frac{s}{\sqrt{s}} + 1 \end{bmatrix} \begin{bmatrix} 0 & 1 \\ 1 & s \end{bmatrix} \quad (4.3)$$

2164 Finally the ABCD matrix of the system in Fig. 4.6 is

$$\begin{bmatrix} \Phi(\omega) \\ I(\omega) \end{bmatrix} = [T_1] \begin{bmatrix} F(\omega) \\ -U(\omega) \end{bmatrix} = \begin{bmatrix} A(s) & B(s) \\ C(s) & D(s) \end{bmatrix} \begin{bmatrix} F(\omega) \\ -U(\omega) \end{bmatrix} = \begin{bmatrix} s & 1 + s^2 \\ \frac{s}{\sqrt{s}} + 1 & \frac{1}{\sqrt{s}} + \frac{s^2}{\sqrt{s}} + s \end{bmatrix} \begin{bmatrix} F(\omega) \\ -U(\omega) \end{bmatrix}, \quad (4.4)$$

2165 where $\Delta_{T1} = -1$. Converting Eq. 4.4 into an impedance matrix, Eq. 2.7 is used to
 2166 give us

$$Z_1 = \begin{bmatrix} z_{11} & z_{12} \\ z_{21} & z_{22} \end{bmatrix}, \quad (4.5)$$

2167 where

$$z_{11} = \frac{s}{\frac{s}{\sqrt{s}} + 1} = \frac{s\sqrt{s}}{s + \sqrt{s}} (\equiv s || \sqrt{s}), \quad (4.6)$$

2168

$$z_{12} = \frac{-1}{\frac{s}{\sqrt{s}} + 1} = -\frac{\sqrt{s}}{s + \sqrt{s}}, \quad (4.7)$$

2169

$$z_{21} = \frac{1}{\frac{s}{\sqrt{s}} + 1} = \frac{\sqrt{s}}{s + \sqrt{s}}, \quad (4.8)$$

2170

$$z_{22} = \frac{\frac{1}{\sqrt{s}} + \frac{s^2}{\sqrt{s}} + s}{\frac{s}{\sqrt{s}} + 1} = \frac{1 + s^2 + s\sqrt{s}}{s + \sqrt{s}}. \quad (4.9)$$

2171 By substituting ‘ s ’ with ‘ $j\omega$ ’ one can easily find that all impedances of this system
 2172 (Eq. 4.6, 4.7, 4.8, and 4.9) are complex quantities, meaning that all have both real
 2173 and imaginary parts in each frequency point. The results shown in Eq. 4.6 - Eq. 4.9
 2174 are a counter example that does not follow the traditional approach of a lossless LC
 2175 network. In the other words, a lossy network has been realized without having a

2176 resistor in a system. We will show in the next section that this is due to existence
 2177 of the semi-inductor in a system by comparing a case where the semi-inductor does
 2178 not exist.

2179 Using Eq. 2.46, Z_{mot} of this system can be calculated as

$$Z_{mot1} = \frac{1}{\left(\frac{s}{\sqrt{s}} + 1\right)\left(\frac{1}{\sqrt{s}} + \frac{s^2}{\sqrt{s}} + s\right)} = \frac{s}{\sqrt{s} + s + s^2 + 2s^2\sqrt{s} + s^3} \quad (4.10)$$

For computational benefits, we can convert Eq. 4.10 to an admittance (Y_{mot}) to investigate the real part of Z_{mot} ,

$$\begin{aligned} Y_{mot1} &= 1 + (\sqrt{s})^{-1} + s + 2s\sqrt{s} + s^2 = 1 + (\sqrt{j\omega})^{-1} + j\omega + 2j\omega\sqrt{j\omega} + (j\omega)^2 \\ &= \left(1 - \omega^2 - \frac{2\omega\sqrt{\omega}}{\sqrt{2}} + \frac{\sqrt{\omega}}{\sqrt{2\omega}}\right) + j\left(\frac{2\omega\sqrt{\omega}}{\sqrt{2}} - \frac{\sqrt{\omega}}{\sqrt{2\omega}} + \omega\right). \end{aligned} \quad (4.11)$$

2180 Since ω is always greater than 0, the real part of Eq. 4.11 can have negative real
 2181 parts if the equation satisfies

$$1 - \omega^2 - \frac{2\omega\sqrt{\omega}}{\sqrt{2}} + \frac{\sqrt{\omega}}{\sqrt{2\omega}} < 0. \quad (4.12)$$

2182 For example, if we have an angular frequency $\omega=1$ [rad/sec], Eq. 4.12 is satisfied
 2183 $\left(1 - 1 - \sqrt{2} - \frac{\sqrt{2}}{2} = -\frac{1}{\sqrt{2}} < 0\right)$. We can generalize if Y_{mot} is none positive then Z_{mot} is
 2184 also not positive. In this specific example, any angular frequency (ω) which satisfies
 2185 Eq. 4.12 can have negative resistance in Z_{mot} (Fig. 4.9). This Z_{mot} is not a positive
 2186 definite quantity, which means it does not conserve energy of the network.

2187 Figure 4.7 represents the simulated Hunt parameters (Eq. 4.6-4.9). All impedances
 2188 are complex meaning both real and imaginary parts have frequency dependance. The
 2189 two transfer impedances have same magnitude but have 180 degree angle difference
 2190 in complex domain. The input impedance is inductive, but as frequency increases
 2191 the angle approaches 45 degree. The output impedance behaves like a resonator with
 2192 damping. Figure 4.8 shows the motional impedance and input impedances with both
 2193 open and short circuit conditions. To help understand better, one can think the open

2194 circuit impedance when a system is demagnetized, and the short circuit condition is
 2195 the system's (i.e., a transducer) free oscillation in vacuum.

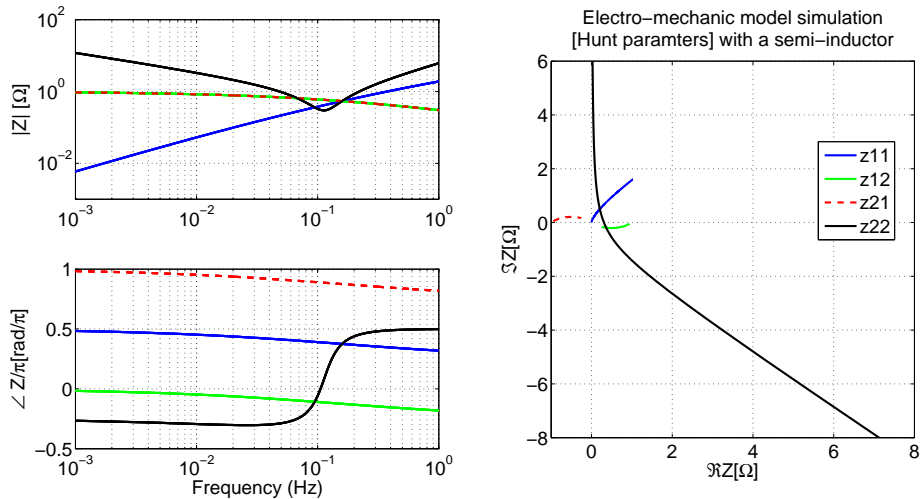


Figure 4.7: Computed Hunt parameters based on a simple electro-mechanic network shown in Fig. 4.6 (Eq. 4.6-4.9). All parameters K , L , G , and m are set to be 1 for a simple computation.

2196 4.4 Calibration results from both the modified and the 2197 manufactured probes

2198 The probe's source calibration is the first and perhaps most critical step to char-
 2199 acterize the probe system. Stable and accurate source parameters enable precise
 2200 computation of the acoustic load such as a human ear. In the previous experimen-
 2201 tation, we discussed several issues of existing probes and found the most common
 2202 reason for calibration failure was crosstalk. Based on a solid understanding of the
 2203 problem in the system, we physically modified and manufactured the probes to min-
 2204 imize the crosstalk effect in the system to calibrate the system above 6 kHz. As a
 2205 result, the modified system can pass 4-cavity (4C) calibration (Allen, 1986) above 10
 2206 kHz. The 4C calibration computes the 4C lengths (L_k) and Norton parameters $P_s(f)$,
 2207 $Y_s(f)$ based on the measured four cavity pressures, using a least-squares procedure.

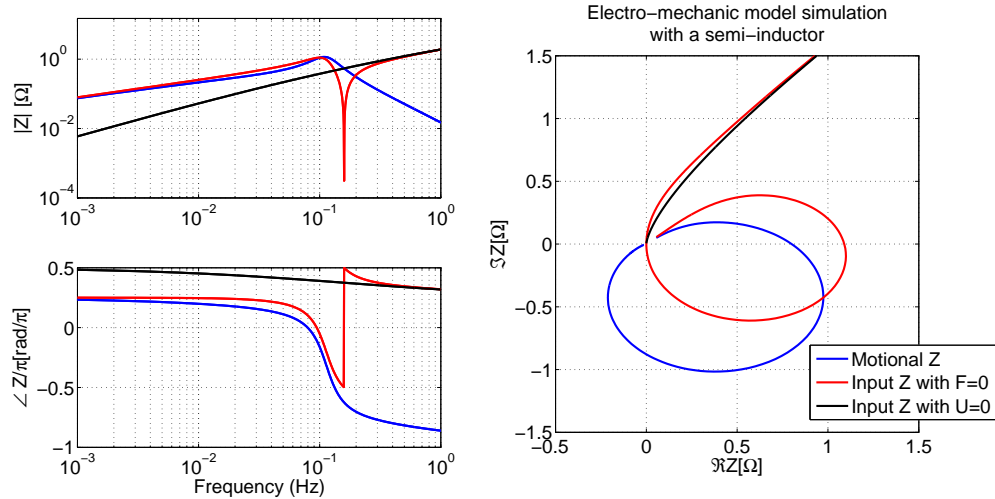


Figure 4.8: Computed motional impedance(Eq. 4.10), and input impedances with both open(Eq. 4.6) and short circuit conditions(Eq. 4.10+Eq. 4.6) based on a simple electro-mechanic network shown in Fig. 4.6.

2208 Also the MA16 and the MA17 (our manufactured prototype probes) have compa-
 2209 rable performance to the modified ER10C as shown in Fig. 4.10.

2210 We believe that this study shows the electrical crosstalk may be a general problem
 2211 for OAE hearing probe devices, which needs to be carefully addressed in the design
 2212 process. This solution supports the importance of the $\dot{\mathbf{D}}$ neglected in classical KCL
 2213 as discussed in section 2.5.2, the displacement current due to time varying electrical
 2214 field. The capacitive coupling in the wire should be carefully considered to design a
 2215 probe.

2216 4.4.1 The modified ER10C

2217 The modification includes the modified ER10C containing a +14dB differential am-
 2218 plifier, and a modified APU (Mimosa Acoustics) with a +20dB differential amplifier
 2219 whose output is fed directly into the APU's codec buffer amplifier. This modified
 2220 system picture is shown in Fig. 4.11.

2221 Compared to the original ER10C, this modified probe showed better performance

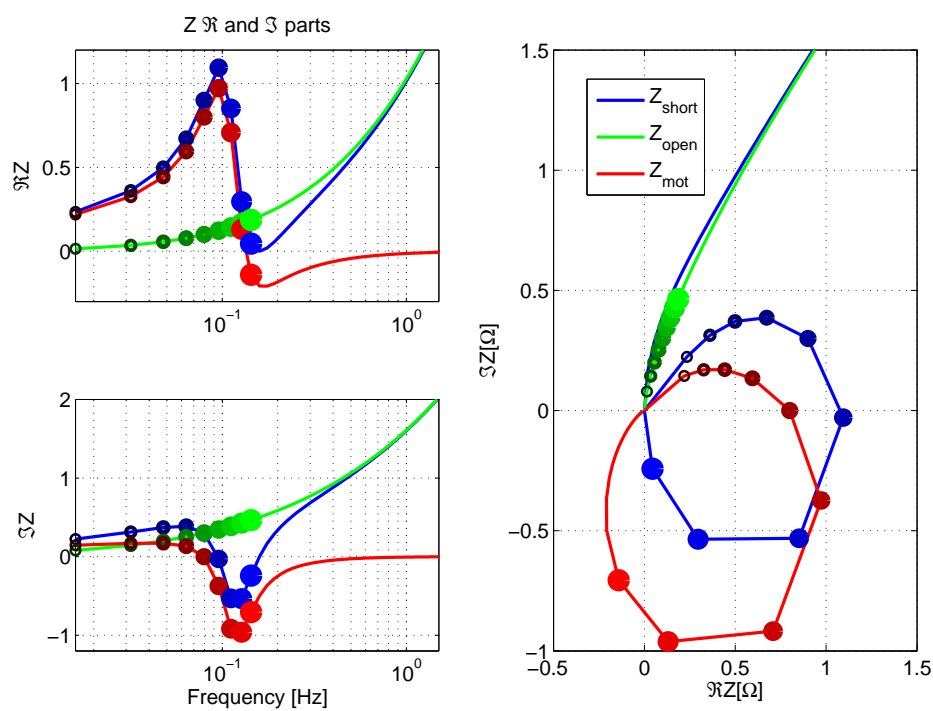


Figure 4.9: Real and imaginary parts of a simple electro-mechanic network shown in Fig. 4.6. The the marker's size indicates increment in frequency. Between 8th and 9th frequency points, the real parts of Z_{mot} goes to negative.

Draft of November 2, 2014 at 17:33

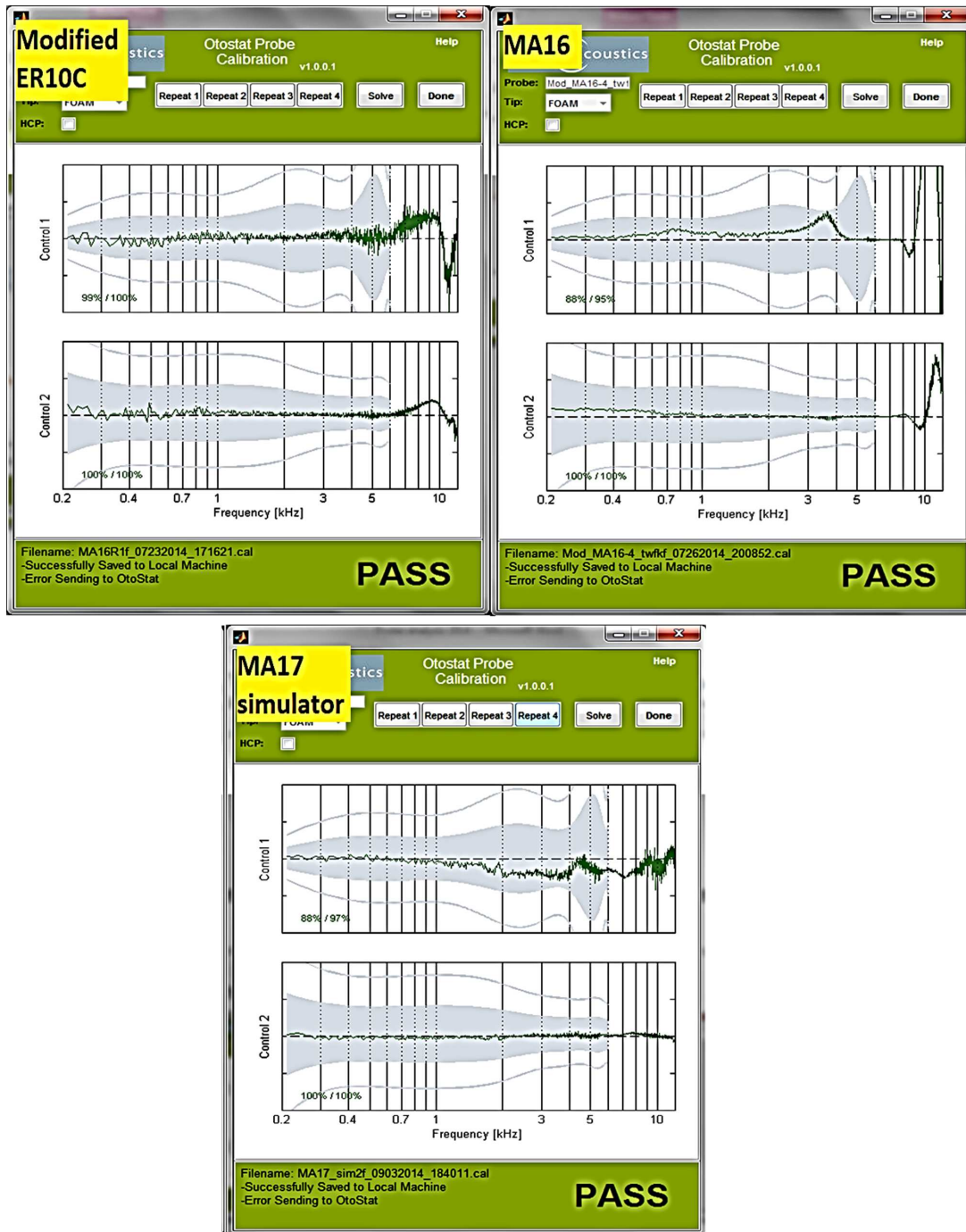


Figure 4.10: (Left figure) Source parameter calibration result from the modified ER10C to diminish the crosstalk effect. The probe can be calibrated above 10 kHz. Based on this result, we concluded that the crosstalk was interfering with the calibration procedure. (Middle figure) MA16 calibration result. This result demonstrates that we made our own system which can pass the 4C calibration above 10 kHz as well, for the first time. (Right figure) MA17 simulator calibration result. To overcome some drawbacks of the MA16, especially the size, we have proposed a new probe design, namely MA17. Before manufacturing the probe, we simulated acoustics of the probe's structure to support the basic idea of the suggested design.

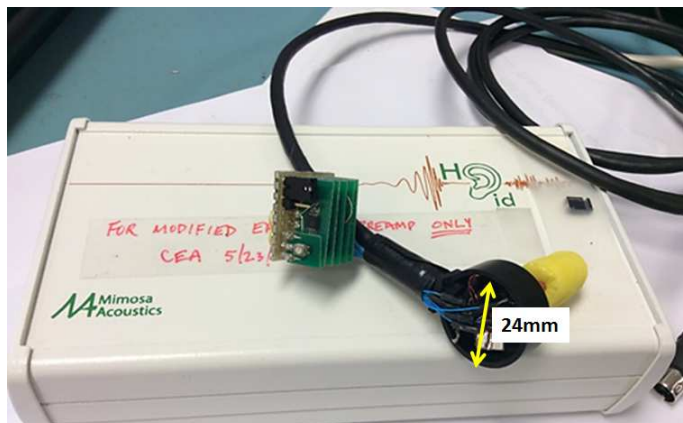


Figure 4.11: The purpose of this modification is to reduce crosstalk due to the long wire of ER10C probe. This reveals that small changes in the wire may lead significant property changes of the probe. The key idea is to amplify the microphone signal before it passes through the long wire. Near the probe's head we placed amplifier as shown in this picture.

2222 as demonstrated in Fig. 4.12. This figure investigates before and after characteris-
2223 tics of the ER10C modification compared to the theoretical values, particularly the
2224 change in sharpness of the acoustic null in each cavity (raw pressure data in a cavity
2225 with four different lengths). For example, if crosstalk is present at high frequen-
2226 cies, the pressure data around its corresponding null for the shortest cavity will be
2227 contaminated as shown (noisy notch in Fig. 4.12), hard to match by theoretical com-
2228 putation. With the low crosstalk probe, cleaner and sharper pressure acoustic nulls
2229 are detected, especially for the shortest cavity. One can also calculate the reflectance
2230 Γ of each cavity theoretically (Keefe, 1984), assuming that the load cavities have
2231 perfect cylindrical shape.

2232 This result will provide fundamental and operational understanding of not only
2233 ER10C system but also hearing measurement devices in general.

2234 4.4.2 Prototype probes: MA16 and MA17

2235 Some efforts to make our own probe to substitute the ER10C can be found in the
2236 series of prototype probes that were made (i.e., MA4-8,6,12,13,14,16,17 series). Each

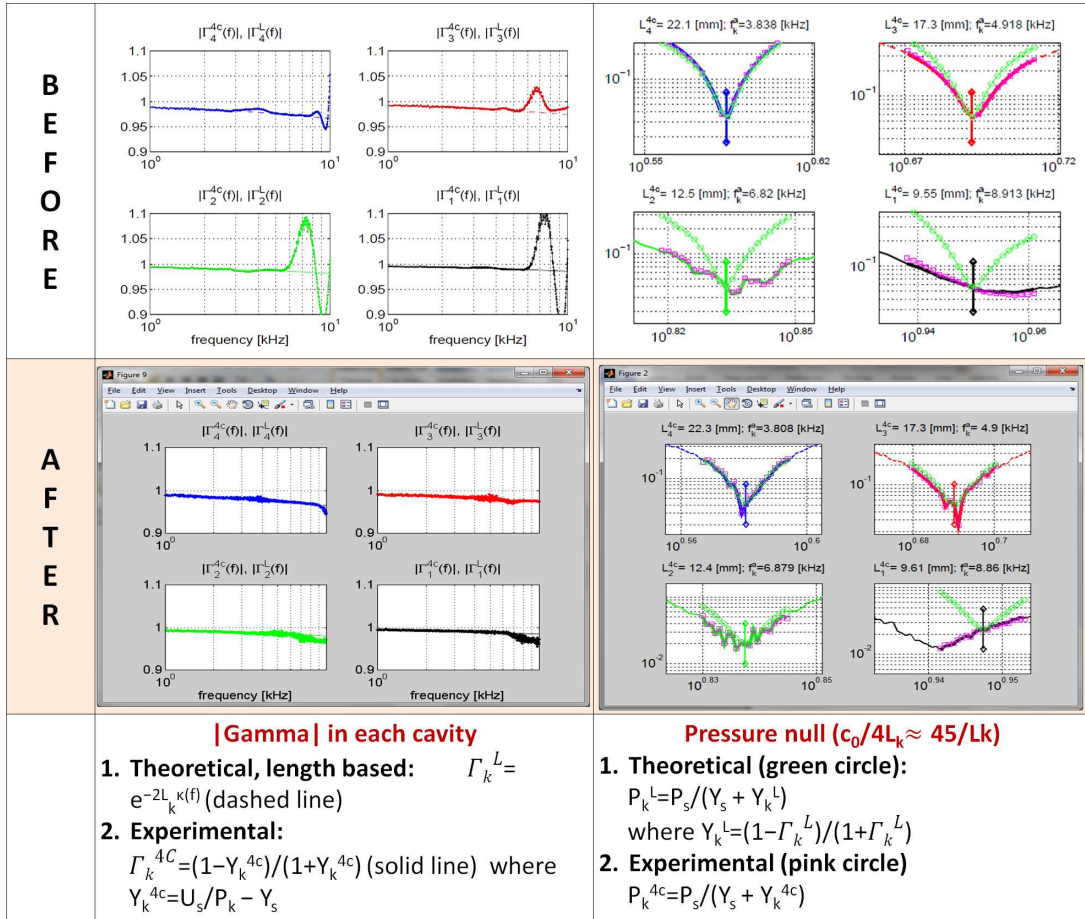
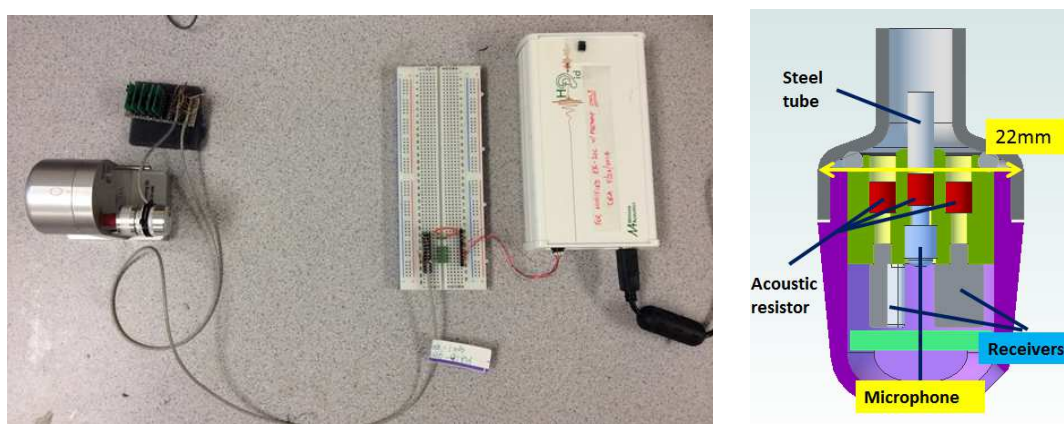


Figure 4.12: This figure shows improvement caused by the ER10C modification before and after. It gives a clear evidence that crosstalk was the source of the problem in the ER10C which has kept users from calibrating the probe above 6 kHz. Now the system can pass 4C calibration above 10 kHz. Note that all data and results are from preliminary tests. Some of the details are Mimosa Acoustics confidential information which will not be addressed here.

2237 series has 4-6 probes to demonstrate the strategy or idea highlighted at each stage.
2238 Finally we have demonstrated that our manufactured MA16 probe has a compatible
2239 performance to the modified ER10C probe which has the best performance on the
2240 market. Design of the MA17 is currently in progress to overcome drawbacks observed
2241 in the previous series, MA16. Compared to the our target size specification, the size
2242 of MA16 is too large. Figure 4.13 (a) shows the MA16 probe when it is inserted in
the MA cavity. The inside structure of the MA16 head is shown in Fig. 4.13 (b).



(a) The MA16 inserted in MA cavity (b) Schematic representation of MA16

Figure 4.13: (a) MA16 is used with the modified APU (right side white box) is used for audio processing. (b) Two speakers (lower two sided) and one microphone (in the middle) are used. The red parts represent acoustic resistors.

2243 Based appreciation of the fundamental theories relevant to the design of a hearing
2244 measurement probe, we proposed the MA17. Before manufacturing the probe, the
2245 probe's acoustic characteristics were simulated using the MA17 simulator (Fig. 4.14).
2246 The Knowles FG23652 microphone and ED27045 receiver were used for the simulator.
2247 The ER7C was used as a reference microphone. To hold the transducers in a syringe,
2248 a piece of cut-foam was used, and cotton was used to center the microphones. The
2249 key idea of this structure is to line up all transducers inside of the probe. Also for the
2250 4C calibration, when we change cavity lengths, the junction between probe's head
2251 and the cavity entry is smooth. Therefore the acoustic load (cavity) can be more
2252 similar to the ideal cylinder shape. To change the length using a piston, we need to
2253

Draft of November 2, 2014 at 17:33

2254 open and close a small hole (using a piece of putty) to adjust the pressure inside the syringe every time we change the cavity length.

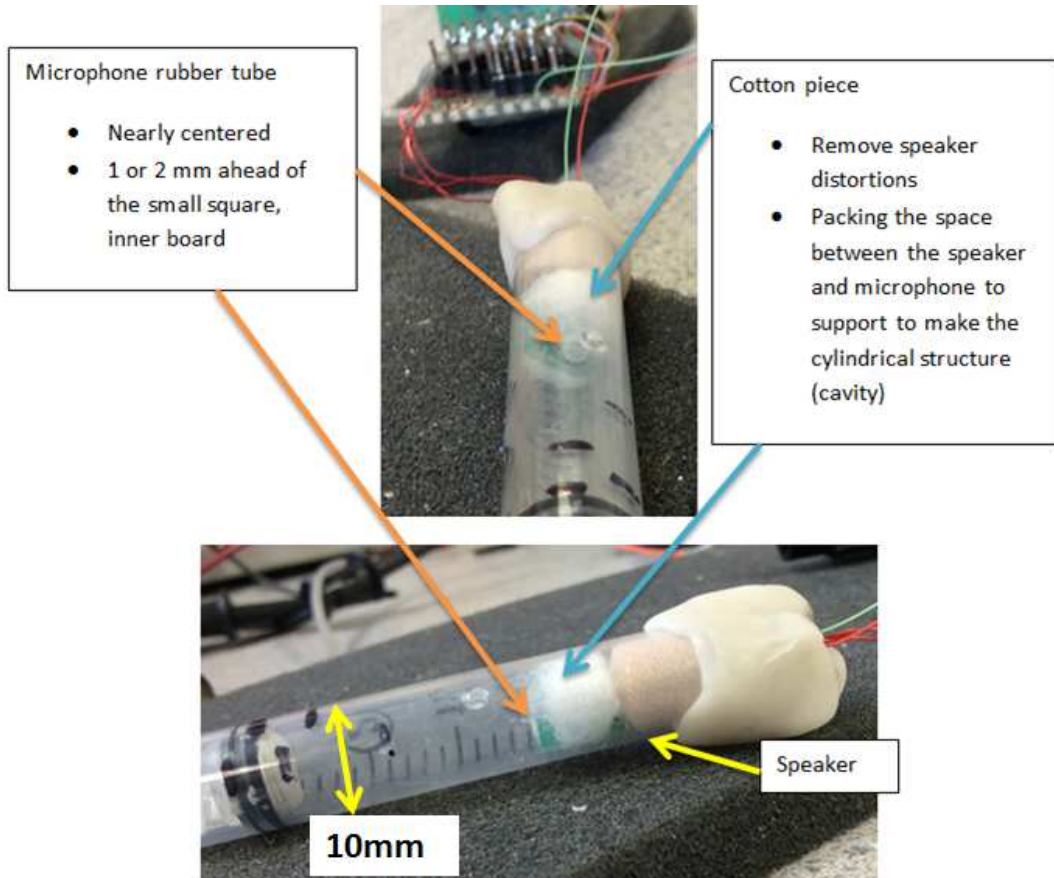


Figure 4.14: The MA17 simulator was made to simulate proposed design of the MA17. Due to the lined up transducers, the size of the probe can be greatly minimized.

2255

CHAPTER 5

CONCLUSIONS AND CONTRIBUTIONS

2256 In this study, we have discussed the critical elements of a BAR including a gyrator,
2257 and a semi-inductor along with the two-port network properties. Starting by solving
2258 for the Hunt parameters of the receiver, we have proposed a new circuit model which
2259 contains these elements, the gyrator and the semi-inductor. An intuitive design of an
2260 electromagnetic transducer has been enabled by using the gyrator thereby avoiding
2261 the mobility method, which can be confusing to explain or teach. Moreover, we have
2262 shown an improved high frequency matching by using the semi-inductors, especially
2263 for the electrical impedance, $Z_{in}(s)$.

2264 The model has been verified by comparing the experimental data (obtained from
2265 laser, vacuum, and pressure measurements) to theoretical data (obtained through
2266 model simulations). All the comparisons are in excellent agreement with the experi-
2267 mental results. The electrical input impedance data matches up to 23[kHz] (Fig. 4.3).
2268 A major advantage of the proposed receiver model is that the acoustic Thevenin pres-
2269 sure can be calculated directly from electrical input impedance measurements.

2270 Summary of the actual contributions from this study beyond the BAR model are

- 2271 1. The uniqueness of our BAR model includes i) extending the circuit theory
2272 to include anti-reciprocal networks, ii) semi inductor networks, and iii) non
2273 quasi-static networks by means of transmission line in the refined circuit model
2274 (Fig. 1.1). These are uniquely necessary components of the BAR transducer.
- 2275 2. In-depth investigation of the gyrator's impedance matrix form. Reinterpret-
2276 ing the formula via electromagnetic basics and explaining the anti-reciprocal
2277 characteristic due to Lenz's Law.

- 2278 3. Explaining the “matrix composition method”, which are characterized by the
2279 Möbius transformation. This appears to be a generalization of the ABCD
2280 (Transmission) matrix cascading method, one of the most powerful computa-
2281 tional analyzing tools in circuit theory.
- 2282 4. A demonstration that Z_{mot} is not a physically realizable PR impedance, sup-
2283 porting by PR property Using a simplified electro-mechanic model simulation.
2284 Historical analysis of the concept of impedance, such as development of AC
2285 impedance by Kennelly, also contributes to understanding nature of the Z_{mot} .
- 2286 5. The derivation of KCL, KVL from Maxwell’s equations. This follows from a
2287 Galilean transformation of ME, which is an approximation to Einstein’s theory
2288 of special relativity.

2289 In summary, this analysis puts the electro-magnetic transducer’s theory on a firm
2290 theoretical basis since its invention by A. G. Bell in 1876.

APPENDIX A

DEFINITION OF ENERGY CONSERVATION, STARTING FROM MODALITY

2291 In the field of engineering or physics, each bears an analogy to the others. If someone
2292 asks the meaning of the field in this context, answer would be ‘an area with a specific
2293 way of how a particle feels a force’. This means that there is a generalization with
2294 differences in each area. At this point, we can define the difference as a modality
2295 which refers a status of having characteristics in a given condition.

2296 Two general variables are used to describe a modality by their product, and their
2297 ratio. The two conjugate variables come in pairs; a generalized force and a flow. They
2298 could be either a **vector** (\mathbf{v} , in bold) or a scalar (s), and also can vary spatially. And
2299 a product of these two variables defines the power, while a ratio of them defines the
2300 impedance, which is usually defined in frequency domain.

2301 Some examples of the conjugate variables in each modality are described in table
A.1, and examples of power and impedance are described in table A.2. An frequency

Modality	Conjugate variables (vector in bold)	
	Generalized force [unit]	Flow [unit]
Electric	Voltage (Φ) [V]	Current (I) [A]
Mechanic	Force (\mathbf{F}) [N]	Particle velocity (\mathbf{U}) [m/s]
Acoustic	Pressure (P) [N/m^2]	Volume velocity (\mathbf{V}) [$(ms)^{-1}$]
Electro-Magnetic	Electric field (\mathbf{E}) [V/m]	Magnetic field (\mathbf{H}) [A/m]

Table A.1: Example of modalities and their conjugate variables. Upper case symbols are used for the frequency domain variables. The time domain representation of each variable can be described using the lower case of the same character, except in the EM case. But general Electro-Magnetic (EM) theories consider the time domain and its traditional notation uses capital letter for the time domain analysis. Note that in the electric field, $\mathbf{E} = -\nabla\Phi$, where Φ is scalar potential, the voltage.

2302

2303 (phasor or time-harmonic) domain of EM expressions are also common. In this case,
 2304 a different notation (i.e., *under – line* or *italic*) is used based on the author’s choice.
 2305 The EM wave can be decomposed into the sum of the sinusoidal waves. The EM
 2306 wave phasor form is to analyze the waves’ propagation if they are oscillating at a
 single frequency.

Modality	Product in time domain	Ratio (Impedance Z) in frequency domain
Electric	$\phi(t)i(t)$	$Z_e = \Phi/I$
Mechanic	$\mathbf{f}(t) \cdot \mathbf{u}(t)$ (inner product)	$Z_m = F/U$
Acoustic	$p(t)\mathbf{v}(t)$ (intensity)	$Z_a = P/V$
Electro-Magnetic (EM)	$\mathcal{P} = \mathbf{E} \times \mathbf{H}$ (Poynting vector)	$\eta = \underline{\mathbf{E}}/\underline{\mathbf{H}}$

Table A.2: Power and impedance definitions for each modalities in table A.1. In general, power concept (a product of conjugate variables) can be used in time domain, however the impedance (a ratio) is thought of in the frequency domain. Assuming causality, the Laplace transformation can be applied to convert the impedance to the time domain.

2307

2308 One can define a system using single modality or a combination of them. For the
 2309 combination of the modalities, ‘n’-port network concept is required. (This discussion
 2310 will be followed in next.) Independent from how many modalities exist in a system,
 2311 there is a well-known law that one can apply to every system. The law of the energy
 2312 conservation is expressed as (Van Valkenburg (1960); Cheng and Arnold (2013))

$$e(t) \equiv \int_{-\infty}^t power(t)dt \geq 0, \quad (\text{A.1})$$

2313 where the total delivered energy $e(t)$ which is an integration of the power over time
 2314 should be than greater than (or equal to) zero, and $power(t)$ is work done per unit
 2315 time defined as a potential times a net flow. Simply speaking, Eq. A.1 means we can
 2316 not have more energy than we supply.

2317 Let’s take an example of an electric modality case in time domain power ($power_e$).

$$power_e(t) = \phi(t)i(t) = (i(t) \star z(t))i(t), \quad (\text{A.2})$$

2318 where $i(t)$ is the net current (the current flow integrated by its affected area therefore

2319 it is a scalar) in time domain which is not zero, $z(t)$ is an inverse Laplace transform of
 2320 an impedance ($Z=\Phi/I$) in frequency domain, $e(t)$ is a voltage in time, and \star denotes
 2321 a convolution operator.

2322 In EM, a Poynting vector (\mathcal{P}), represents the power density, a rate of energy
 2323 transfer per unit area,

$$\mathcal{P} = \mathbf{E} \times \mathbf{H}. \quad (\text{A.3})$$

2324 Note that a cross product is used to consider the spatial variation of each variable.
 2325 The units for \mathcal{P} , \mathbf{E} , and \mathbf{H} are $[W/m^2]$, $[V/m]$, and $[A/m]$ respectively. The directions
 2326 of \mathcal{P} , \mathbf{E} , and \mathbf{H} vectors follow the right hand rule. By integration of this Poynting
 2327 vector over the effective surface area A , we have a scalar power in unit of $[W]$ in
 2328 electro-magnetic field ($power_{EM}$),

$$power_{EM} = \int_s \mathcal{P} \cdot d\mathbf{A} = \int_s (\mathbf{E} \times \mathbf{H}) \cdot d\mathbf{A}. \quad (\text{A.4})$$

2329 In the field of acoustic, the power is a measure of sound energy per unit time which
 2330 is defined as intensity times area $\mathbf{A}[m^2]$ ($power_a$),

$$power_a = p(t)\mathbf{u}(t) \cdot \mathbf{A}, \quad (\text{A.5})$$

2331 where $p(t)\mathbf{u}(t)$ defines the intensity.

2332 To take into account the power concept in frequency domain, one must use the
 2333 Laplace transform (\mathcal{L})'s convolution theorem. Therefore a proper way to describe
 2334 the instantaneous power in Laplace frequency domain extending from Eq. A.2 is

$$power_e(t) = \phi(t)i(t) \xleftrightarrow{\mathcal{L}} Power(s)|_{s=j\omega} = \Phi(\omega) \star I(\omega) \quad (\text{A.6})$$

2335 where $j = \sqrt{-1}$, ω is the angular frequency and 's' is the Laplace frequency. Com-
 2336 pared to an usual power definition $P = \Phi I$, this is an unusual expression. However
 2337 based on Eq. A.2, a product relationship becomes a convolution via Laplace trans-
 2338 form. ¹

¹If it is not true, then more explanation should be followed to make that point clear

APPENDIX B

TELLEGEN'S THEOREM & KCL/KVL

2339 Tellegen's theorem (Eq. B.1) states that the complex power, \mathcal{S} , dissipated in any
 2340 circuit's components (or branches) sums to zero,

$$\sum \mathcal{S}_i = 0, \quad (\text{B.1})$$

2341 where 'i' is branches in a circuit and, $\mathcal{S} = \Phi I^* = R + jQ$ is complex power measured.
 2342 The \mathcal{S} has both real (R) and imaginary (Q) parts.

$$R = \Re \mathcal{S} = \Re(\Phi I^*), \quad (\text{B.2a})$$

2343

$$Q = \Im \mathcal{S} = \Im(\Phi I^*) \quad (\text{B.2b})$$

2344 where 'R' represents the average power measured in Watt [W], and 'Q' shows the
 2345 reactive power measured in Volt-Amps Reactive [VAR].

2346 Therefore the total power (P_{total}) of the electro-mechanic system (Fig. 2.1) can be
 2347 described as

$$P_{total} = \Phi I^* + FU^* = \Re(\Phi I^*) + \Re(FU^*) + j\Im(\Phi I^*) + j\Im(FU^*) = P_{avg} + jP_{reactive}, \quad (\text{B.3})$$

2348 where

$$P_{avg} = \Re \Phi I^* + \Re FU^* = \frac{1}{2}(\Phi I^* + \Phi^* I) + \frac{1}{2}(FU^* + F^* U) \quad (\text{B.4a})$$

2349

$$P_{reactive} = \Im \Phi I^* + \Im FU^* = \frac{1}{2}(\Phi I^* - \Phi^* I) + \frac{1}{2}(FU^* - F^* U). \quad (\text{B.4b})$$

For any lossless network, the P_{avg} goes to zero. McMillan (1946) describes an elemen-

tary two-port network to generalize the system's total power using the impedance components of the system. Here, we revisit the steps using Hunt parameters introduced in 1954.

The total averaged input power (P_{avg}) of an electro-mechanic system can be calculated from Eq. 2.1,

$$\begin{aligned}
 P_{avg} &= \frac{1}{2}[\Phi I^* + \Phi^* I + F U^* + F^* U] \\
 &= \frac{1}{2}[(Z_e I + T_{em} U) I^* + (Z_e I + T_{em} U)^* I + (T_{em} I + Z_m U) U^* + (T_{me} I + Z_m U)^* U] \\
 &= \frac{1}{2}[(Z_e + Z_e^*) I I^* + (Z_m + Z_m^*) U U^* + (T_{em} + T_{me}^*) I^* U + (T_{em}^* + T_{me}) I U^*], \quad (\text{B.5})
 \end{aligned}$$

2350 where ‘*’ is the complex conjugation operator. In lossless network, the real part of
 2351 the power, P_{avg} is zero. Therefore Eq. B.5 vanishes for all I and U, then we have the
 2352 following conditions on the Hunt parameters,

$$Z_e = -Z_e^*, \quad (\text{B.6})$$

2353

$$Z_m = -Z_m^*, \quad (\text{B.7})$$

2354

$$T_{em} = -T_{me}^*. \quad (\text{B.8})$$

2355 Eq. B.6 and Eq. B.7 show Z_e and Z_m are purely imaginary in lossless system. If any
 2356 loss is added to the system, Z_e and Z_m can not have negative real part (resistance)
 2357 to obey the conservation of energy law. Only positive resistance is allowed.

2358 Eq. B.5 tells us a general idea about reciprocity. If F is 90 degree out of the
 2359 phase with ‘I’, then T_{em} and T_{me} should be imaginary, therefore we have $T_{em} = T_{me}$
 2360 (Eq. 2.3, 2.4). A condenser transducer is a real world example of this ‘reciprocal’
 2361 case.

2362 In an electromagnetic transducer, on the other hand, F is in phase with I , therefore
 2363 the F is proportional to the I . In this case, T_{em} is real, therefore to satisfy Eq. B.8,
 2364 $T_{me} = -T_{em}$. This is the definition of the ‘anti-reciprocity’, the two transfer impedances
 2365 are real and have different signs. This specific conditions are also discussed in Tellegen

2366 (1948). It is a lossless LC network with anti-reciprocity characteristic considering
 2367 only Brune's impedances (except resistors).

2368 Two-port network without a Semi-inductor

2369 Similar to Eq. 4.2, Eq. B.9 is a corresponding ABCD matrix representation of a simple
 2370 two-port network depicted in Fig. B.1. In this figure, the semi-inductor is excluded
 from the electrical side.

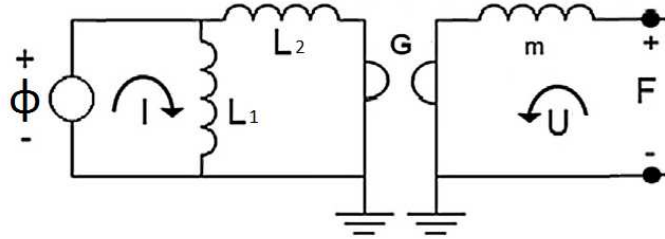


Figure B.1: A simple anti-reciprocal network without a semi-inductor

2371

$$\begin{bmatrix} \Phi(\omega) \\ I(\omega) \end{bmatrix} = \begin{bmatrix} 1 & 0 \\ \frac{1}{sL_2} & 1 \end{bmatrix} \begin{bmatrix} 1 & sL_1 \\ 0 & 1 \end{bmatrix} \begin{bmatrix} 0 & G \\ \frac{1}{G} & 0 \end{bmatrix} \begin{bmatrix} 1 & 0 \\ \frac{1}{sm} & 1 \end{bmatrix} \begin{bmatrix} F(\omega) \\ -U(\omega) \end{bmatrix}, \quad (\text{B.9})$$

2372 where s is the Laplace frequency ($\sigma + j\omega$) and L_1 , L_2 , G , and m are the inductance
 2373 1 and 2, the gyration coefficient, and the mass of the system respectively.

2374 For a simple analysis, the ABCD matrix part in Eq. B.9 is separated, and L_1 , L_2 ,
 2375 G , and m are set to be '1'. The whole equation is rewritten as

$$\begin{bmatrix} 1 & 0 \\ \frac{1}{s} & 1 \end{bmatrix} \begin{bmatrix} 1 & s \\ 0 & 1 \end{bmatrix} \begin{bmatrix} 0 & 1 \\ 1 & 0 \end{bmatrix} \begin{bmatrix} 1 & 0 \\ \frac{1}{s} & 1 \end{bmatrix} = \begin{bmatrix} 1 & s \\ s & s^2 + 1 \end{bmatrix} \begin{bmatrix} \frac{1}{s} & 1 \\ 1 & 0 \end{bmatrix} \quad (\text{B.10})$$

2376 Finally we have the second giant ABCD matrix to represent the system in Fig. B.1.

$$\begin{bmatrix} \Phi(\omega) \\ I(\omega) \end{bmatrix} = [T_2] \begin{bmatrix} F(\omega) \\ -U(\omega) \end{bmatrix} = \begin{bmatrix} A(s)' & B(s)' \\ C(s)' & D(s)' \end{bmatrix} \begin{bmatrix} F(\omega) \\ -U(\omega) \end{bmatrix} = \begin{bmatrix} \frac{1}{s} + s & 1 \\ 2 + s^2 & s \end{bmatrix} \begin{bmatrix} F(\omega) \\ -U(\omega) \end{bmatrix}, \quad (\text{B.11})$$

2377 where $\Delta_{T_2} = -1$. Converting Eq. B.11 into an impedance matrix, Eq. 2.7 is used to
2378 give us

$$Z_2 = \begin{bmatrix} z'_{11} & z'_{12} \\ z'_{21} & z'_{22} \end{bmatrix}, \quad (\text{B.12})$$

2379 where

$$z'_{11} = \frac{\frac{1}{s} + s}{2 + s^2} = \frac{1 + s^2}{2s + s^3}, \quad (\text{B.13})$$

2380

$$z'_{12} = -\frac{1}{2 + s^2}, \quad (\text{B.14})$$

2381

$$z'_{21} = \frac{1}{2 + s^2}, \quad (\text{B.15})$$

2382

$$z'_{22} = \frac{s}{2 + s^2}. \quad (\text{B.16})$$

2383 Note that this network is a typical lossless LC network which contains only Brune's
2384 impedances. Therefore z'_{11} and z'_{22} are purely imaginary while z'_{12} and z'_{21} are purely real.

2385 Based on Eq. 2.46, Z_{mot} of this system can be computed as follows,

$$Z_{mot2} = \frac{1}{s(2 + s^2)} = \frac{1}{2s + s^3}. \quad (\text{B.17})$$

2386 Substituting the Laplace frequency 's' to be $j\omega$ in Eq. B.17,

$$Z_{mot2}|_{s=j\omega} = \frac{1}{2j\omega + (j\omega)^3} = j \frac{1}{\omega^3 - 2\omega}. \quad (\text{B.18})$$

2387 There is no real part in Eq. B.18. In this specific case, any angular frequencies (ω)
2388 cannot have real part. Z_{mot} is always purely imaginary.

2389 Figure B.2 represents the simulated Hunt parameters (Eq. B.13-B.16). The two
2390 transfer impedances are real, and they are equal in magnitude but different in signs.

2391 The input impedance is purely inductive, and the output impedance behaves like
 2392 a resonator. Figure B.3 shows the motional impedance and input impedances with
 2393 both open and short circuit conditions. Compared to Fig. 4.8, all are purely imagi-
 2394 nary, with no loss in this system (real part is zero).

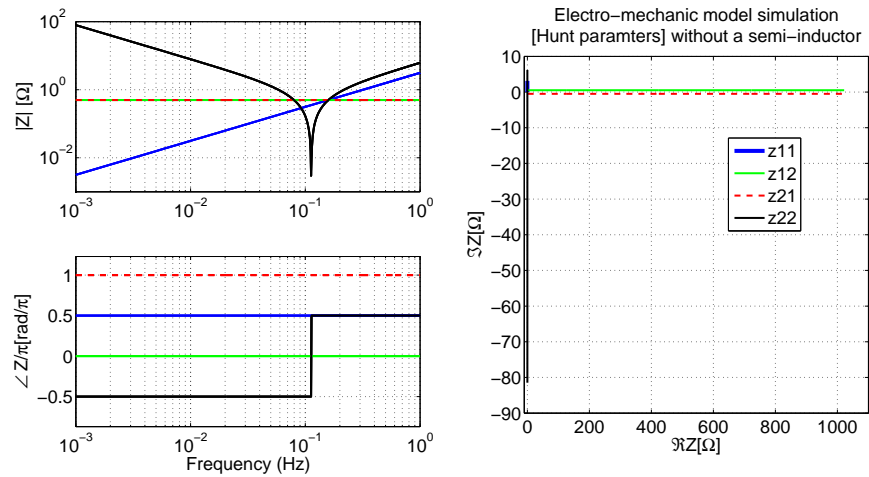


Figure B.2: Computed Hunt parameters based on a simple electro-mechanic network shown in Fig. B.1 (Eq. B.13-B.16). All parameters L_1 , L_2 , G , and m are set to be 1 for a simple computation.

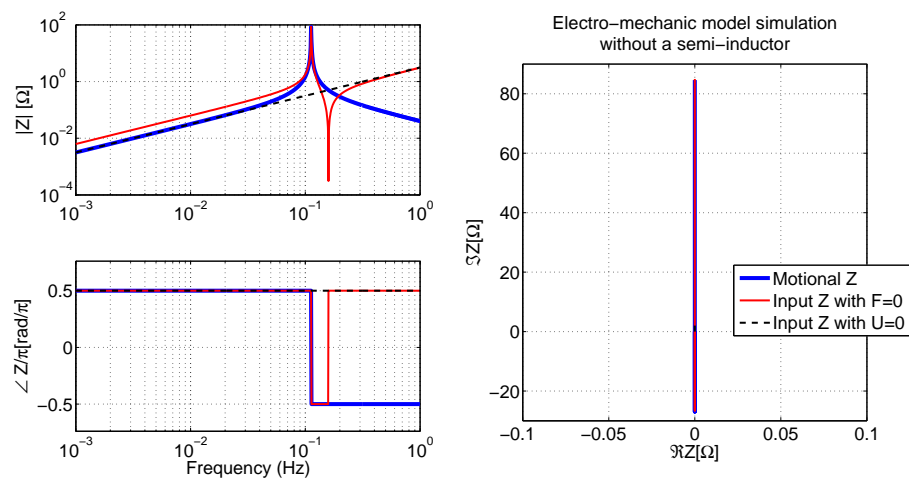


Figure B.3: Computed motional impedance(Eq. B.18), input impedances with both open(Eq. B.13) and short circuit conditions(Eq. B.18+Eq. B.13) based on a simple electro-mechanic network shown in Fig. B.1.

APPENDIX C

SENSITIVITY ANALYSIS OF ED SERIES SPICE MODEL

2395 Figure C.1 shows the Knowles Electronics commercial SPICE circuit model (Killion,
2396 1992). This SPICE model contains a gyrator and is meant to be equivalent to the
2397 physical system, but does not accordingly represent the system in an one-to-one
2398 physical manner.

2399 In order to fully understand each component, we implemented the Knowles PSpice
2400 model in Matlab using transmission matrices. Unlike PSpice, Matlab provides a more
2401 flexible platform for a matrix model manipulation. Matlab does not critically depend
2402 on the user's operating system (Knowles' PSpice model is inflexibly tied to both the
2403 Cadence Orcad Schematics and Capture, and Windows XP). PSpice requires a DC
2404 path to ground from all nodes, thus R1, RK512, RK513, and RK514 components
2405 have been added for this purpose.

2406 We then performed a *sensitivity analysis* on the Matlab model by changing each
2407 component value by +/- 20% to determine those components for which the output
2408 changed by less than -50[dB], within the frequency range of 0.1 - 10[kHz]. Once
2409 the small effect components were determined, we removed the components from the
2410 original PSpice design for a further Matlab analysis. To compare the difference
2411 between the original and the reduced components condition, we calculate each error
2412 computed across frequencies,

$$e(f) = \frac{|'Original' - 'Small effect'|}{|'Original'|}, \quad (C.1)$$

2413 where f is frequency. Our Matlab simulation result is shown in Fig. C.2(a) with
2414 the CMAG value defined in the PSpice circuit (in Fig. C.1, CMAG=0.92e-7). The

2415 ‘Original’ simulation contains all circuit elements without any modification, whereas
 2416 the ‘Small effect’ simulation excludes the small effect components in Fig. C.1. The
 2417 PSpice sensitivity analysis for the semi-capacitor is performed using Knowles PSpice
 2418 library for the CMAG component¹ shown in Fig. C.2(b). The most important result
 2419 of this sensitivity analysis was that the semi-capacitor in the PSpice model is one of
 2420 these ‘small effect’ components.

2421 Using a series semi-capacitor on the right side of the gyrator is mathematically
 2422 equivalent to using a shunt semi-inductor on the left side of the gyrator, because
 2423 of mobility and impedance analogies. However, ideally, circuit elements should be
 2424 properly associated with their physical properties. It is important to take advantage
 2425 of using a gyrator to describe the anti-reciprocity for a physically intuitive model of
 2426 the system. The gyrator is the bridge between the electrical and mechanical systems.
 2427 For this reason the coil of the receiver should be represented on the electrical side.
 2428 This realization further motivated our objective to design a simplified and rigorous
 2429 BAR model.

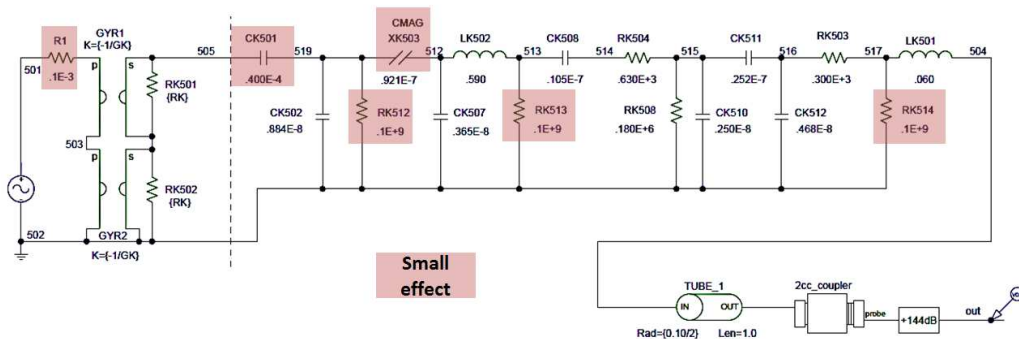


Figure C.1: Knowles PSpice model of the ED receiver: The refined PSpice circuit model of ED receiver by reducing ‘small effect’ components which are marked in red. R1, RK512, RK513, and RK514 resistors were added to maintain DC stability of PSpice. Note that the Spice model represents all ED series receivers, including ED7045, ED1744, ED1913, and etc., such that specific parameter value of components vary for each specific receiver.

¹This simulation result was provided by Knowles Electronics.

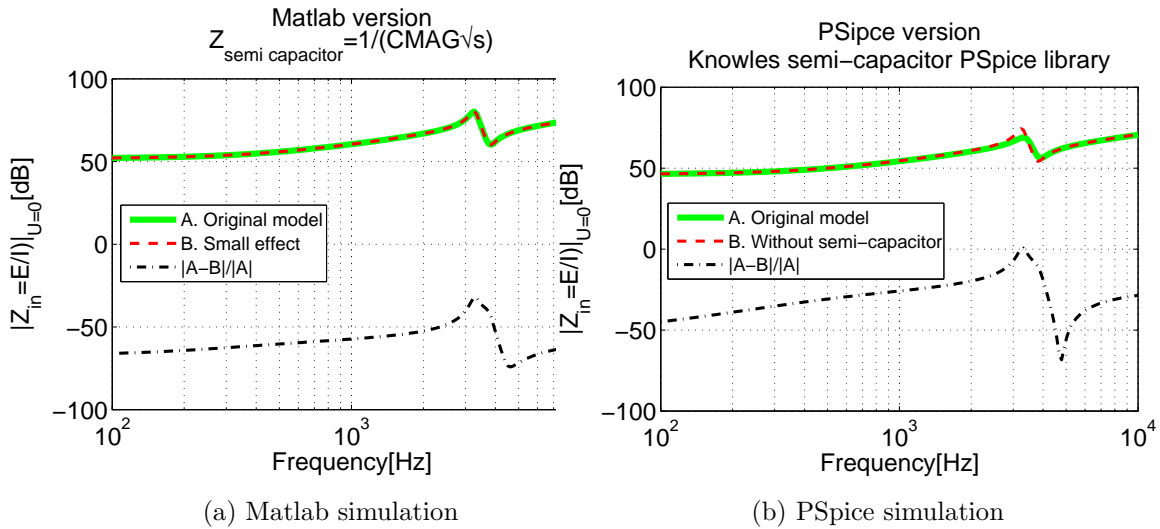


Figure C.2: The simulated electrical input impedance' magnitude, $|Z_{in}|$, in dB scale. (a) shows the sensitivity analysis using Matlab based on Fig. C.1 where $s = j\omega$. The 'A. original model' and the 'B. Small effect' conditions are marked with a thick green line and a dashed red line, respectively. The 'B. Small effect' is the simulated result when all 'small effect' components in Fig. C.1 are removed in the original PSpice circuit. It represents summed-up sensitivities of 'small effect' components in Fig. C.1. (b) represents the sensitivity of the CMAG component only. This analysis is provided by Knowles Electronics using their PSpice library for the CMAG component (This result is plotted in Matlab but the data is acquired via PSpice simulation). Similar to the (a), 'A. Original model' shows the PSpice simulation including all components in Fig. C.1, whereas 'B. Without semi-capacitor' simulates the original PSpice circuit only without the semi-capacitor. For both simulations (a) and (b), the difference between the original response and the reduced response is calculated based on Eq. C.1 shown as black dashed line.

APPENDIX D

Z_{MOT} : SPATIAL RELATIONSHIPS BETWEEN Φ , I , B , F , AND I

2430 In this section, we will research the fundamental spatial relationship of signals based
2431 on Maxwell's equation. There are four well-known Maxwell's equations both in inte-
2432 gral and differential forms. Maxwell's equations can be reduced into two main equa-
2433 tions, Faraday's law and Ampere's law. When Maxwell developed electro magnetic
2434 relationship into mathematical equations, he ended up with 37 quaternion equations
2435 to described all relationships in electro magnetic world. Later on Olive Heaviside
2436 reorganized Maxwell's quaternion equations into four reduced complex vector rela-
2437 tionships using the ∇ operator.

2438 Therefore it is a reasonable idea to revisit electro-mechanic parameter's relation-
2439 ship in spatial domain. In quaternion, 3 spatial rotation parameters (i,j, and k) are
2440 defined which have the following properties

$$i^2 = j^2 = k^2 = ijk = (k)k = -1. \quad (D.1)$$

2441 Note Eq. D.1 is noncommutative, also i or j are different from the imaginary param-
2442 eter of Laplace complex time-frequency domain.

2443 Faraday-lenz's law explains generator (a relationship between Φ and U through B)

$$\Phi = l(U \times B), \quad (D.2)$$

2444 while Ampere's law is applying for explaining motor action (a relationship between
2445 F and I through B),

$$F = l(I \times B). \quad (D.3)$$

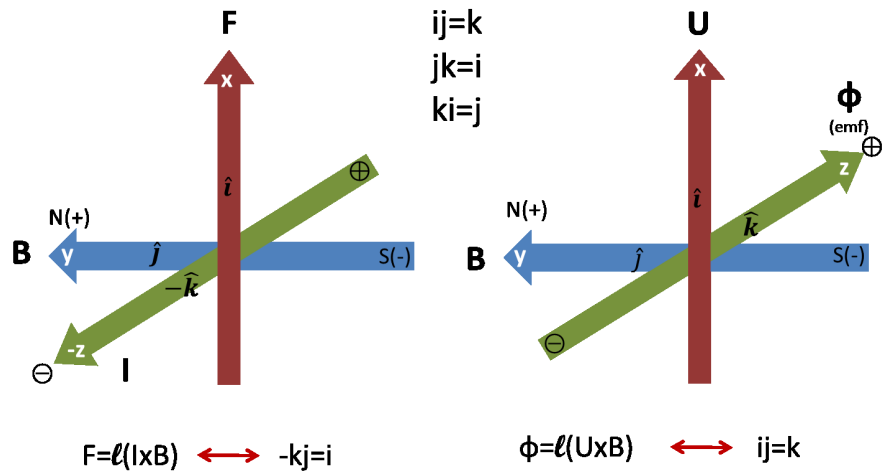


Figure D.1: Electro-mechanic system's variables in spatial domain by BeranekBeranek (1954)

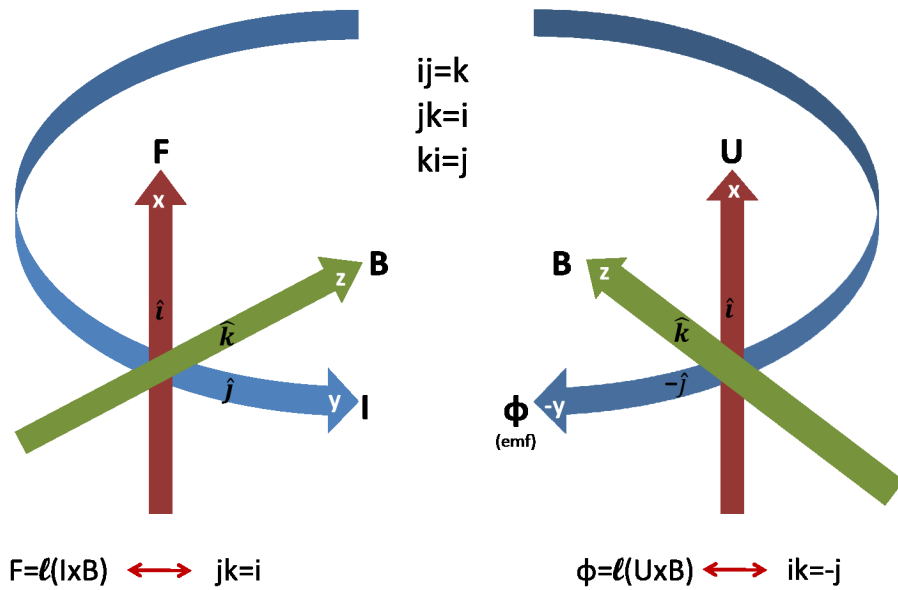


Figure D.2: Equivalent with Fig. D.1. The choice of each geometry is adapted from Hunt's book Hunt (1954)

Draft of November 2, 2014 at 17:33

2446 Let's consider Fig. D.2 picturing variables in 3D spatial domain. Considering the
 2447 spatial relationship of each variable shown in Fig. D.2, Eq. 2.1 is rewritten as

$$\begin{bmatrix} \Phi_x \hat{i} + \Phi_y \hat{j} + \Phi_z \hat{k} \\ F_x \hat{i} + F_y \hat{j} + F_z \hat{k} \end{bmatrix} = \begin{bmatrix} Z_e & T_{em} \\ T_{me} & Z_m \end{bmatrix} \begin{bmatrix} I_x \hat{i} + I_y \hat{j} + I_z \hat{k} \\ U_x \hat{i} + U_y \hat{j} + U_z \hat{k} \end{bmatrix} \quad (\text{D.4})$$

2448 We can rewrite Eq. D.4 consider the spatial relationship of each parameter depicted
 2449 in Fig. D.2,

$$\begin{bmatrix} 0\hat{i} + \Phi_y \hat{j} + 0\hat{k} \\ F_x \hat{i} + 0\hat{j} + 0\hat{k} \end{bmatrix} = \begin{bmatrix} Z_e & T_{em} \\ T_{me} & Z_m \end{bmatrix} \begin{bmatrix} 0\hat{i} + I_y \hat{j} + 0\hat{k} \\ U_x \hat{i} + 0\hat{j} + 0\hat{k} \end{bmatrix} \quad (\text{D.5})$$

2450 To finalize each relationship in Eq. D.5 we have,

$$\begin{bmatrix} \Phi_y \hat{j} \\ F_x \hat{i} \end{bmatrix} = \begin{bmatrix} Z_e & T_{em} \hat{k} \\ T_{me}(-\hat{k}) & Z_m \end{bmatrix} \begin{bmatrix} I_y \hat{j} \\ U_x \hat{i} \end{bmatrix}. \quad (\text{D.6})$$

2451 Considering spatial rotations in each parameter in Eq. D.6, we can repeat Z_{mot}
 2452 derivation shown in Eq. 2.40 and Eq. 2.41.

$$\Phi_y \hat{j} = Z_e I_y \hat{j} + T_{em} \hat{k} U_x \hat{i} = Z_e I_y \hat{j} + T_{em} U_x \hat{j} \quad (\text{D.7a})$$

2453

$$F_x \hat{i} = T_{me}(-\hat{k}) I_y \hat{j} + Z_m U_x \hat{i} = -T_{me} I_y \hat{i} + Z_m U_x \hat{i} \quad (\text{D.7b})$$

2454 Set $F_x \hat{i}$ to be zero, we have

$$\frac{\Phi_y}{I_y} = Z_e + T_{em} \frac{U_x}{I_y} \quad (\text{D.8a})$$

2455

$$\frac{U_x}{I_y} = -\frac{T_{me}}{Z_m} \quad (\text{D.8b})$$

2456 Plugging Eq. D.8b into Eq. D.8a, finally we have the same Eq. 2.42

$$Z_{in}|_{F_x=0} = \frac{\Phi_y}{I_y} = Z_e - \frac{T_{em} T_{me}}{Z_m}. \quad (\text{D.9})$$

2457 The result shown in Eq. D.9 is as same as Eq. 2.42, no spatial dependency is observed.

2458 Therefore the spatial relation is already considered in motional impedance formula

Draft of November 2, 2014 at 17:33

²⁴⁵⁹ shown in Eq. 2.46.

APPENDIX E

CALCULATION OF HUNT PARAMETERS

2460 Equation 2.12 includes three unknown Hunt parameters (Z_e , Z_a and T_a) that we
 2461 wish to find. In order to solve for three unknown parameters, 3 different electrical
 2462 input impedances ($Z_{in|A}$, $Z_{in|B}$, and $Z_{in|C}$) are measured corresponding to three known
 2463 acoustic loads, A, B, and C. The load conditions differ in a length of the tubing,
 2464 attached to the receiver's port. Each tube has different impedance denoted as $Z_{L|A}$,
 2465 $Z_{L|B}$, and $Z_{L|C}$, where $Z_{L|A} = Z_0 \coth(a \cdot tube_length)$ (for the blocked-end tube, $V =$
 2466 0), Z_0 is the characteristic impedance of a tube, and a is the complex propagation
 2467 function. Parameters a and Z_0 parameters assume viscous and thermal loss (Keefe,
 2468 1984). In $20^\circ[C]$ room temperature, $c = 334.8[m/s]$. Define diameter of $Z_{L|A,B,C} \approx$
 2469 $1.4[mm]$

2470 Substituting these for Z_L in Eq. 2.12:

$$Z_{in|A} = \frac{\Phi}{I} = Z_e + \frac{T_a^2}{Z_{L|A} + Z_a} \quad (E.1)$$

2471

$$Z_{in|B} = \frac{\Phi}{I} = Z_e + \frac{T_a^2}{Z_{L|B} + Z_a}$$

2472

$$Z_{in|C} = \frac{\Phi}{I} = Z_e + \frac{T_a^2}{Z_{L|C} + Z_a}.$$

2473 Given these three measured impedances, we can solve for Z_a , T_a , and Z_e via the
 2474 following procedure:

- 2475 1. Subtract two electrical impedance measurements to eliminate Z_e , such as

$$Z_{in|C} - Z_{in|A} = \frac{T_a^2}{Z_a + Z_{L|C}} - \frac{T_a^2}{Z_a + Z_{L|A}}. \quad (\text{E.2})$$

2. Take the ratio of various terms as defined by Eq. E.2,

$$\left(\frac{Z_a - Z_{L|B}}{Z_{in|C} - Z_{in|A}} \right) = \left(\frac{Z_{in|A} - Z_{in|C}}{Z_{in|B} - Z_{in|C}} \right) \left(\frac{Z_{L|C} - Z_{L|B}}{Z_{L|C} - Z_{L|A}} \right).$$

- 2476 From this we may solve for the first unknown Z_a ,

$$Z_a = \frac{(Z_{in|A} - Z_{in|C})(Z_{L|C} - Z_{L|B})(Z_{in|C} - Z_{in|A})}{(Z_{in|B} - Z_{in|C})(Z_{L|C} - Z_{L|A})} + Z_{L|B}. \quad (\text{E.3})$$

- 2477 3. Next we find T_a by substituting Z_a into Eq. E.2

$$T_a = \sqrt{\frac{(Z_{in|C} - Z_{in|A})(Z_a + Z_{L|C})(Z_a + Z_{L|A})}{Z_{L|A} - Z_{L|C}}}. \quad (\text{E.4})$$

- 2478 4. Finally Z_e is given by Eq. E.1

$$Z_e = \left(\frac{T_a^2}{Z_{L|A} + Z_a} \right) - Z_{in|A}. \quad (\text{E.5})$$

APPENDIX F

HYSTERESIS LOOP FOR A FERROMAGNETIC MATERIAL: \mathbf{B} VS. \mathbf{H}

2479 The word ‘*Hysteresis*’ is originated from the Greek, *hystérēsis*, meaning that a state
 2480 of lagging behind or late, the outcome depends on history of past inputs, as well as
 2481 current inputs. In the field of magnetism, \mathbf{B} and \mathbf{H} relationship in ferromagnetic
 2482 materials shows this hysteresis characteristic, plotting of this relationship, we call
 2483 it as ‘Hysteresis loop.’ The key formula for studying this effect is well known as
 2484 $\mathbf{B} = \mu\mathbf{H}$, however the most important thing to discern is ‘Whose’ \mathbf{B} , \mathbf{H} , and μ ,

$$\underbrace{\mathbf{B}}_{\text{Material's}} = \overbrace{\mu}^{\text{Material's}} \underbrace{\mathbf{H}}_{\text{Applied}}. \quad (\text{F.1})$$

2485 where $\mathbf{B}[Wb/m^2]$ is the total magnetic density in (ferromagnetic) material, $\mathbf{H}[A/m]$
 2486 is the external applied magnetic field to the material, and $\mu[H/m]$ is the permeabil-
 2487 ity (one of properties, showing how easily the material can be magnetized) of the
 2488 material.

2489 Figure F.1 visualizes magnetization process in a ferromagnetic material with a
 2490 greatly simplified way. Without applied \mathbf{H} , the ferromagnetic material (i.e., iron,
 2491 nickel., etc...) does not show any magnetic properties (left figure in Fig. F.1) having
 2492 net $\mathbf{B}=0$. Once it is exposure to external magnetic field \mathbf{H} , this material exhibits
 2493 characteristics as shown in the right drawing of Fig. F.1. Now the net $\mathbf{B} \neq 0$, it has
 2494 the same magnetic direction with the applied magnetic field. This is the simplified
 2495 description of the magnetization, details of this process needs heavy duty knowledge
 2496 in quantum mechanic which is not relevant in our study Ulaby (2007).

2497 Based on the magnetization process, we can discuss magnetic hysteresis. Figure

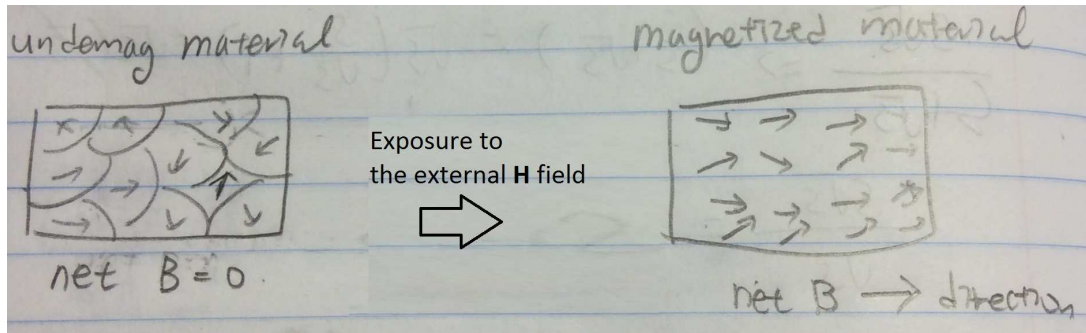


Figure F.1: Simplified magnetization process. Undemagnetized ferromagnetic material's net $\mathbf{B}=0$. When ferromagnetic material is exposure to the magnetic field \mathbf{H} , the net magnetic intensity (\mathbf{B}) of the material is not longer 0. It becomes magnetized with the same direction of the applied \mathbf{H} . Note that details of this process (i.e., breaking the domain walls) needs heavy duty knowledge in quantum mechanic which is not relevant to discuss in our study Ulaby (2007).

2498 F.2 depicts a typical hysteresis loop shown in the ferromagnetic materials. In general
 2499 (not in a ferromagnetic material), \mathbf{H} and \mathbf{B} hold linear relationship, meaning that μ
 2500 of the material is constant. However it is not true for the ferromagnetic materials,
 2501 as we can see in Fig. F.2. The shape of the curve has a specific pattern, each step of
 2502 the curve needs to be explained. In Fig. F.2, the x-axis represents magnetic field \mathbf{H}
 2503 that is applied to the material, and the y-axis shows the magnetic intensity (\mathbf{B}) of
 2504 the material.

- 2505 1. ($O \rightarrow A$): The material's initial position starts from O , as strength of the \mathbf{H}
 2506 is increased to its positive maximum saturation point (1), the material's \mathbf{B} is
 2507 also increased to reach the point A
- 2508 2. ($A \rightarrow B_r$): Then the \mathbf{H} starts to decrease to be zero, but the material's mag-
 2509 netic property still remains at B_r . This point is named as a residual magnetic
 2510 point. At this point, the ferromagnetic material has magnetic characteristic
 2511 without applied magnetic field, therefore it becomes permanent magnet.
- 2512 3. ($B_r \rightarrow C$): As \mathbf{H} is increased its amplitude to the opposite direction (the direc-
 2513 tion of \mathbf{H} is still backward), \mathbf{B} becomes zero at C . The descending from B_r to C
 2514 is called demagnetization, permanent magnet loses its magnetic characteristic
 2515 within this process.

Draft of November 2, 2014 at 17:33

- 2516 4. ($C \rightarrow D$): The line goes down to D , when the \mathbf{H} reaches its (negative) maxi-
2517 mum saturation limits at 2 (red).
- 2518 5. ($D \rightarrow A$): Finally, \mathbf{H} is reversing its direction (i.e., current with sine wave,
2519 passing through $f = \pi/2$) and goes through the portion of the hysteresis loop
2520 from D to A .

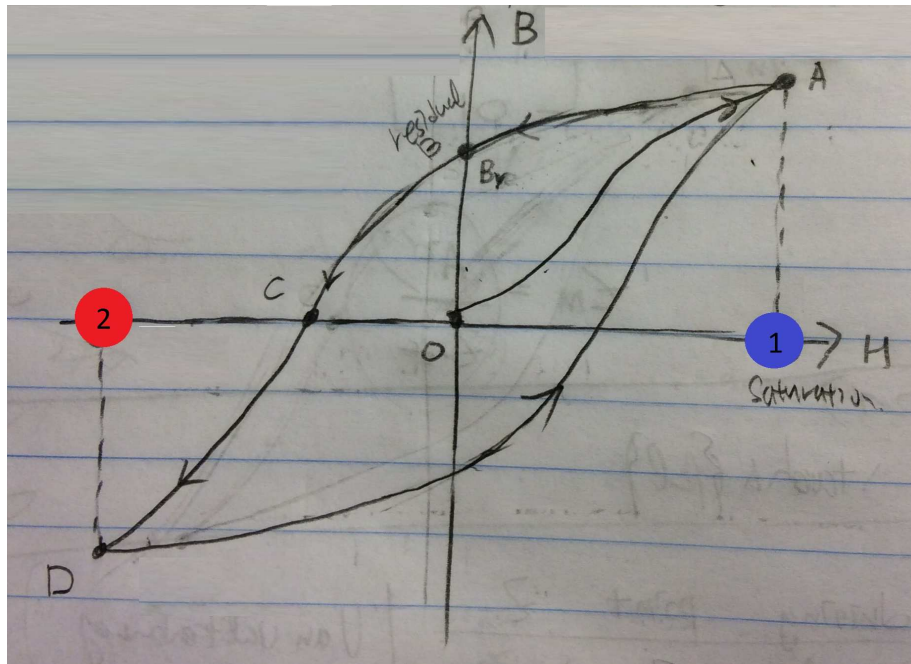


Figure F.2: A typical hysteresis curve in ferromagnetic materials. The x-axis represents magnetic field \mathbf{H} that is applied to the material, and the y-axis shows the magnetic intensity (\mathbf{B}) of the material. On the loop, there are five marked points, O , A , B_r , C , D , and two colored points on the x-axis blue(1) and red(2). The blue and red points are two saturation limits of \mathbf{H} in each direction (\pm). The material's initial position starts from O , as strength of the \mathbf{H} is increased to its positive maximum saturation point (1), the material's \mathbf{B} is also increased to reach the point A . Then the \mathbf{H} starts to decrease to be zero, but the material's magnetic property still remains at B_r . This point is named as a residual magnetic point. At this point, the ferromagnetic material has magnetic characteristic without applied magnetic field, therefore it becomes permanent magnet. As \mathbf{H} is increased its amplitude to the opposite direction (the direction of \mathbf{H} is still backward), \mathbf{B} becomes zero at C . The descending from B_r to C is called demagnetization, permanent magnet loses its magnetic characteristic within this process. The line goes down to D , when the \mathbf{H} reaches its (negative) maximum saturation limits at 2 (red). Finally, \mathbf{H} is reversing its direction (i.e., current with sine wave, passing through $f = \pi/2$) and goes through the portion of the hysteresis loop from D to A and repeating $A \rightarrow B_r \rightarrow C \rightarrow D \dots$ until \mathbf{H} becomes zero

REFERENCES

- 2521 Allen, J., 1986. Measurement of eardrum acoustic impedance, in: Allen, J., Hall,
2522 J., Hubbard, A., Neely, S., Tubis, A. (Eds.), *Peripheral Auditory Mechanisms*.
2523 Springer Berlin Heidelberg. volume 64 of *Lecture Notes in Biomathematics*, pp.
2524 44–51.
- 2525 Bauer, B.B., 1953. A miniature microphone for transistor amplifiers. *The Journal of*
2526 *the Acoustical Society of America* 25, 867–869.
- 2527 Beranek, L.L., 1954. *Acoustics*. McGraw-Hill.
- 2528 Beranek, L.L., Mellow, T.J., 2014. *Acoustics sound fields and transducers*. Waltham,
2529 MA.
- 2530 Boas, R.P., 1987. *Invitation to complex analysis*. New York, NY.
- 2531 Brune, O., 1931. Synthesis of a finite two-terminal network whose driving-point
2532 impedance is a prescribed function of frequency. Ph.D. thesis. Massachusetts
2533 Institute of Technology, Massachusetts.
- 2534 Carlin, H.J., Giordano, A.B., 1964. *Network theory, an introduction to reciprocal*
2535 *and nonreciprocal circuits*. Englewood Cliffs NJ.
- 2536 Cheng, S., Arnold, D.P., 2013. Defining the coupling coefficient for electrodynamic
2537 transducers. *JASA* 134(5), 3561–3672.
- 2538 Fay, R.D., Hall, W.M., 1933. The determination of the acoustical output of a thele-
2539 phone receiver from input measurements. *Journal of Acoustic Science of America*
2540 V, 46–56.
- 2541 Firestone, F.A., 1938. The mobility method of computing the vibration of linear me-
2542 chanical and acoustical systems. *The Journal of the Acoustical Society of America*
2543 10.

Draft of November 2, 2014 at 17:33

- 2544 Hanna, C.R., 1925. Design of telephone receivers for loud speaking purposes. *Radio*
2545 *Engineers, Proceedings of the Institute of* 13(4), 437–460.
- 2546 Hunt, F.V., 1954. *Electroacoustics: The analysis of transduction and its historical*
2547 *background.* Harvard University Press. Harvard University, Massachusetts.
- 2548 Jensen, J., Agerkvist, F.T., Harte, J.M., 2011. Nonlinear time-domain modeling of
2549 balanced-armature receivers. *J. Audio Eng. Soc* 59, 91–101.
- 2550 Keefe, D.H., 1984. Acoustical wave propagation in cylindrical ducts: Transmission
2551 line parameter approximations for isothermal and nonisothermal boundary condi-
2552 tions. *Journal of the Acoustical Society of America* 75, 58–62.
- 2553 Kennelly, A., 1925. The measurement of acoustic impedance with the aid of the
2554 telephone receiver. *Journal of the Franklin Institute (JFI)* 200, 467–487.
- 2555 Kennelly, A., Affel, H., 1915. The mechanics of telephone-receiver diaphragms, as
2556 derived from their motional impedance circles. *Proc. Am. Ac. Arts and Sci.* 51(8),
2557 421–482.
- 2558 Kennelly, A., Kurokawa, K., 1921. Acoustic impedance and its measurement. *Proc.*
2559 *Am. Ac. Arts and Sci.* 56(1), 3–42.
- 2560 Kennelly, A., Nukiyama, H., 1919. Electromagnetic theory of the telephone receiver
2561 with special reference to motional impedance. The 348th meeting of the American
2562 Institute of Electrical Engineers (A.I.E.E.) .
- 2563 Kennelly, A., Pierce, G., 1912. The impedance of telephone receivers as affected by
2564 the motion of their diaphragms. *Proc. Am. Ac. Arts and Sci.* 48, 113–151.
- 2565 Killion, M.C., 1992. Elmer Victor Carlson: A lifetime of achievement. *The Bulletin*
2566 *of the American Auditory Society* 17, 10–21.
- 2567 Kim, N., Allen, J.B., 2013. Two-port network analysis and modeling of a balanced
2568 armature receiver. *Hearing Research* 301, 156–167.
- 2569 Lewin, W., 2002a. Lecture 16: Non-conservative fields - do not trust your intuition.
2570 *University Lecture, Electricity and Magnetism (Physics 8.02).*
- 2571 Lewin, W., 2002b. Lecture 20: Faraday’s law - most physics college books have it
2572 wrong! *University Lecture, Electricity and Magnetism (Physics 8.02).*

Draft of November 2, 2014 at 17:33

- 2573 Lin, F., Niparko, J.K., Ferrucci, L., 2011. Hearing loss prevalence in the United
2574 States. *Archives of Internal Medicine* 171(20), 1851–1853.
- 2575 Lynch, T.J., Nedzelnitsky, V., Peake, W.T., 1982. Input impedance of the cochlea
2576 in cat. *The Journal of the Acoustical Society of America* 72, 108–130.
- 2577 McMillan, E., 1946. Violation of the reciprocity theorem in linear passive electromechanical system. *J. Acoust. Soc. Am.* 18, 344–347.
- 2579 Mott, E.E., Miner, R.C., 1951. The ring armature telephone receiver. *The Bell*
2580 *System Technical Journal* , 110–140.
- 2581 Parent, P., Allen, J.B., 2010. Wave model of the human tympanic membrane. *Hearing*
2582 *Research* 263, 152–167.
- 2583 Puria, S., Allen, J.B., 1998. Measurements and model of the cat middle ear: evidence
2584 of tympanic membrane acoustic delay. *J Acoust Society of America* 104, 3463–81.
- 2585 Robinson, S.R., Allen, J.B., 2013. Characterizing the ear canal acoustic impedance
2586 and reflectance by pole-zero fitting. *Hearing Research* 301, 168–182.
- 2587 S. Ramo, J.R.W., Duzer, T.V., 1965. *Fields and waves in communication electronics.*
2588 New York, NY.
- 2589 Serwy, R., 2012. The limits of Brunes impedance. Master’s thesis. University of
2590 Illinois at Urbana-Champaign, Illinois.
- 2591 Sommerfeld, A., 1964. *Electrodynamics.* Academic Press INC.. London, United
2592 Kingdom.
- 2593 Tellegen, B., 1948. The gyrator, a new electric network element. *Philips Res. Rep t.*
2594 *3*, 81–101.
- 2595 Thorborg, K., Unruh, A.D., Struck, C.J., 2007. A model of loudspeaker driver
2596 impedance incorporating eddy currents in the pole structure. *J. Audio Eng. Soc.* .
- 2597 T.S.Littler, 1934. Motional impedance diagram. *Journal of Acoustic Science of*
2598 *America V*, 235–241.
- 2599 Ulaby, F.T., 2007. *Fundamentals of Applied Electromagnetics*, 5th ed. Prentice-Hall,
2600 Upper Saddle River, NJ.

Draft of November 2, 2014 at 17:33

- 2601 Van Valkenburg, M.E., 1960. Introduction to Modern Network Synthesis. Wiley,
2602 NY.
- 2603 Van Valkenburg, M.E., 1964. Network Analysis. Prentice-Hall, Englewood Cliffs,
2604 NJ. 2nd edition.
- 2605 Vanderkooy, J., 1989. A model of loudspeaker driver impedance incorporating eddy
2606 currents in the pole structure. *J. Audio Eng. Soc.* 37(3), 119–128.
- 2607 Warren, D.M., LoPresti, J.L., 2006. A ladder network impedance model for lossy
2608 wave phenomena. *The Journal of the Acoustical Society of America* (abst) 119(5),
2609 3377.
- 2610 Weece, R., Allen, J., 2010. A clinical method for calibration of bone conduction
2611 transducers to measure the mastoid impedance. *Hearing Research* 263, 216–223.
- 2612 Wegel, R.L., 1921. Theory of magneto-mechanical systems as applied to telephone
2613 receivers and similar structures. *Journal of the American Institute of Electrical*
2614 *Engineers* 40, 791–802.
- 2615 Woodson, H.H., Melcher, J.R., 1968. Electromechanical dynamics. John Wiley and
2616 Sons. New york, London, Sydney.